7-31-2013 12:00 AM

Study of Stability Analysis of a Grid-Connected Doubly Fed Induction Generator (DFIG)-based small Wind Farm

Baishakhi Dhar, *The University of Western Ontario*

Supervisor: Dr. Tarlochan S Sidhu, *The University of Western Ontario*
Joint Supervisor: Dr.Amirnaser Yazdani, *The University of Western Ontario*
A thesis submitted in partial fulfillment of the requirements for the Master of Engineering Science degree in Electrical and Computer Engineering

Study of Stability Analysis of a Grid-Connected Doubly Fed Induction Generator (DFIG)-based small Wind Farm

(Thesis format: Monograph)

by

Baishakhi Dhar

Graduate Program

In

Engineering Science

Department of Electrical and Computer Engineering

A thesis is submitted in partial fulfillment

of the requirements for the degree of

Master of Engineering Science

The School of Graduate and Postdoctoral Studies

University Of Western Ontario

London, Ontario, Canada

Abstract

Wind is the most reliable, clean and fast-developing renewable energy source. The DFIG-based variable speed wind turbine system is now the most popular in wind power industry. With power being so in-demanding, a large wind farm needs to be developed to produce more power from a stable system. But before such a large wind farm is installed, better understanding is needed of the system's intrinsic dynamic behavior, range of stability region and parametric effects on system stability. Hence, a small wind farm with two identical DFIG-based wind turbines connected to a grid network has been considered for this study.

A detailed non-linear mathematical model of grid-connected single DFIG-based wind turbine system as well as a grid-connected multi DFIG-based wind turbine system in a dq-frame has been developed. Linearization of these non-linear mathematical models for both the systems has been performed from the set of developed non-linear equations. These two linearized dynamic models provide an analytical platform for determining the robustness and stability of the two systems. The linearized models are then verified with the simulation results of non-linear systems designed in a PSCAD/EMTDC environment. This step is needed to check the performance accuracy of the linearized models. The small-signal stability, the system's parametric effects on stability and the modal analysis of two developed linearized models have been studied. Participation factor analysis has been employed to determine system parametric effects on each eigenmode. The intrinsic dynamic behavior of a single wind turbine connected to a grid and multi wind turbines connected to a grid (a small wind farm) are observed to be identical in nature at the same operating conditions and system parameters.

Acknowledgements

The author remembers with gratitude the constant guidance, suggestions and encouragement forwarded by several respected persons and knows well that is not possible to express indebtedness for all those valuable assistances by writing some lines. She therefore, acknowledges in this page, the assistance rendered by all the concerned persons, as a token her of gratitude.

The author likes to express her sincere gratitude and thanks to her supervisors Dr. Tarlochan Singh Sidhu and Dr. Amirnaser Yazdani for their financial support, invaluable supervision, kind and persistent valuable suggestion, advice, guidance, help and encouragement from without which this thesis would not have been a reality.

The author is also thankful for financial support from Faculty of Engineering of the Western University.

Finally, the author wishes to express her profound gratitude to her beloved husband for providing the necessary atmosphere of understanding and support during most crucial and disheartening moments.

Table of Contents

List of Tables

Chapter 1

Chapter 4

List of Figures

Chapter 1

Chapter 2

Chapter 3

Chapter 4

Nomenclature

V_s	Stator voltage
i_s	Stator current
i_r	Rotor current
V_r	Rotor voltage
V_a	Grid-side converter ac-side terminal voltage
i_a	Grid-side converter ac-side terminal current
P_r	Rotor active power
Q_r	Rotor reactive power
P_s	Stator active power
Q_s	Stator reactive power
P_a	Ac-side terminal active power of grid-side converter
Q_a	Ac-side terminal reactive power of grid-side converter
L_m	Magnetizing inductance
L_s	Stator inductance
L_r	Rotor inductance
R_r	Rotor resistance
R_s	Stator resistance
λ	Stator flux

s1	Subscript used for DFIG-based wind turbine 1
s2	Subscript used for DFIG-based wind turbine 2
d	Subscript used for direct axis component of a variable
q	Subscript used for quadrature axis component of a variable
V	Voltage at PCC
ω_0	Grid steady state angular frequency
ω_r	Rotor angular speed
J	Moment of inertia
τ_s	Stator time constant
τ_r	Rotor time constant
T_{tur}	Turbine torque
T_e	Electrical torqur
L_{link}	Linking inductance between machine and PCC
N_{tc}	Turn ratio of transformer T_{rs}
N_{tg}	Turn ratio of transformer T_{rg}
R_g	Resistance at Transmission line
R_a	Grid-side converter ac-side terminal resistance
L_a	Grid-side converter ac-side terminal inductance
V_g	Grid Voltage
C_f	Shunt capacitor at PCC

C_{dc} DC side capacitor of two VSC

V_{dc} Voltage across C_{dc}

C_{link} Shunt capacitor at machine and linking inductance meet point

i_{clink} Current across capacitor C_{link}

i_{link} Current across L_{link}

L_g Inductance at Transmission line

ω_l Angular frequency of PLL reference frame

θ_l Reference frame angel of PLL

ρ_s Stator flux phase-angle

ω Angular frequency of stator flux

ζ Damping factor

f_{osc} Frequency of Oscillation

Abbreviations

DFIG	Doubly Fed Induction Generator
VSC	Voltage Source Converter
USSR	Union of Soviet Socialist Republics
GWEO	Global Wind Energy Outlook
HAWT	Horizontal Axis Wind Turbine
VAWT	Vertical Axis Wind Turbine
FRC	Fully Rated Converter
IGBT	Insulated Gate Bipolar Transistor
PWM	Pulse Width Modulation
PCC	Point of Common Coupling
PLL	Phase Locked Loop

Chapter 1
Introduction

In recent years, nations have sought alternative renewable energy resources to meet their rapidly growing demands of power, mainly due to the rapid increase of fuel costs and rising pollution levels. Continuously trimming down traditional energy resources as well as preservation of non-renewable energy resources are the two main causes of increased fuel costs. Pollution levels keep increasing, mainly due to long-term use of fossil fuels and increase in population. Different types of renewable energy sources are Biomass Energy, Hydro-Power Energy, Solar Energy, and Wind Energy. Among all these renewable energy sources, wind energy is most in-demand, as wind is a clean source of energy, with no waste products created during wind power generation. Wind power generation does not need any fuel and is able to supply considerable level of energy to meet world demand.

1.1 Historical Background of Wind Power

Wind power has been used from many years, since humans first started of use of sailboats and sailing ships. Ackermann [1] stated that at least from the 7^{th} century BC, vertical axis windmills were used in the Afghan highlands to grind grain. It has been found that horizontal axis windmills were used in about 1000 AD by Persian, Chinese and Tibetan people. The use of horizontal axis windmills reached the Mediterranean countries and

Central Europe from Persia and the Middle East. In around 1150 AD, this type of windmill reached England; in 1180 AD it reached France, in 1222 AD Germany, and in around 1259 AD, Denmark. Between the 12th to 19th centuries, windmill performance was constantly enhanced, and by the end of the 19th century, typical European windmills were developed, with a rotor of 25 m in diameter, and stocks reaching up to 30 m [1]. In the mid-1700's, Dutch settlers established windmills in America [2]. By 1800, 90% of power used in industry in the Netherlands was from wind power [1]. In the United States of America (USA), between 1880 and 1930, around 6.5 million units of windmills were installed by different companies to provide water for farm animals [2].

1.2 Growth of Electricity Demand

Burton et al. [3] stated, 12 kW DC windmill generator was developed to produce electricity in the late 19th century by Brush in USA and this research was carried out by LaCour in Denmark. In 1931, Union of Soviet Socialist Republics (USSR) constructed 100 kW- 30 m diameter Balaclava wind turbine, which was the first utility scale wind turbine in the world. In 1941, in USA, 1250 kW Smith-Putnam wind turbine was developed that had a steel rotor with diameter of 53m, full-span pitch control and flapping blades to reduce loads. This wind turbine was operated for 1100 hours before a blade spar failed in 1945. This wind turbine remained the largest wind turbine for around 40 years.

A hollow blade, open at tip with 24 m diameter pneumatic wind turbine was constructed in early 1950s in UK to draw air through the tower. In 1956 and in 1963, 200 kW with 24 m diameter Gedser wind turbine and 1.1 MW -35 m diameter wind turbine were

constructed in Denmark and in France, respectively. In between 1950s and 1960s a number of modern, lightweight turbines were developed by U. Hutter in Germany. In spite of this technological progress, it was seen that for much of the 20th century, world had little interest to use wind energy other than in remote residences for battery charging [3].

After a sudden price hike of oil occurred in 1973 because of inadequate fossil-fuel resources, countries like USA, UK, Germany, Sweden took serious steps with a large number of Government-funded programs of research, development and manifestation to investigate cost effective sources of energy. As a result of fact, in between 1975 and 1987, a series of prototype wind turbines starting with 38 m diameter 100 kW Mod-0 and 97.5 m diameter 2.5 MW Mod-5B, respectively, were constructed in USA [3]. Nearly at the same time a 4 MW vertical-axis Darrieus wind turbine and a 34 m diameter Sandia vertical-axis wind turbine were constructed, in Canada and in USA, respectively. Another vertical-axis wind turbine with straight blades using 'H' type rotor was designed by Peter Musgrove and this model was constructed in UK that had a capacity to generate 500 kW power. An entire structure of 3 MW horizontal axis wind turbine was designed and tested in USA, in 1981 that used hydraulic transmission, an alternative to yaw drive [3]. In mid-1980s, a large number of small wind turbines with capacity less than 100 kW were installed in a wind farm with a maximum total capacity of 1.5 MW in California [4]. But for some time, the selection of the number of blades remained undecided and the turbines were constructed with a maximum of three blades. Installed wind turbine capacity was increased from 2.5 GW in 1995 to 12 GW by 2001 [3]. Figure 1.1 shows a statistical review of global cumulative installed wind capacity from 1996 till 2012; a promising

growth of wind energy has been noticed [5]. From 1996 to 2012, an exponential increase of the growth of global cumulative installed wind capacity is observed in Figure 1.1.

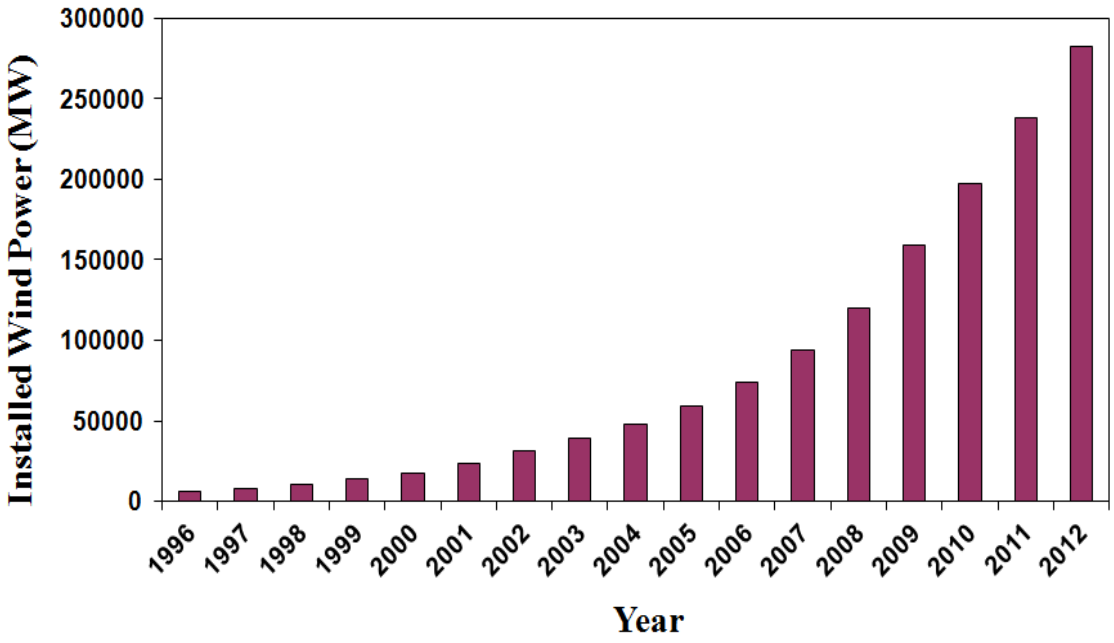

Figure 1.1: Global cumulative installed wind capacity (1996-2012) [5]

As per the 2012 report on global wind energy outlook (GWEO), the growth of global cumulative wind power capacity with three different scenarios in MW unit and wind power share of global electricity demand in percentage, have been plotted for the time period 2011 to 2030, in Figure 1.2 and in Figure 1.3, respectively; while Table 1.1 also lays out the power generation for the three different scenarios [6]. On the basis of current directions and intentions from both national and international energy and climate policy, the "New Policies" scenario is analyzed. The factors related to "Moderate Policies" scenario are mostly similar to "New Policies" scenario; but it also comprises of all policy measures, which are either already implemented in the planning stages or are based on

the commitments of the emission reductions [6]. The most aspiring scenario is 'Advanced Policies' scenario. This consists of unambiguous commitment to renewable energy in line with industry recommendations, the political will to commit to appropriate policies and the stamina to stick with them [6].

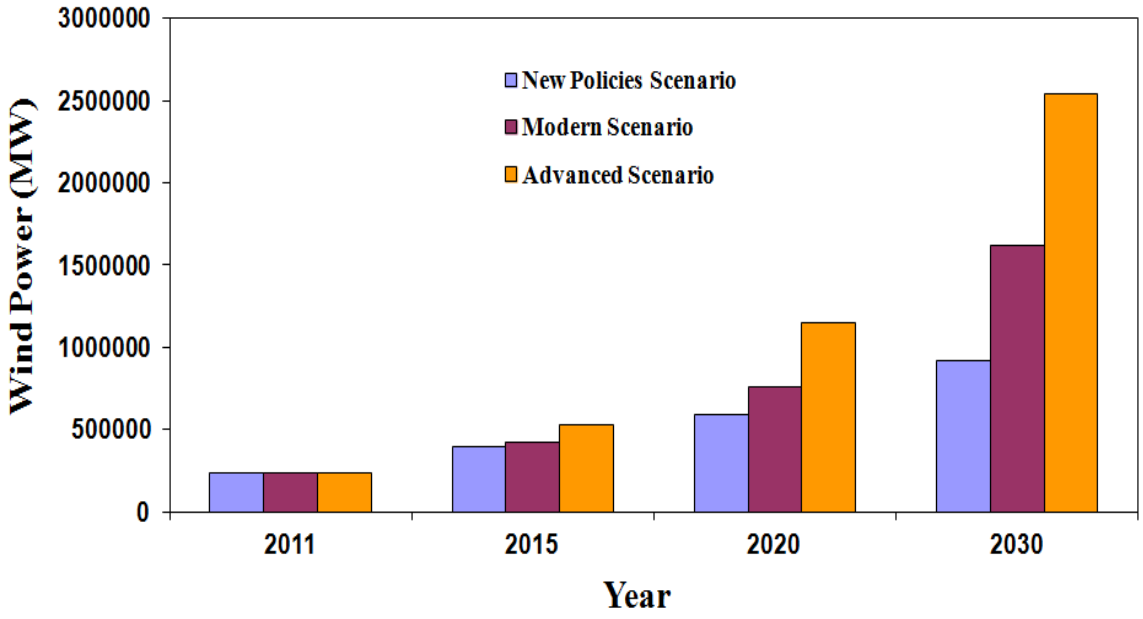

Figure 1.2: Global cumulative wind power capacity (2011-2030) [6]

IEA demand projection of new policies scenario was obtained from Figure 1.3. The projection showed that the wind power share of global electricity demand will increase from 3.5% to 4.7% by 2015 and is projected to be 8% by 2030. But, considering the energy efficiency demand projection of the same scenario, the demand will reach 9% by 2030 [6].

Table 1.1: Three different scenarios for global cumulative wind power capacity (2011-2030) [6]

Different Scenarios	2011	2015	2020	2030
New Policies Scenario [MW]	237,699	397,859	586,729	917,798
Moderate Scenario [MW]	237,699	425,155	759,349	1,617,444
Advanced Scenario [MW]	237,699	530,945	1,149,919	2,541,135

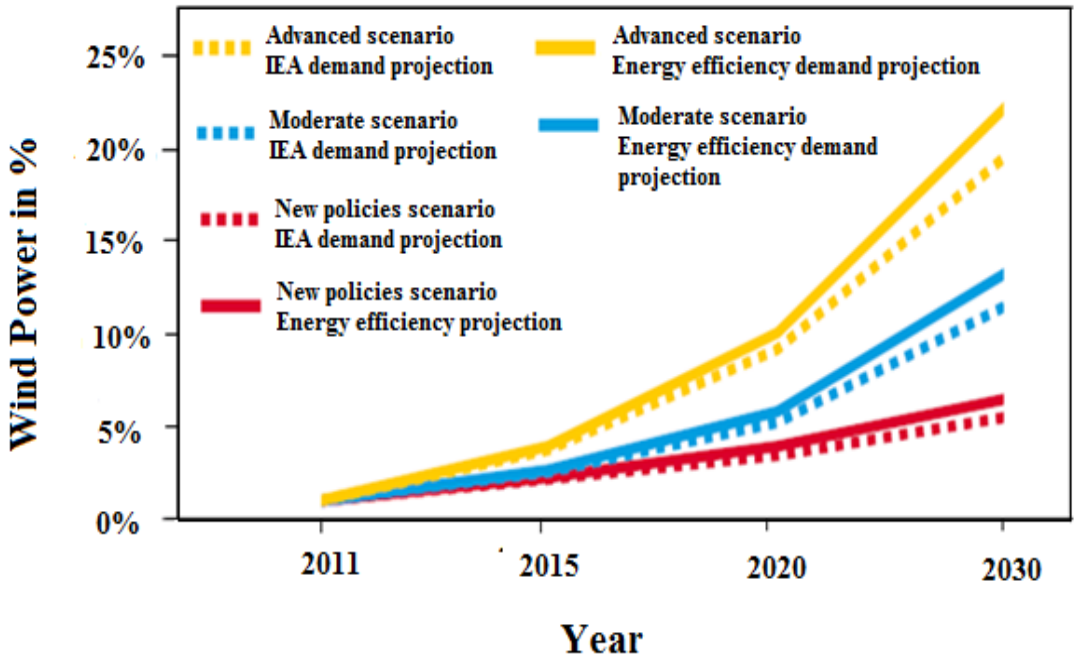

Figure 1.3: Wind power share of global electricity demand (2011-2030) [6]

1.3 Electricity Generation from Wind Power System

Wind turbine generates electricity from wind power to drive electrical machine. If a machine converts kinetic energy of the wind to mechanical energy, and then, this mechanical energy is used to generate electrical energy, that machine is defined as the wind power plant or wind turbine. A detailed description of some fundamental facts of wind turbine such as basic parts, principle of operation and etc. are discussed to get an idea of modern wind turbine system.

1.3.1 Inside of a Wind Turbine

Wind turbine mechanism is exactly the reverse of a fan. Fans use electricity to generate wind, whereas wind turbines use wind to generate electric power. The rotor of wind power system is connected to the main shaft, which spins a generator to produce electricity [7]. Figure 1.4, illustrates a detailed view of the inside of a wind turbine system and its components. Major components of a typical wind turbine system are as follows:

Rotor: The most important part, from both performance and overall cost stand point, of a wind turbine is its rotor; that consists the hub, the high tech blades and a spinner [9,10]. Heaviest components of wind turbine are the hub as it is made of ductile cast iron. For a 2 MW modern wind turbine the weight of the hub is normally in between 8 to 10 tons. The hub can absorb a high level of vibration. The nose cone helps to cover the hub and also to protect it slightly the hub from the environment. Nose cone is made from balsa wood, carbon fiber, and fiberglass [10].

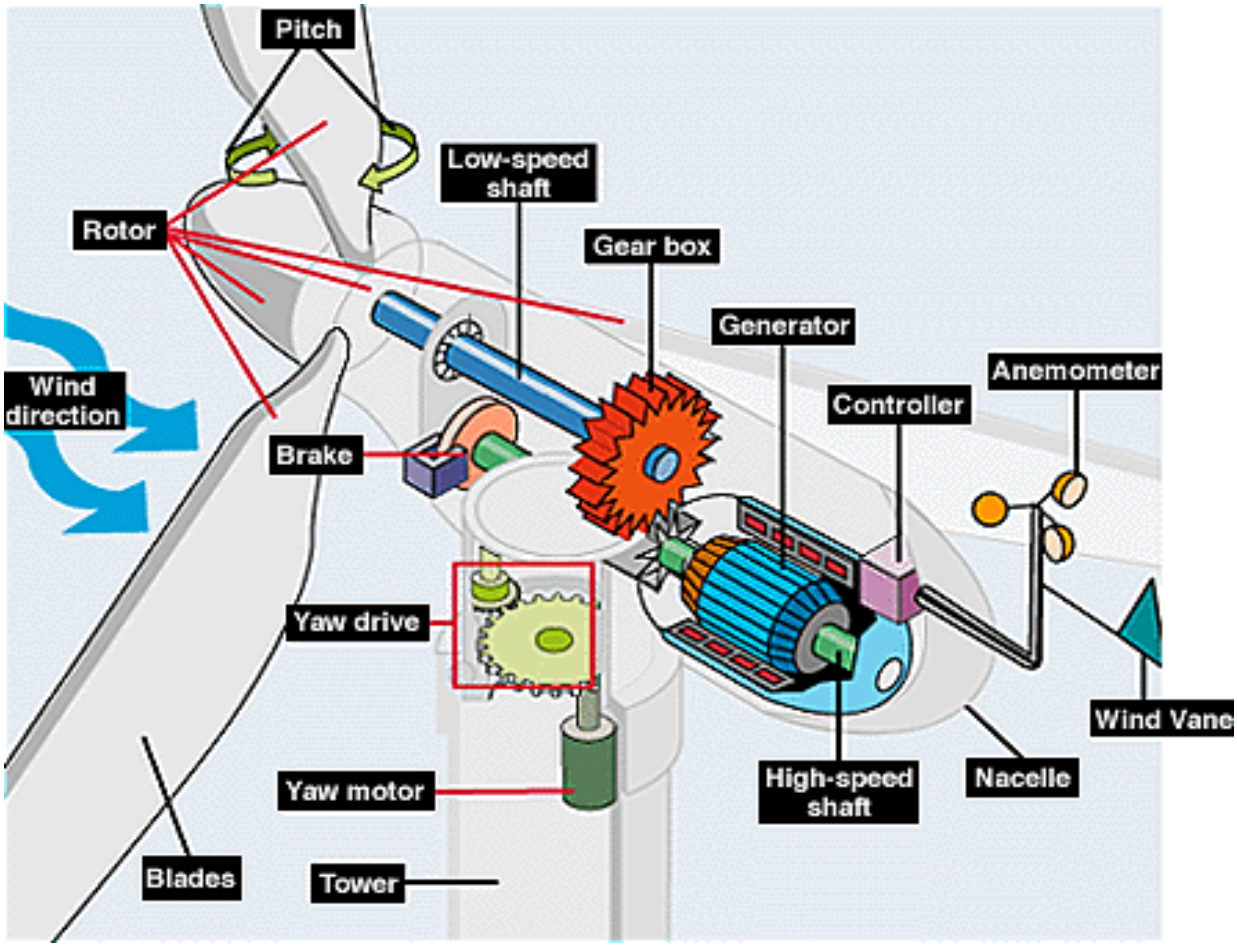

Figure 1.4: Schematic diagram of wind turbine subsystems [8]

One of the most critical and premeditated component of wind turbine system is its blades. The composition of the blades is same as that of the nose cone. To enhance performance of wind turbine in various wind conditions different types of blade are created for a single-turbine. 61.5 m long blade is the world's longest blade made for a 5 MW turbine by LM Glasfiber [10].

Drive Train: This part consists of a low speed shaft, a high speed shaft, a gear box, one or more couplings, support bearings, a brake and a rotating part of generator. The low speed shaft is made on rotor side while the high speed shaft is on the generator side [9]. This drive train is electricity generating system of a wind power system. Gearbox steps up the rate of rotation of the rotor from a low value to a high value suitable for electric generator. As a gear box handles the frequent changes in torque due to changes in wind speed, it must be robust. A lubrication system is used to minimize the wear needed for the gear box system. Mainly parallel shaft and planetary, these two types of gear box are used in wind turbine system. Planetary type gear box is used normally in large wind turbine over 500 kW. Mainly induction generator based wind turbines need gearbox. To stay away from mechanical problem related to gear box, some wind turbines use a direct drive system which connects the rotor directly to a permanent magnet generator [9,10].

Nacelle: A box-like component at the top of tower is connected to the rotor, is called the nacelle. This contains around 8000 components of wind power system like generator, main frame, etc. Nacelle saves the internal components of turbine from weather and is made of fiberglass. The nacelle cover is fixed firmly to the main frame, which also supports all the other components inside the nacelle. The main frames provide proper alignment of drive train components and are also able to withstand large fatigue loads [10].

Yaw System: To keep the rotor shaft properly aligned with the wind a yaw system is needed. A large bearing that connects the main frame to the tower is the main component of yaw drive system. The yaw drive system uses either an electric or hydraulic motor which drives a pinion gear on a vertical shaft through a reducing gearbox. Typically a yaw drive system is used with an upwind wind turbine system, whereas downwind wind power systems are often free from yaw systems. [9]. A brake is also used in a yaw drive system to stop a turbine from turning and stabilizing it during normal operation [10].

Generator: To get constant rotational speed, mainly induction or synchronous generators are used with all wind turbines. Power electronic converters are used with the generators to run wind turbines at variable speed. Squirrel cage induction generators (SQIG) can be used with many grid-connected wind turbines, due to it being rugged by nature, low cost, and driven in a narrow range of speeds, slightly higher than its synchronous speed. Nowadays, doubly fed induction generators (DFIG) have gained popularity in variable speed applications. Main advantages of DFIG are simple configuration, over a wide range of wind speed; wind turbines work efficiently [9].

Tower and Foundation: For use of maximum wind nacelle and generator are situated on the top of the tower [10]. In recent times, lattice towers, concrete towers and free standing steel tube towers are most popular. Depending on the site character, tower is selected. Normally height of a tower varies from 1 to 1.5 times of the rotor diameter. Stiffness of tower plays an important role in wind turbine system dynamics as vibration occurs between rotor and tower. Tower shadow of turbines with downwind rotor must be

considered to have significant effect on power fluctuations, turbine dynamics and noise generation [9].

Controls: To get proper functioning from wind turbine, few instruments like sensors, controllers, power amplifiers, actuators and some intelligent devices like microprocessors and computers are used as control system. Sensors are used to sense and give feedback of wind speed, direction, flow, current, voltage, rotor speed, temperature, vibration levels etc. Electrical circuits and mechanical systems act as controllers to control all the parameters. Different types of switches, hydraulic pumps, electrical amplifiers etc. are the parts of power amplifiers. Motors, magnets, solenoids etc. act as actuators. Few intelligent devices like computers and microprocessors are used to process the inputs of turbine to get proper function from turbine and also at an emergency situation, which help to override the controller to safe overall system [9, 10].

The most fundamental and major components of a typical wind turbine connected to a grid is discussed above. Other than these components, some other components like transformers, power electronic converters and pitch motors etc. are used depending on the complexity of the system to get proper functionality.

1.3.2 Physics of Generating Electricity from Wind Energy

Wind energy is one form of solar energy generated because of temperature and as well as pressure differences in the atmosphere, the rotary motion of the earth, and the irregularities of the earth's surface. Sun heats up the air, forcing the air to rise; this causes a movement of air from high pressure zone to low pressure zone where temperature falls

to balance the differences. Wind turbine first catches wind's kinetic energy which helps to drive generator to produce electricity [11]. The kinetic energy in air with mass m moving with velocity V_w is given by [12]:

$$KE = \frac{1}{2} m V_w^2 \tag{1.1}$$

The power in wind is the Kinetic energy per unit time and as is expressed as:

$$P_w = \frac{1}{2} \dot{m} V_w^2 \ , \tag{1.2}$$

where $\dot{m} = \frac{dm}{dt} = mass\ flow\ rate$

The mass flow rate $\frac{dm}{dt}$ is:

$$\frac{dm}{dt} = \rho A V_w \ , \tag{1.3}$$

where ρ and A are defined as air density and the rotor effective area, respectively. Finally, the wind power equation is:

$$P_w = \frac{1}{2} \rho A V_w^3 \tag{1.4}$$

Power extracted from wind by the turbine blades is the difference between upstream and downstream wind powers and is given by:

$$P_{tur} = \frac{1}{2} mass\ flow\ rate (V_w^2 - V_o^2) \ , \tag{1.5}$$

where V_w is the actual wind speed or upstream wind velocity at the entrance of the rotor blades and V_o is the downstream wind velocity at the exit of rotor. The mass flow rate of the air through rotating blades is then expressed as:

$$mass\ flow\ rate = \rho A \frac{V_w + V_o}{2} \tag{1.6}$$

So the turbine power becomes:

$$P_{tur} = \frac{1}{2}\left[\rho A \frac{(V_w+V_o)}{2}\right](V_w^2 - V_o^2) \quad (1.7)$$

Equation (1.7) is modified to be:

$$P_{tur} = \frac{1}{2}\rho A V_w^3 \frac{\left(1+\frac{V_o}{V_w}\right)\left[1-\left(\frac{V_o}{V_w}\right)^2\right]}{2}, \quad (1.8)$$

where $C_P = \frac{\left(1+\frac{V_o}{V_w}\right)\left[1-\left(\frac{V_o}{V_w}\right)^2\right]}{2}$ (1.9)

is the power coefficient of the rotor. C_P, is the fraction of upstream wind power.

Finally the turbine power P_{tur} from equation (1.8) is rewritten to be:

$$P_{tur} = \frac{1}{2}\rho A V_w^3 C_P \quad (1.10)$$

The power coefficient, C_P, is thus a dimensionless parameter and is the ratio of turbine power P_{tur} to that of wind power P_w.

$$C_P = \frac{P_{tur}}{P_w} \quad (1.11)$$

The maximum value of C_P is defined by Betz limit and is 0.59, as Betz limit states that a turbine can never extract more than 59.3% of wind power. Practically C_P varies from 25% to 40% [13] for the wind turbine. C_P, is a function of the blade pitch angle, β_{pitch} and the tip speed ratio, λ_{blade}. λ_{blade}, is defined as the ratio of upstream wind speed V_w and downstream wind speed V_o.

$$\lambda_{blade} = \frac{V_w}{V_o} \quad (1.12)$$

This, λ_{blade} can also be expressed in terms of turbine angular speed, ω_{tur}, turbine radius, r, and wind speed, V_w, and is given as :

$$\lambda_{blade} = \frac{\omega_{tur} \times r}{V_w} \quad (1.13)$$

The relationship between C_P and tip speed ratio λ_{blade} is then established by using the blade theory of turbine and is given by [14]:

$$C_P = \frac{1}{2}(\lambda_{blade} - 0.022\beta_{pitch}^2 - 5.6)e^{-0.17\lambda_{blade}} \quad (1.14)$$

Figure 1.5 shows the changing behavior of the power coefficient C_p with the changing tip speed ratio λ_{blade}. It can be stated from this figure that, maximum C_p is only achieved at a single tip-speed ratio and for a fixed rotational speed of the wind turbine; this happens only at one single wind speed.

Figure 1.6 shows the nature of the graph for turbine power in per unit value with the change in turbine speed which is in per unit value at different wind speed. This wind speed varies from 6 m/s. to 14 m/s. The maximum turbine power in Figure 1.6 is seen to change for different wind speed.

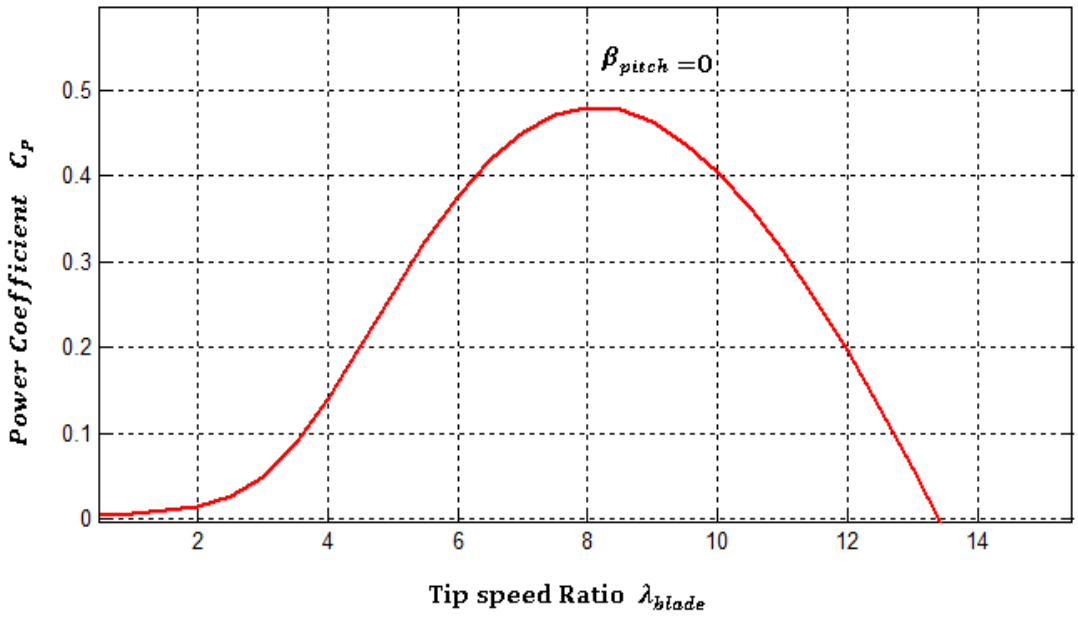

Figure 1.5: Graph of power coefficient, C_p vs. tip speed ratio λ_{blade}

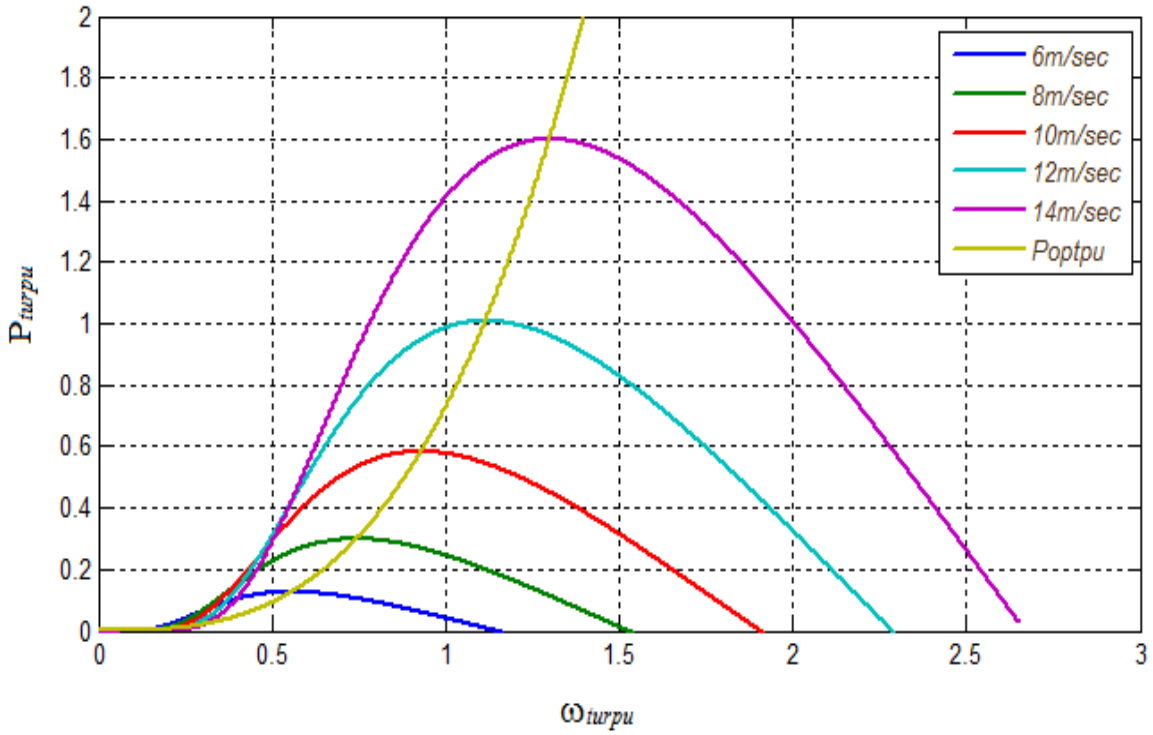

Figure 1.6: Graph of turbine power in per unit vs. turbine speed in per unit

1.3.3 Different Types of Wind Turbine

Wind turbines are classified in two ways. Firstly, the classification depends on the position of the rotor axis of wind power system and secondly, it depends on the variation of wind speed. Wind turbine can be classified into horizontal axis wind turbine (HAWT) and vertical axis wind turbine (VAWT) [15]. Depending on the variation of wind speed wind turbines are also classified into constant speed wind turbine and variable speed wind turbine [16].

HAWT: Most popular commercial wind turbine connected to a grid, in recent times is the HAWT. These mainly consist of two or three bladed rotors. For this type of wind

turbine, the rotor shaft and electrical generator are placed at the top of the tower where wind is less turbulent and wind has more power. Figure 1.7 (a) shows the schematic diagram of HAWT [15].

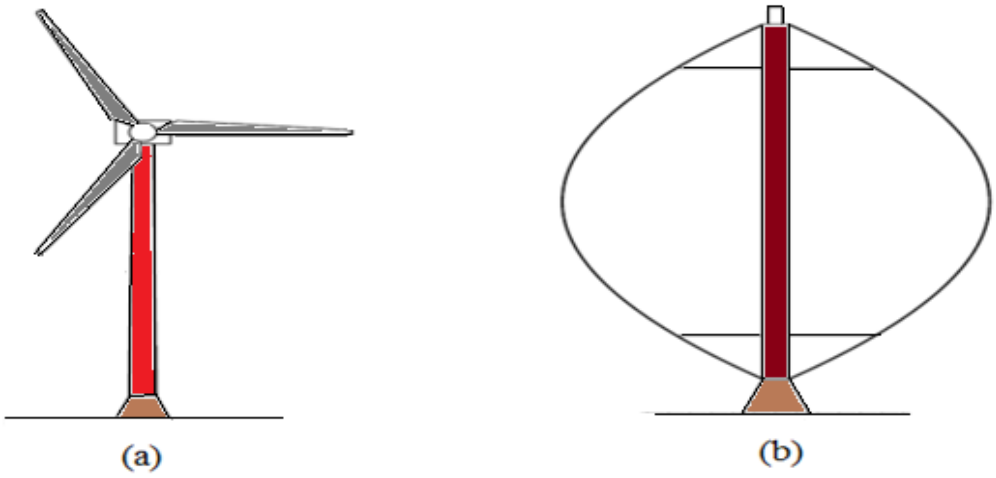

Figure 1.7: (a) Schematic diagram of horizontal axis wind turbine. (b) Schematic diagram of vertical axis wind turbine [15]

VAWT: The main rotor shaft in VAWT is placed vertically in the wind turbine system. Figure 1.7 (b) shows Darrieus rotor type vertical axis wind turbine system which is the most popular type VAWT [15]. The main advantages of this kind of wind turbines are that, the generators and gearboxes are easy to repair and perform maintenance operation of the components as they are placed close to ground, and also this turbine can catch the wind from all direction without any yaw system. Though there are advantages, but this type of wind turbine has many disadvantages like, low starting torque, sensible to design conditions, tendency to stall under blustery wind conditions, used for low power

applications such as battery charging, as output power is very low; thus, minimizes the popularity of VAWT comparing with HAWT [17].

Constant Speed Wind Turbine: This type of turbine is simple in design and is composed of a gearbox, a low speed shaft, a high speed shaft and an asynchronous generator. Figure 1.8 presents the schematic diagram of a constant speed wind turbine system. Mainly squirrel-cage induction generator is used to generate power from such type of system [13]. For this turbine system, a power-electronic converter is not needed since the system works at constant speed, and therefore it is structurally simple. Synchronous frequency is imposed by the grid to the machine because the generator is directly interfaced with the utility grid through a turbine transformer machine. The rotational speed of the asynchronous generator is not exactly constant and varies within ±3% to ±8% of the synchronous speed which is very small, so this type of turbine is considered to be a constant speed type wind turbine system. As asynchronous machines consume reactive power, so power factor correction capacitors is used at each wind turbine to maintain the voltage profile to get stable operation, mainly at non-stiff grid conditions. Though simple in design, this type of turbine system is not able to extract maximum power at different wind speed as it works at almost constant wind speed. The stator of generator is directly connected to a utility grid, so, as a result of fact, any kind of transmission line network will affect directly the wind based generating units of the system [16].

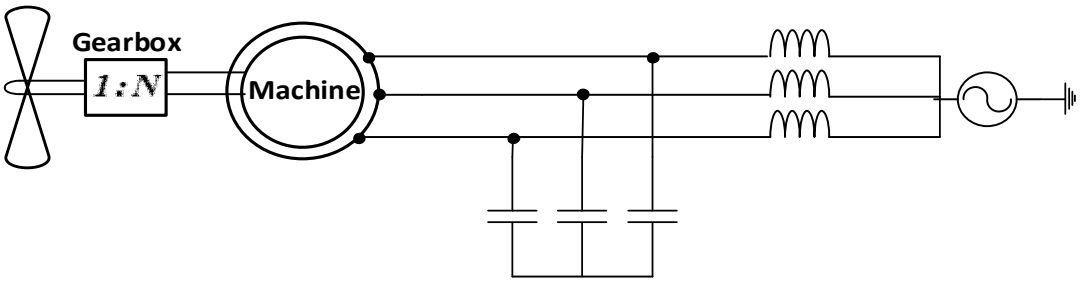

Figure 1.8: Schematic diagram of constant speed wind turbine system [16]

Variable Speed Wind Turbine: Though structurally complex, this type of wind turbine system is more popular comparing with constant speed wind turbine as maximum energy can be generated due to the variability in speed of the turbine system. A solid-state power converter is always used to interface the machine to the transmission system. There are two different types of variable speed wind turbines that are most common nowadays. These are: wind turbine with doubly fed induction generator (DFIG) and wind turbine with fully rated converter (FRC) based on a synchronous or induction generator [13].

- **DFIG Wind Turbine:** Power can be delivered to the grid through both stator and rotor of the machine for this type of variable speed wind turbine system. Depending on the rotational speed of the generator the rotor can also absorb power [13]. The rotor absorbs power from the grid through power converter when the operating speed of generator is lower than the synchronous speed and it delivers power to the grid when the generator operates above the synchronous speed [13]. A schematic diagram of this type of turbine is shown in Figure 1.9 (a). A controllable voltage is injected into the rotor at slip frequency to achieve variable speed of operation. Mainly two

AC/DC IGBT based voltage source converters (VSCs), linked by a DC bus is interfaced in between the rotor winding and electrical network to decouple transmission line electrical frequency from rotor mechanical frequency. Thus, the variable speed operation of wind turbine is possible [13].

- **FRC Wind Turbine:** Figure 1.9 (b) shows a schematic diagram of FRC wind turbine system. A wide range of electrical generators like wound rotor synchronous generator, permanent magnet generator, induction generator etc. can be used for this type of turbine system. Use of the gearbox is optional for FRC wind turbine system. Variable speed operation can be performed as the dynamic operation of electrical generator is effectively separated from the electrical network through power converters [13]. A diode rectifier or a PWM VSC can be used as generator side converter and only PWM VSC can be used as grid side converter. Each type of converter can independently deliver or absorb reactive power independently. Mainly DC bud voltage is controlled by the grid side converter whereas generator side converter controls the torque applied to the generator. But reverse control strategy is also applicable for these two types of converters [13].

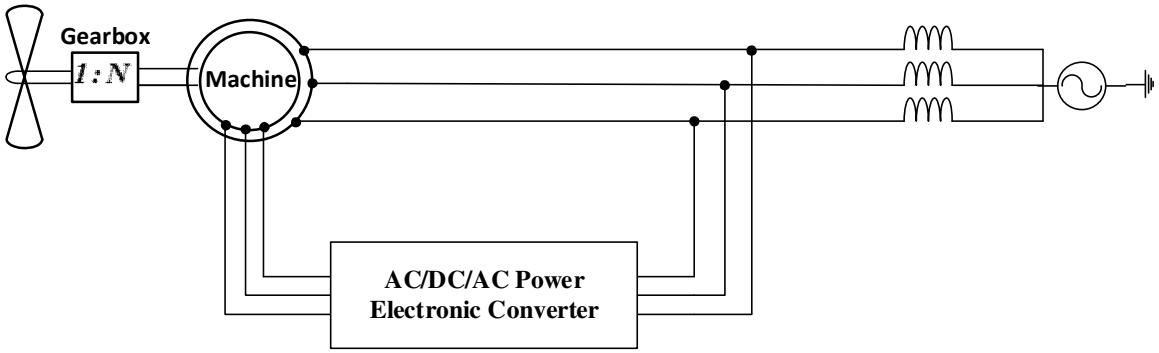

(a)

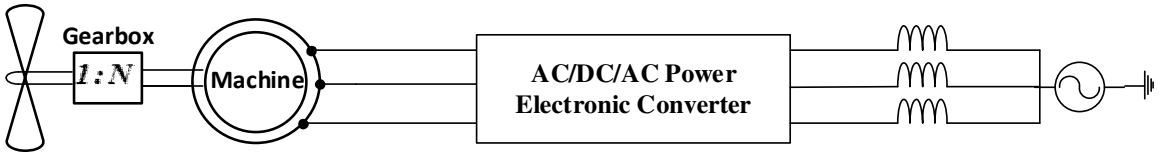

(b)

Figure 1.9: (a) Schematic diagram of DFIG variable speed wind turbine system [16] (b) Schematic diagram of FRC variable speed wind turbine system [16]

1.4 Survey of Existing Work

As shown in section 1.2, the demand for wind power to meet global electricity demand has been increasing. In Recent years, variable-speed DFIG-type wind-power systems have become commercially very popular for generating wind power, but because of the erratic nature of wind velocity, extensive research has been done to analyze system stability and sensitivity for the changes of different system parameters to get efficient and economic production of wind energy from a stable wind-power-generating system. A brief review of previous research shows the relation between system modeling and stability analysis of a DFIG wind turbine system. Different models of grid-connected DFIG with one or two mass drive trains and with or without stator transients have been

formulated mathematically and compared with each other using eigenvalues and participation factor analysis [18]. Rouco and Zamora [19] developed detailed non-linear and corresponding linear mathematical models of DFIG systems for wind power applications. They offered a reduced order model of the detailed models using eigenvalues of the state matrix and corresponding participation factor analysis. A comparative study has also been carried out on the detailed models and the proposed reduced order models [19]. Modal analysis, with a 7^{th} order grid-connected DFIG-based system, has been performed for, better understanding of basic dynamics of the system, model justification and control system design [20]. This study was carried out by changing the modal properties for different operating points, grid strengths and system parameters. [21] has designed damping controllers of DFIG for damping electromechanical oscillation by eigenvalue sensitivity analysis with respect to some parameters. A detailed mathematical model of DFIG has been developed, to analyze eigenvalue sensitivity with respect to machine and control parameters, and to evaluate their impacts on system stability; it has also been shown that without proper controller tuning, a Hopf bifurcation can occur for various reasons [22]. [23] has presented a study on participation factor analysis using eigenvalue of a mathematically developed DFIG-based wind-power unit interfaced with the grid through a series compensated transmission lines. The influence of the system parameters on stability of the system has also been studied.

1.5 Scope of the Thesis

As the literature review makes clear, considerable research has been carried out to analyze system stability and modal analysis in a single DFIG-based-turbine connected to a grid. However, a very few research has been performed to clarify the intrinsic dynamic behavior of a wind farm comprised of multi-turbine systems. As wind power is very much in demand nowadays, being a non-conventional energy resource to generate electric power, it is necessary to construct large wind farms that can produce maximum power from a stable system. Hence, this thesis is motivated by the desire to contribute to the better understanding of the intrinsic dynamic behavior, range of stability region and system's parametric effects on the system stability of a small wind farm. To achieve these, a small wind farm with two identical DFIG-based wind turbines connected to a grid network needs to be established.

1.6 Thesis Objectives

The objectives of the thesis are

- To develop a linearized mathematical model from a non-linear DFIG-based single wind power system connected to a grid. Also on the basis of this model, to establish a linearized model of a small DFIG-based wind farm connected to a distribution network.
- To validate the established linearized mathematical models by comparing the simulation results from both the linear and non-linear models.
- To study and analyze the system stability, eigenvalue sensitivity and modal properties for the models of both systems.

1.7 Methodology

The following methodology is used in order to carry out the objectives:

- non-linear analytical models of a grid-connected DFIG-based single-turbine and a grid-connected DFIG-based multi-turbine systems are established.
- to clarify the dynamic behavior of both the systems, linearized mathematical models are developed from the non-linear models.
- to validate the linearized models for a single-turbine system and the wind farm, the simulation results of the linear and non-linear models are compared separately.
- to examine the system stability and fundamental dynamic behavior, participation factor analysis and eigenvalue sensitivity analysis are performed for different operating conditions and system parameters.

1.8 Thesis Layout

Thesis is organized in the following manner:

- Chapter 2 develops mathematical linearized models of a DFIG-based wind turbine system connected to a grid and a small wind farm involving two identical DFIG-based wind turbines connected to a grid around an equilibrium point, including all the control system blocks, system and network equations, based on non-linear models.
- Chapter 3 deals with the validation of linearized system performance with non-linear models developed in a PSCAD/EMTDC environment for a single-turbine connected to a grid and as well as for a multi-turbine connected to a grid.

- Chapter 4 presents system stability analysis and modal analysis of the linearized models developed in Chapter 2 to determine the intrinsic dynamics for model justification and for useful control system block design in order to achieve wide range system stability with maximum output power.
- Finally, Chapter 5, summarizes and concludes the thesis and presents the scope of future work.

Chapter 2

Mathematical Modeling and Control of Grid-Connected DFIG-based Wind Energy Conversion System

This chapter develops a non-linear mathematical model of a DFIG-based wind power system connected to a grid. A linearization is performed on the same system for small-signal stability analysis. Two of these, identical DFIG-based wind power systems are then considered to be connected in parallel with a distribution network through a Point of Common Coupling (PCC). The resulting design is then referred to as a small wind farm connected to a grid. A non-linear mathematical model of this wind farm is then developed and linearization is performed.

The non-linear equations for both the models established on "dqo" frame are used, which simplify the analysis of three phase circuits, transform AC quantities into DC quantities, decouple DFIG torque and flux, and also avoid the time varying mutually coupled inductances of the overall systems [16]. From each of the system equations, the o-axis components are eliminated. The variables with the d- and q-axis components are denoted by subscripts "d" and "q"; for instance as, V_g is represented as V_{gd} and V_{gq}, respectively .

Each of the individual wind power systems consists of individual control system blocks, back-to-back voltage source converters (VSCs), and a phase locked loop (PLL). An in-depth description of each of these blocks for both in linear and non-linear mathematical forms is presented here.

2.1 Grid-Connected Single DFIG-based Wind Power System

Figure 2.1 presents a schematic diagram of a grid-connected single DFIG-based wind turbine system. All the parametric values used for the system are mentioned in the appendix A. The turbine is interfaced with the grid through a linking inductance, L_{link}, a transformer, T_{rg}, and a transmission line where an ideal voltage source, V_g , is the grid as mentioned in Figure 2.1. The high voltage side of the T_{rg} is connected with V_g. The stator of the DFIG is directly connected to L_{link}, while the rotor is connected through the ac-dc-ac back-to-back VSCs to L_{link}. Figure 2.1 shows the two back-to-back converters, rotor side and grid side converters that are referred to as VSC1 and VSC2, respectively. Thus capacitors, C_{link} and C_f provide a low-impedance path for switching harmonics, which are generated by VSCs. The voltage at PCC is V, where L_{link} and T_{rg}, are connected. The transmission line consists of resistance, R_g, and inductance, L_g, connected in series. The mechanical dynamics of Figure 2.1 is described by

$$J\frac{d\omega_r}{dt} = T_{tur} - T_e, \tag{2.1}$$

where J is the moment of inertia, ω_r is the machine rotor speed, T_{tur} is considered to be turbine torque and T_e is the electrical torque [13, 16, 24] .

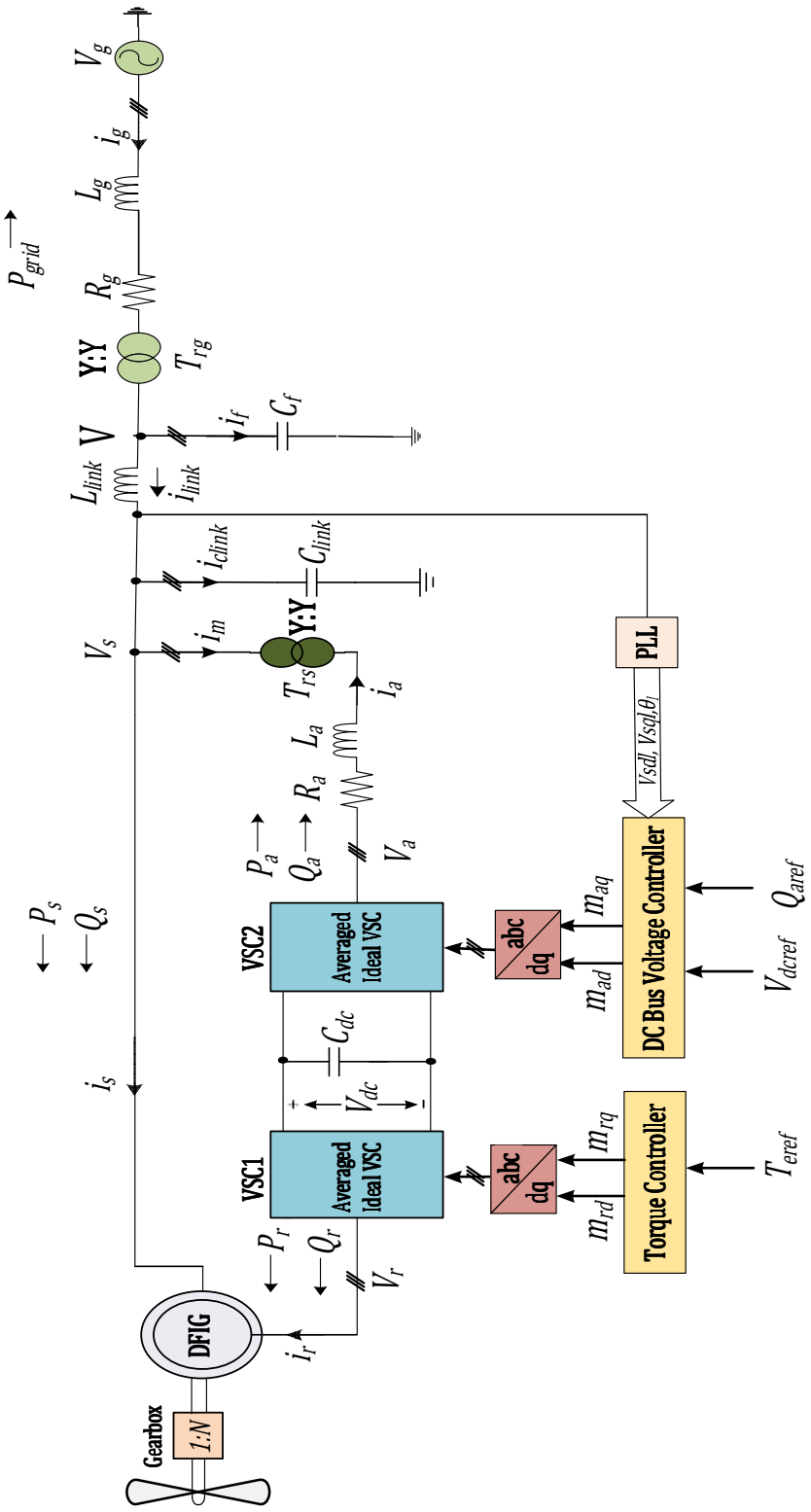

Figure 2.1: Schematic diagram of grid-connected DFIG-based single wind power system

Equation (2.1) is significant in analyzing the stability of the wind power system as it helps to describe the effect of any mismatch between the electrical and the mechanical torques generated by the turbine. A detailed description and a non-linear mathematical model of each block of the overall system as shown in Figure 2.1 is synchronously developed.

2.1.1 Stator Flux Observer

Figure 2.2 presents a schematic diagram of the stator flux observer. This flux observer helps to calculate the stator flux angle, ρ_s. This angle is considered as the transformation angle for transforming space phasor equations to dq-frame equations.

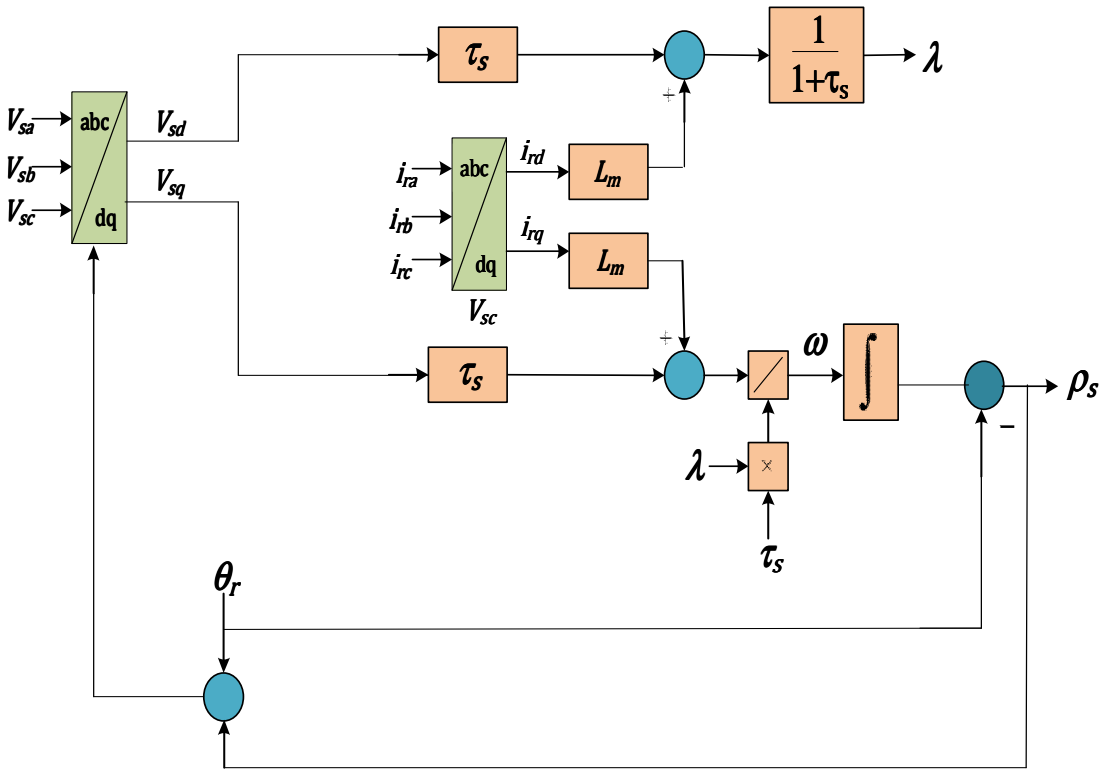

Figure 2.2: Schematic diagram of stator flux observer

The space phasor equation governed by the dynamics of three phase DFIG machine can be represented in machine stator flux equation [16] as

$$\frac{d\vec{\lambda}_s}{dt} = \vec{V}_s - R_s\vec{i}_s \tag{2.2}$$

where, λ_s is stator flux of DFIG, V_s is stator voltage, i_s is stator current and R_s is stator resistance. In the dq-frame, the equation (2.2) is expressed as,

$$\frac{d\lambda_{sd}}{dt} = V_{sd} - R_s i_{sd} + \omega\lambda_{sq} \tag{2.3}$$

$$\frac{d\lambda_{sq}}{dt} = V_{sq} - R_s i_{sq} - \omega\lambda_{sd} \tag{2.4}$$

where $\omega = \frac{d\rho_s}{dt}$

$$\lambda_{sd} = L_s i_{sd} + L_m i_{rd} \tag{2.5}$$

$$\lambda_{sq} = L_s i_{sq} + L_m i_{rq} \tag{2.6}$$

where L_s, L_r and L_m are the stator, rotor, and magnetizing inductances, respectively.

To be able to control the machine's torque independently from the machine's flux (see Section 2.1.2), the angle ρ_s is controlled (by the proper control of ω) in such a way that $\lambda_{sq} = 0$ and $\lambda_{sd} = \lambda$. So equations (2.3) and (2.4) are then substituted to become,

$$\frac{d\lambda}{dt} = V_{sd} - R_s i_{sd} \tag{2.7}$$

$$\frac{d\rho_s}{dt} = \frac{1}{\lambda}(V_{sq} - R_s i_{sq}) \tag{2.8}$$

The dq-frame currents, i_{sd} and i_{sq} are eliminated from equations (2.7) and (2.8) by substituting equations (2.5) and (2.6). The two equations are then rewritten in terms of i_{rd} and i_{rq}.

$$\frac{d\lambda}{dt} = -\frac{\lambda}{\tau_s} + V_{sd} + \frac{L_m i_{rd}}{\tau_s} \tag{2.9}$$

$$\frac{d\rho_s}{dt} = \frac{1}{\lambda}(V_{sq} + \frac{L_m i_{rq}}{\tau_s}) \tag{2.10}$$

where i_{rd} and i_{rq} are the d- and q-axis components of rotor currents, respectively and $\tau_s = \frac{L_s}{R_s}$ is called the stator time constant.

2.1.2 Torque/ Flux Controller

The machine torque equation is written as,

$$T_e = \frac{3}{2}\frac{L_m}{L_s}\lambda i_{rq} \tag{2.11}$$

It is observed from (2.11) that machine's electrical torque is controlled linearly by the rotor q-axis current i_{rq}.

Under steady-state condition, the stator flux and stator voltage of DFIG are sinusoidal waveforms with amplitudes $\hat{\lambda}$ and $\hat{V_s}$, respectively. As $\lambda_{sq} = 0$, $\lambda_{sd} = \lambda = \hat{\lambda}$, thenignoring R_s from equation (2.7), at steady state condition, $V_{sd} = 0$ and as

$\sqrt{{V_{sd}}^2 + {V_{sq}}^2} = \hat{V}_s$ is the peak value of the line to neutral voltage and is a constant, V_{sq}, which becomes $\hat{V}_s$. Also, at steady state condition, $\omega = \omega_0$, where ω_0 is the machine's nominal frequency. Then $\hat{\lambda} \approx \frac{\hat{V}_s}{\omega_0}$. Considering all the assumptions, the machine torque equation can be rewritten as

$$T_e = \frac{3}{2}\frac{L_m}{L_s}\frac{\hat{V}_s}{\omega_0} i_{rq} \tag{2.12}$$

T_e can also be represented in terms of ω_r, and the equation is given by [16],

$$T_e = k_{opt}\omega_r^2 \tag{2.13}$$

where k_{opt} is a constant. The value of k_{opt} depends on the wind-turbine's design specification and characteristics. A detail description for k_{opt} is as given in Hilal et al. [25]. To extract the maximum possible electrical power from a variable speed wind power system, T_e is expressed as T_{eref} and is given by

$$T_{eref} = k_{opt}\omega_r^2 \tag{2.14}$$

From equations (2.12) and (2.14), the expression for i_{rq} is obtained. This i_{rq} is represented as i_{rqref} which controls the electrical torque. The expression of i_{rqref} is schematically shown in Figure 2.3.

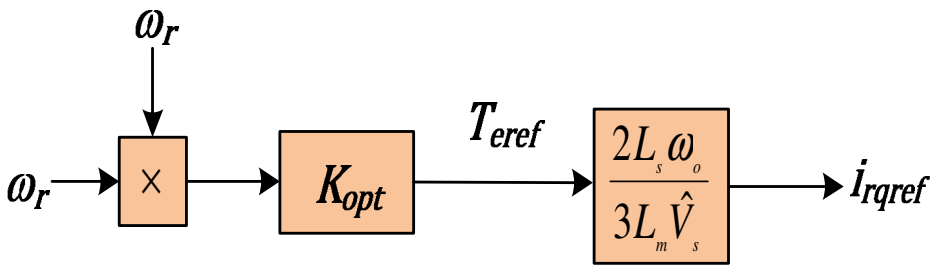

Figure 2.3: Schematic diagram of rotor q-axis reference current generator

Figure 2.4 presents the schematic diagram of the d- and q- axis current controllers of the rotor side converter VSC1 [16] , where $\eta = (L_r - \frac{L_m^2}{L_s})$ and $K_r(s)$ is a PI controller; the values of which are given in appendix A.

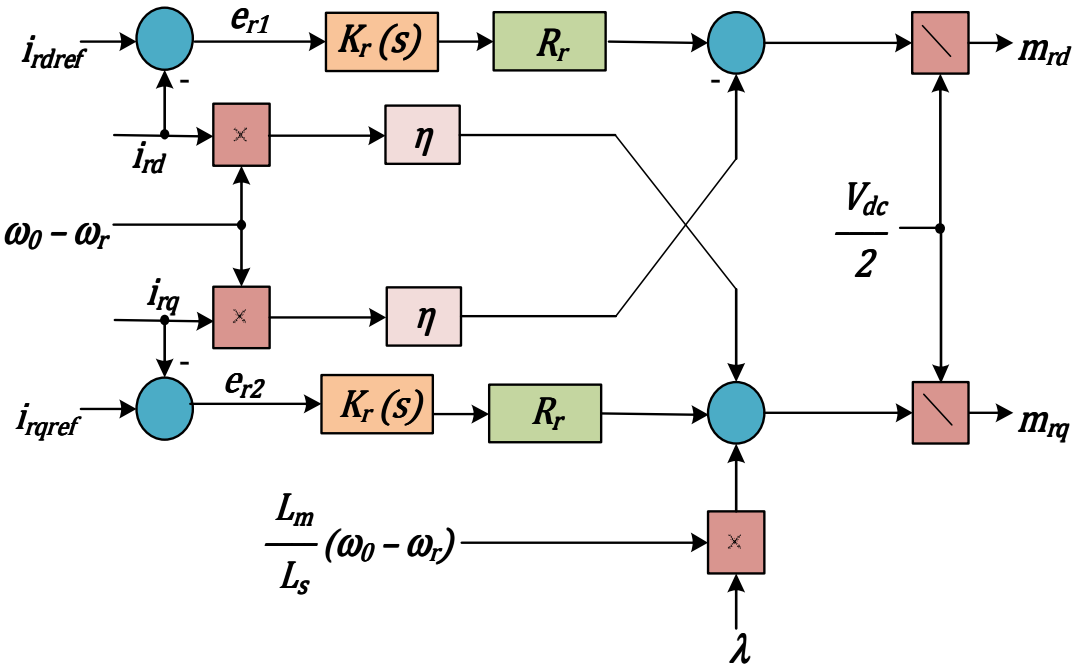

Figure 2.4: Block diagram of machine rotor current control loop

The rotor d- and q- axis currents i_{rd} and i_{rq} are controlled through their corresponding reference current control commands i_{rdref} and i_{rqref}, respectively; m_{rd} and m_{rq} are the modulating signals and stand as the output of the controller, as described in Figure 2.4. Modulating signals m_{rd} and m_{rq} are transformed into their "abc" frame, and the signal is presented as m_{rabc} . Switching sequences in the rotor side converters are controlled by the modulating signals m_{rabc}.

2.1.3 Phase Locked Loop (PLL)

The schematic diagram of PLL for synchronizing the utility voltages with controlled voltages is shown in Figure 2.5.

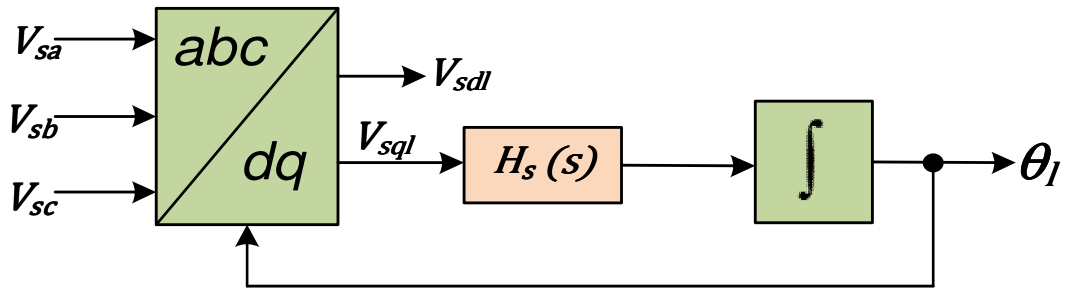

Figure 2.5: Schematic diagram of PLL

From the above schematic diagram, the following equation is derived;

$$\frac{d\theta_l}{dt} = H_s(s)V_{sql} \qquad (2.15)$$

where $H_s(s)$ is a compensator. The transfer function of $H_s(s)$ is given in the appendix A. As the PLL frame and the stator flux frame angles are different so, the PLL voltages, V_{sdl} and V_{sql}, are expressed in terms of stator flux voltages.

$$V_{sdl} = V_{sd}\cos(\rho_s - \theta_l) - V_{sq}\sin(\rho_s - \theta_l) \tag{2.16}$$

$$V_{sql} = V_{sd}\sin(\rho_s - \theta_l) + V_{sq}\cos(\rho_s - \theta_l) \tag{2.17}$$

$H_s(s)$ changes θ_l in a way so that $V_{sql} = 0$ and $V_{sdl} = \hat{V}_s$. A detailed design and operation of PLL are mentioned in [16].

2.1.4 Back -to-back VSC Converters & DC Bus Voltage Controller

In Figure 2.1, two back-to-back converters, VSC1 and VSC2 are used. They both are connected to each other at their DC voltage end with a capacitor C_{dc} .The active power flowing through these converters is expressed by the power balance equation as:

$$\frac{C_{dc}}{2}\frac{dV_{dc}^2}{dt} = -P_r - P_a \tag{2.18}$$

where P_r is the machine rotor power and is considered as disturbance input; P_a is the power leaving the AC side terminals of VSC2.

The rotor power P_r can be expressed in terms of rotor voltages V_{rd}, V_{rq} and rotor current i_{rd} and i_{rq}.

$$P_r = \frac{3}{2}Re(\vec{V}_r\vec{i}_r^{\,*}) = \frac{3}{2}(V_{rd}i_{rd} + V_{rq}i_{rq}) \tag{2.19}$$

Also P_a can be represented as:

$$P_a = \frac{3}{2} Re\left(\vec{V}_a \vec{i}_a{}^*\right)$$

As, $V_{ad} = \frac{3\,V_{sdl}}{2N_{tc}}$; and $V_{aq} = \frac{3\,V_{sql}}{2N_{tc}}$;

$$P_a = \frac{3}{2N_{tc}} (V_{sdl} i_{ad} + V_{sql} i_{aq}) \tag{2.20}$$

where N_{tc} is turn ratio of the transformer, T_{rs}. V_{ad}, V_{aq} and i_{ad}, i_{aq} are d-and q-axis components of voltage and current, respectively, of the ac-side terminal of VSC2 in Figure 2.1.

Based on equation (2.18) and equation (2.20), is the dc voltage V_{dc} is controlled by i_{ad} only, because in the previous section, $V_{sql} = 0$. Figure 2.6 illustrates the current control loop for DC bus voltage regulation. The ac side d- and q- axis current components i_{ad} and i_{aq} of VSC2 are controlled through their corresponding reference current control commands i_{adref} and i_{aqref}, respectively; m_{ad} and m_{aq} are the modulating signals, and stand as the output of the controller, as described in Figure 2.6. Modulating signals m_{ad} and m_{aq} are transformed into their "abc" frame, and the signal is presented as m_{aabc} . Switching sequences in the grid side converters are controlled by the modulating signals m_{aabc}.

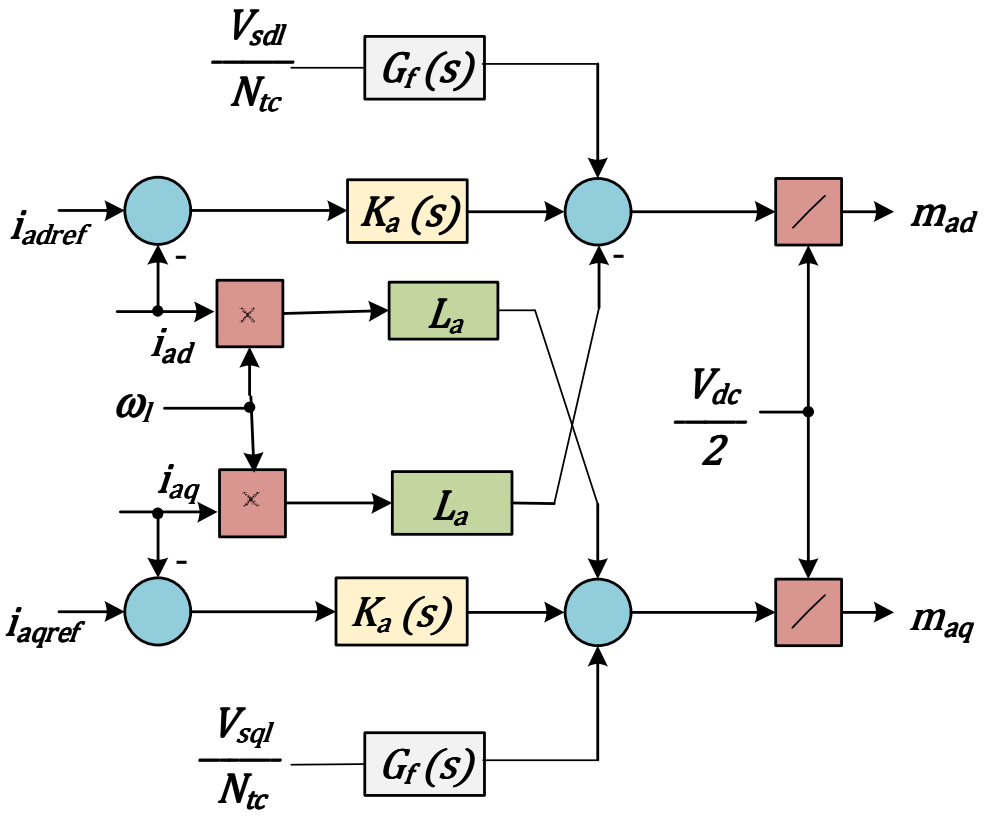

Figure 2.6: Schematic diagram of current control loop for grid side VSC System

Figure 2.7 (a) shows the schematic diagram of DC-bus voltage controller with feed-forward scheme. This figure shows that the effect of P_r on V_{dc} can be ignored by using a feedforward term, which measures P_r through filter K_{pr}. Transfer function of K_{pr} is given in the Appendix A.

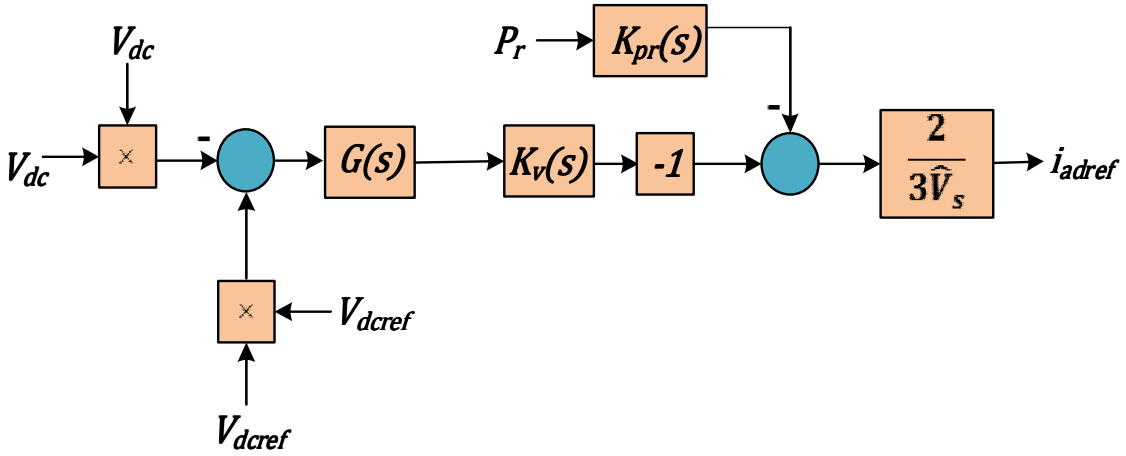

(a)

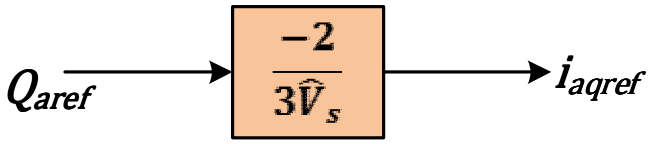

(b)

Figure 2.7: (a) Schematic diagram of dc voltage controller with feed-forward scheme (b) Reference signal generator

Figure 2.7 (b) shows schematically a reference signal generator, by which i_{aqref} can be controlled through reactive power Q_{aref}.

2.1.5 Distribution Network

The distribution network of Figure 2.1 is described by the set of space phasor equations as:

$$\vec{V_g} = L_g \frac{d\vec{i_g}}{dt} + R_g \vec{i_g} + N_{tg} \vec{V} \tag{2.21}$$

$$C_f \frac{d\vec{V}}{dt} = N_{tg} \vec{i_g} - \vec{i}_{link} \tag{2.22}$$

$$C_{link} \frac{d\vec{V_s}}{dt} = \vec{i}_{link} - \vec{i_s} - \vec{i_m} \tag{2.23}$$

$$L_{link} \frac{d\vec{i}_{link}}{dt} = \vec{V} - \vec{V_s} \tag{2.24}$$

It is assumed here that the grid voltage V_g is a balanced three phase voltage. These space phasor equations are then converted in the dq frame as represented below:

$$V_{gd} = L_g \frac{di_{gd}}{dt} + R_g i_{gd} + N_{tg} V_d - \omega L_g i_{gq} \tag{2.25}$$

$$V_{gq} = L_g \frac{di_{gq}}{dt} + R_g i_{gq} + N_{tg} V_q + \omega L_g i_{gd} \tag{2.26}$$

$$C_f \frac{dV_d}{dt} = N_{tg} i_{gd} - i_{linkd} + \omega C_f V_q \tag{2.27}$$

$$C_f \frac{dV_q}{dt} = N_{tg} i_{gq} - i_{linkq} - \omega C_f V_d \tag{2.28}$$

$$C_{link} \frac{dV_{sd}}{dt} = i_{linkd} - i_{sd} - i_{md} + \omega C_{link} V_q \tag{2.29}$$

$$C_{link} \frac{dV_{sq}}{dt} = i_{linkq} - i_{sq} - i_{mq} - \omega C_{link} V_d \tag{2.30}$$

$$L_{link} \frac{di_{linkd}}{dt} = V_d - V_{sd} + \omega L_{link} i_{linkq} \tag{2.31}$$

$$L_{link}\frac{di_{linkq}}{dt} = V_q - V_{sq} - \omega L_{link} i_{linkd} \quad (2.32)$$

The mathematical model of the distribution network is presented in the dq-frame. This model is a set of non-linear equations, expressed from equations (2.25) to (2.32).

2.2 Grid-Connected Two Identical DFIG-based Wind Power Systems

Figure 2.8 illustrates a schematic diagram of grid-connected two DFIG-based wind power systems representing a small wind farm. Wind turbine 1 and wind turbine 2 as denoted in Figure 2.8 are identical, and all the system parameters, including the control system blocks, are also the same as was used in Figure 2.1. The two DFIG-based wind turbines are connected in parallel with each other and with the grid through the PCC. The non-linear mathematical equations remain the same for wind turbine 1, wind turbine 2 and the distribution network as developed in the previous section for the system based on Figure 2.1.

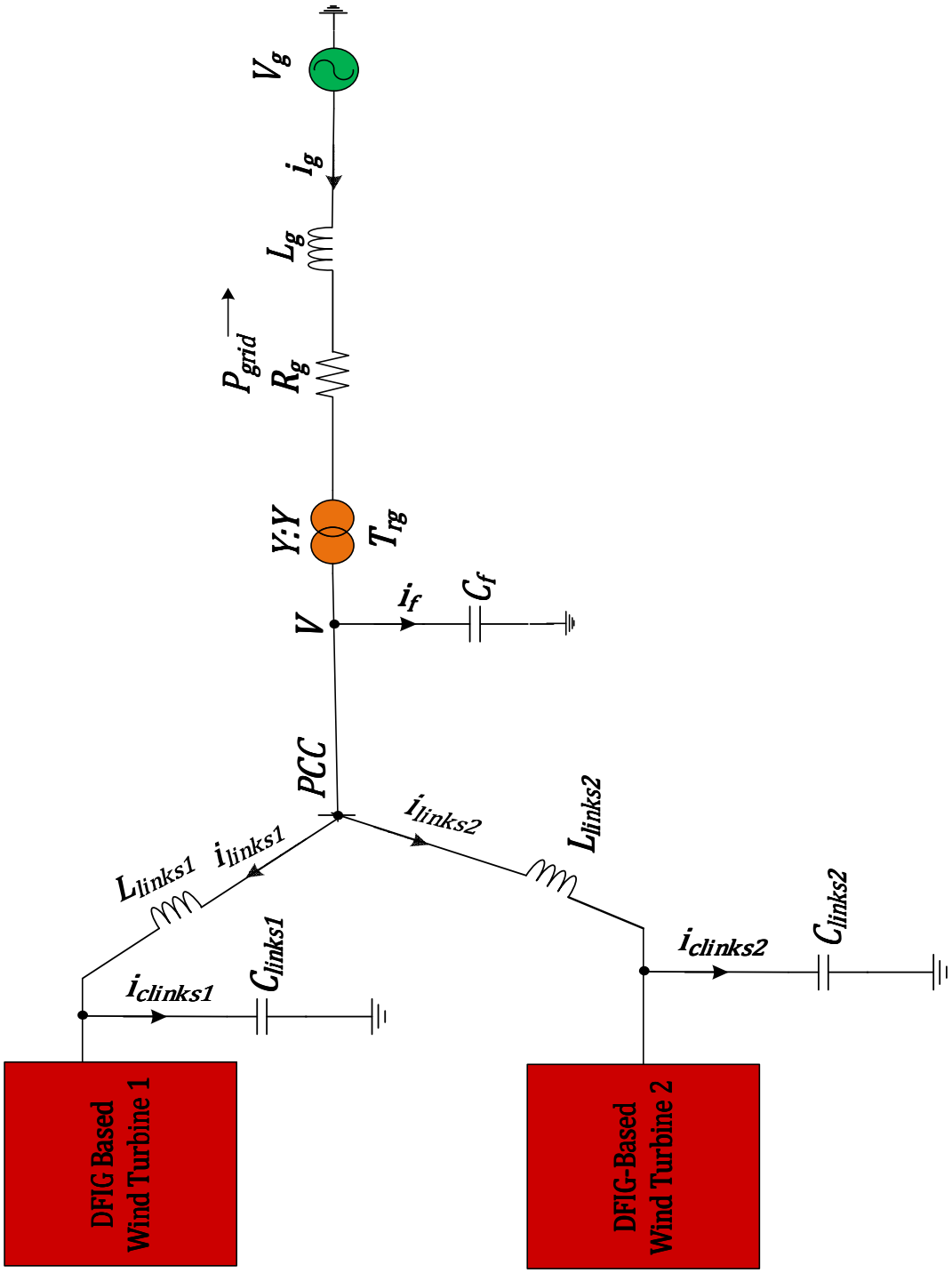

Figure 2.8: Schematic diagram of grid-connected two DFIG-based wind power systems.

2.3 Model Linearization

Both the DFIG-based wind power systems in Figure 2.1 and 2.8 are described by the non-linear set of equations (mathematical models). Although accurate, these models provide little insight into the stability of the system and its robustness. These equations are suitable for large signal analysis and simulation studies. Additionally, from these non-linear equations it is not easily understood how each mode is influenced by the systems and network parameters. Thus, to assist the analysis, the equations are linearized for a system's steady state operating point. Some terms, like system state, state matrix, state vector, etc., play an important role in establishing linearized models and also in studying the stability analysis of the systems.

The mathematically developed models in previous sections are presented in the following general form, as 1st order non-linear differential equations:

$$\dot{X} = f(X, U, t) \tag{2.33}$$

where

$$X = \begin{bmatrix} x_1 \\ x_2 \\ . \\ . \\ x_n \end{bmatrix}; \qquad U = \begin{bmatrix} u_1 \\ u_2 \\ . \\ . \\ u_r \end{bmatrix}; \qquad f = \begin{bmatrix} f_1 \\ f_2 \\ . \\ . \\ f_n \end{bmatrix}; \qquad \dot{X} = \begin{bmatrix} \dot{x_1} \\ \dot{x_2} \\ . \\ . \\ \dot{x_n} \end{bmatrix}$$

where X is the state vector, U is the input vector, $\dot{X}$ is the derivative of the state vector, t is the time, $x_1, x_2, \ldots, x_n$ are the state variables with n number of states or state variables of the system, $u_1, u_2, \ldots, u_n$ are the inputs with r number of input variables, and f is the vector of non-linear differential equation [26]. $\dot{x_1}, \dot{x_2}, \ldots, \dot{x_n}$ are the derivative of state

variables with respect to time. For autonomous systems, time, t, should be ignored in equation (2.33), as the derivatives of the state variables are not explicit functions of time [26].

$$y = g(X, U) \tag{2.34}$$

$$y = \begin{bmatrix} y_1 \\ y_2 \\ \cdot \\ \cdot \\ y_m \end{bmatrix}; \quad \text{and} \quad g = \begin{bmatrix} g_1 \\ g_2 \\ \cdot \\ \cdot \\ g_m \end{bmatrix};$$

where y is the output vector ; g is the vector of non-linear differential equation; y_1, y_2 are the output variables with m number of outputs [26].

For the system of Figure 2.1, the states of overall systems are

$$X = [X_s^T \;\; X_c^T \;\; X_{pll}^T \;\; X_g^T]^T, \tag{2.35}$$

where X_s is the state vector of a DFIG-based wind turbine; X_c is the controller's state vector, X_{pll} is the state vector of PLL, and X_g is the state vector generated due to the transmission line. All the state variables of equation (2.35) are expanded as:

$$X_s = [\lambda \;\; \alpha \;\; V_{sd} \; V_{sq} \; V_{dc} \; \omega_r \; \beta_l \; i_{rd} \; i_{rq} \; i_{ad} \, i_{aq} \, i_{linkd} \; i_{linkq} \,]^T \tag{2.36}$$

$$X_c = [x_{ird} \;\; x_{irq} \;\; x_{iad} \;\; x_{iaq} \, x_{v1} \;\; x_{v2} \;\; x_{pr} \;\; x_{fd} \;\; x_{fq}]^T \tag{2.37}$$

$$X_{pll} = [h_1 \;\; h_2 \;\; h_3 \;\; h_4 \;\; h_5]^T \tag{2.38}$$

$$X_g = [\, i_{gd} \;\; i_{gq} \;\; V_d \;\; V_q]^T \tag{2.39}$$

where

$$\alpha = \omega_0 t - \rho_s$$

$$\beta_l = \omega_0 t - \theta_l$$

x_{ird} , and x_{irq} are generated due to controller $K_r(s)$, used in Figure 2.4.

x_{iad} , x_{iaq}, and x_{fd}, x_{fq} are created due to compensators $K_a(s)$, and $G_f(s)$, respectively, in Figure 2.6.

x_{v1} , x_{v2} , and x_{pr} are generated due to controllers $G(s)$, $K_v(s)$ and $K_{pr}(s)$, respectively, in Figure 2.7(a).

X_{pll} is generated due to one 5th order compensator used in the PLL block, $H_s(s)$ in Figure 2.5.

The input vector U for the system of Figure 2.1 is given by:

$$U = [U_s^T \quad U_g^T]^T \tag{2.40}$$

where U_s and U_g are expanded as

$$U_s = [P_{tur}\ i_{rdref}\ V_{linkref}\ Q_{aref}]^T \tag{2.41}$$

$$U_g = [\hat{V}_g]^T \tag{2.42}$$

U_s is the input vector applied to the DFIG-based wind turbine, where P_{tur} is the turbine power; and $U_g$is the input vector generated due to grid voltage V_g, where $\hat{V}_g$ is the peak value of the grid line to neutral voltage. For the mathematical model developed for Figure 2.1, 31 state equations are generated.

Figure 2.8 has two identical DFIG-based wind turbines, so for this case, X_s, X_c, X_{pll}, and U_s are generated twice. A few states generated due to the distribution network from the model based in Figure 2.1 remain common for the overall system in Figure 2.8. Thus, as a result, 58 state equations are mathematically created. A liniearization method

considering initial state vector, X_0, and initial input vector $U_{0,}$ around the state vector, X, and input vector, U, are needed to linearize the non-linear differential equations in (2.33) and (2.34). 1st order differential equation of X_0 is expressed as:

$$\dot{X}_0 = f(X_0\, U_0) = 0 \tag{2.43}$$

The final linearized differential equations mathematically modeled from the developed non-linear models are then written as:

$$\Delta\dot{X} = A\Delta X + B\Delta U \tag{2.44}$$

$$\Delta y = C\Delta X + D\Delta U \tag{2.45}$$

In equations (2.44) and (2.45), ΔX is the state vector with dimension n; A is the system state matrix with size $n \times n$; ΔU is the input vector with dimension r; B is the system input matrix with size $n \times r$; Δy is the output vector with dimension m; C is the output matrix with size $m \times n$, and D is the feedforward matrix with size $m \times r$.

where

$$A = \begin{bmatrix} \frac{\partial f_1}{\partial x_1} \cdots \cdots \frac{\partial f_1}{\partial x_n} \\ \cdots \cdots \cdots \\ \frac{\partial f_n}{\partial x_1} \cdots \cdots \frac{\partial f_n}{\partial x_n} \end{bmatrix}; \qquad B = \begin{bmatrix} \frac{\partial f_1}{\partial u_1} \cdots \cdots \frac{\partial f_1}{\partial u_r} \\ \cdots \cdots \cdots \\ \frac{\partial f_n}{\partial u_1} \cdots \cdots \frac{\partial f_n}{\partial u_r} \end{bmatrix} \tag{2.46}$$

$$C = \begin{bmatrix} \frac{\partial g_1}{\partial x_1} \cdots \cdots \frac{\partial g_1}{\partial x_n} \\ \cdots \cdots \cdots \\ \frac{\partial g_m}{\partial x_1} \cdots \cdots \frac{\partial g_m}{\partial x_n} \end{bmatrix}; \qquad D = \begin{bmatrix} \frac{\partial g_1}{\partial u_1} \cdots \cdots \frac{\partial g_1}{\partial u_r} \\ \cdots \cdots \cdots \\ \frac{\partial g_m}{\partial u_1} \cdots \cdots \frac{\partial g_m}{\partial u_r} \end{bmatrix}$$

n number of eigenvalues are generated from state matrix A, as the size of the matrix is $n \times n$. Eigenvalue is denoted as λ_i, where i varies from 1 to n [26]. State matrix A is also represented as,

$$A = \begin{bmatrix} a_{11} \dots \dots . a_{1n} \\ \dots \dots \dots \cdot \cdot \\ a_{n1} \dots \dots a_{nn} \end{bmatrix}; \quad (2.47)$$

where a_{kj} is the element of A in kth row and jth column.

A detailed linearized mathematical model of the wind farm is expressed in Appendix B, From this section, it is determined that as each eigenvalue corresponds to the each eigenmode of the system, thus total 31 eigenmodes and 58 eigenmodes are generated from linearized mathematical model of systems in Figure 2.1 and Figure 2.8, respectively.

2.4 Summary and Conclusions

This chapter has established a detailed non-linear mathematical model of a DFIG-based single wind turbine system connected to a grid as well as a multi DFIG-based wind turbine system connected to a distribution network in the dq-frame. It has also provided each control system block used for both the systems, and provided a detailed description of each block in the dq-frame. Linearization of mathematical model for both the systems has been performed from the set of developed non-linear equations. These two linearized dynamic models provide an analytical platform for determining the robustness and stability of the two systems. A total of 31 states for grid-connected single wind power system plus 58 state equations for grid-connected two DFIG-based wind power systems have been determined. Additionally, this chapter describes how close observation makes

decoupling of the d-and q-axis current components of rotor side and grid side converters possible with the proper selection of angular speed of dq-frame.

Chapter 3

Model Validation and Simulation Result

In this chapter, simulation studies are carried out on a detailed switched model of a grid-connected DFIG-based single wind turbine, as well as on the switched model of a grid-connected small wind farm. The simulations are conducted in PSCAD/EMTDC environment and performed to ensure the algebraic accuracy of the linearized models of Chapter 2. The linearized models are simulated in the MATLAB/SIMULINK software environment, and their responses are compared with those obtained from the switched models of the PSCAD/EMTDC environment. Hence, the switched models are considered in this thesis as the equivalents of experimental set-ups. Since the linearized models approximate the small-signal behaviors of their corresponding non-linear switched counterparts, the levels of test disturbances have been kept to about or less than 10% of their corresponding nominal values. Two different case studies are conducted on each switched model and their corresponding linearized model at a 13.5 m/s wind speed. In case study 1, a 10% step change of grid signal at t=5.0 s is imposed. In case study 2, a step change in dc link voltage of VSCs is applied from 1200V to 1350V at t=5.0 s.

3.1 Case Study 1

In this case study, 10% step change in grid voltage is imposed at 13.5m/s wind speed and 1 μH linking inductances to the models of both the systems developed in the PSCAD/EMTDC and MATLAB/SIMULINK environment for validation. The results, achieved from linear and non-linear models are then compared. The simulation results for case study 1 are presented from Figure 3.1 to Figure 3.8. Figure 3.1 presents simulation results of rotor speed ω_r, ω_{rs1}, and ω_{rs2} of each turbine. Figure 3.2 describes dc link voltages V_{dc}, V_{dcs1},V_{dcs2} of ac-dc-ac back to back VSCs of both the systems. Figure 3.3 and Figure 3.4 presents simulation results of stator fluxes λ, $\lambda_{s1}, \lambda_{s2}$ and electrical torques T_e, T_{es1}, T_{es2}, respectively, of each of the turbines. Figure 3.5 and Figure 3.6 compares the simulation results of active power components of rotor side (P_r, P_{rs1}, P_{rs2}) and grid side converters (P_a, P_{as1}, P_{as2}) , respectively. Figure 3.7 and Figure 3.8 present simulation results of reactive power components of rotor side (Q_r, Q_{rs1},Q_{rs2}) and grid side converters (Q_a, Q_{as1},Q_{as2}), respectively.

In these figures, left columns represent the simulation results, achieved from linearized models whereas right columns represents the simulation results of non-linear models. It is noticed that the graphs of linearized models closely agree with the results from PSCAD/EMTDC environment [27].

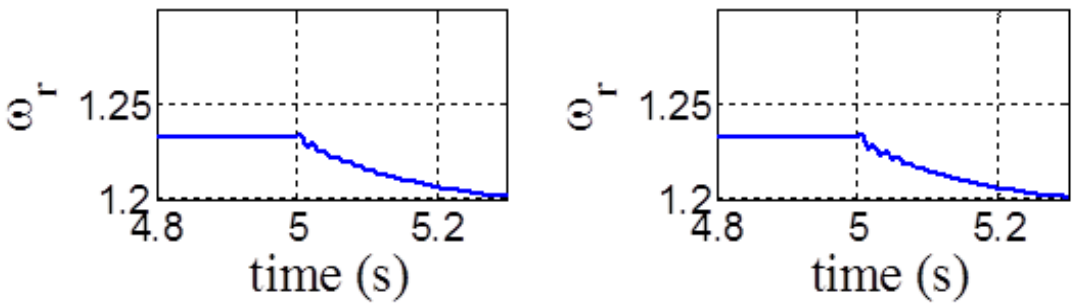

(a)

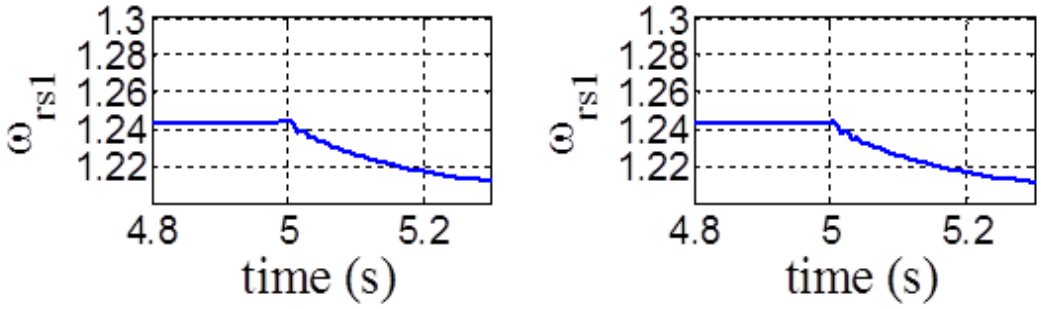

(b)

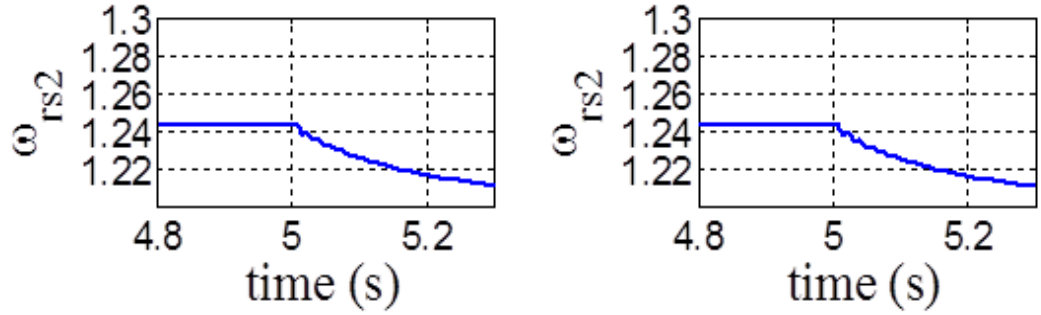

(c)

Figure 3.1: Responses of rotor speed of wind turbines (a) Response of wind turbine of Figure 2.1 (b) Response of Wind Turbine 1 of Figure 2.8 (c) Response of Wind Turbine 2 of Figure 2.8

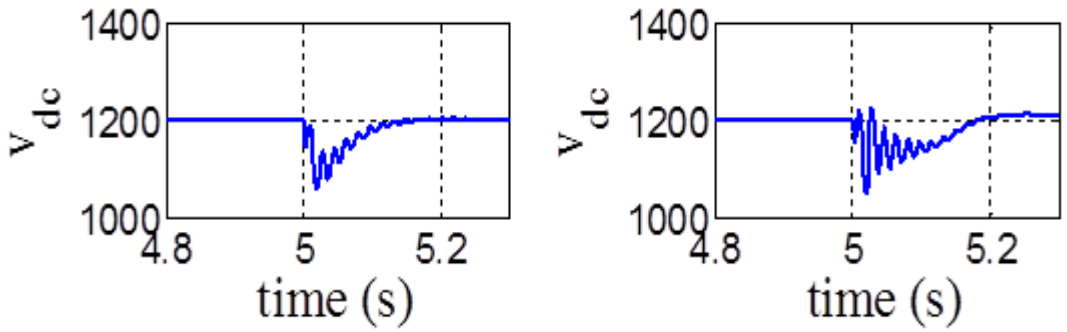

(a)

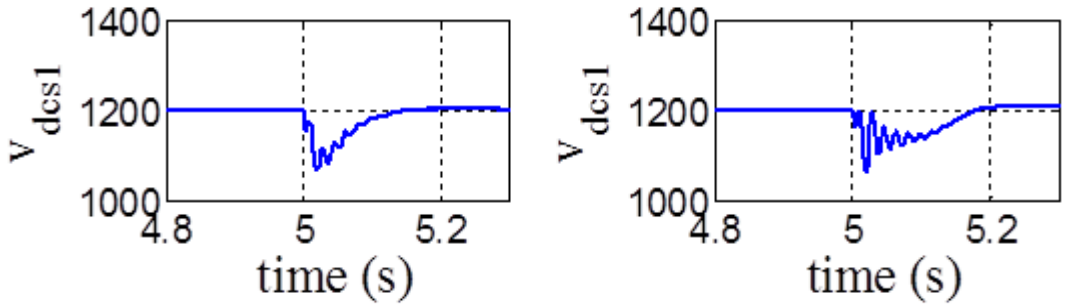

(b)

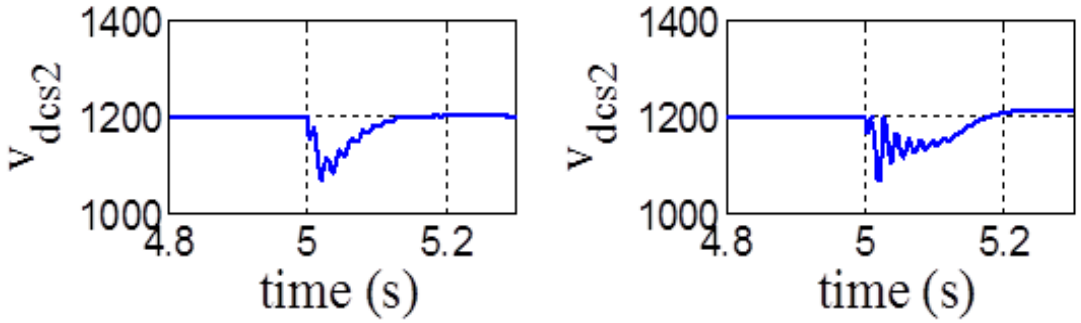

(c)

Figure 3.2: Responses of dc link voltages of ac-dc-ac back to back VSCs (a) Response of Figure 2.1 (b) Response of Wind Turbine 1 of Figure 2.8 (c) Response of Wind Turbine 2 of Figure 2.8

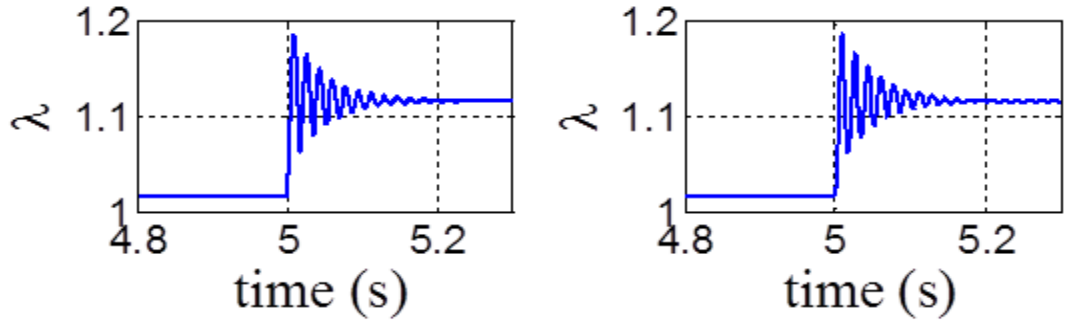

(a)

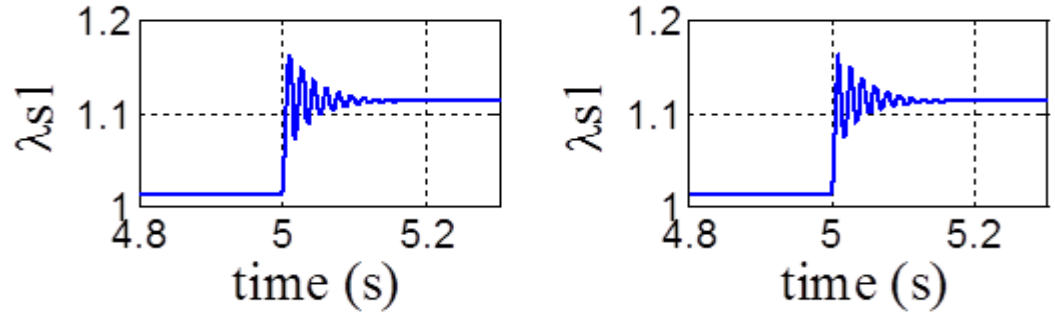

(b)

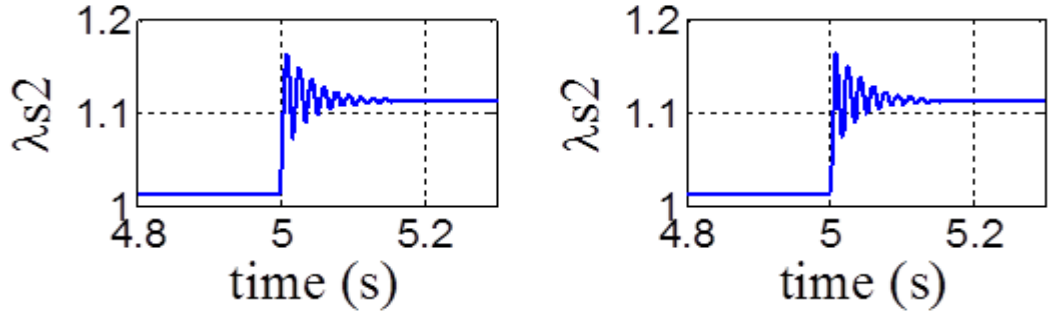

(c)

Figure 3.3: Responses of stator fluxes of wind turbines (a) Response of wind turbine of Figure 2.1 (b) Response of Wind Turbine 1 of Figure 2.8 (c) Response of Wind Turbine 2 of Figure 2.8

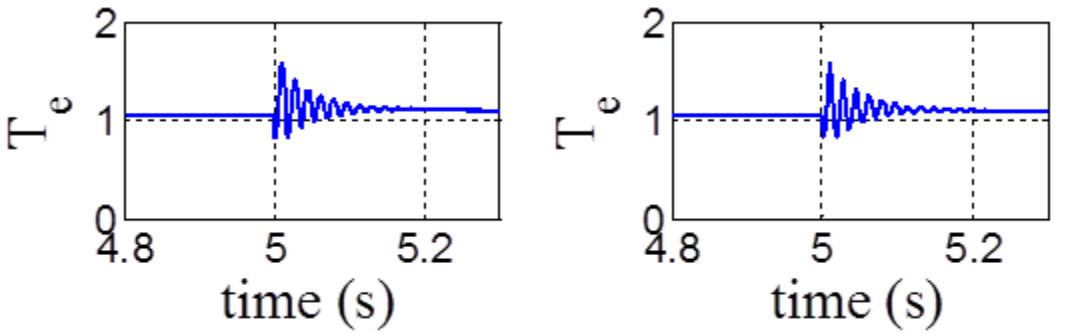

(a)

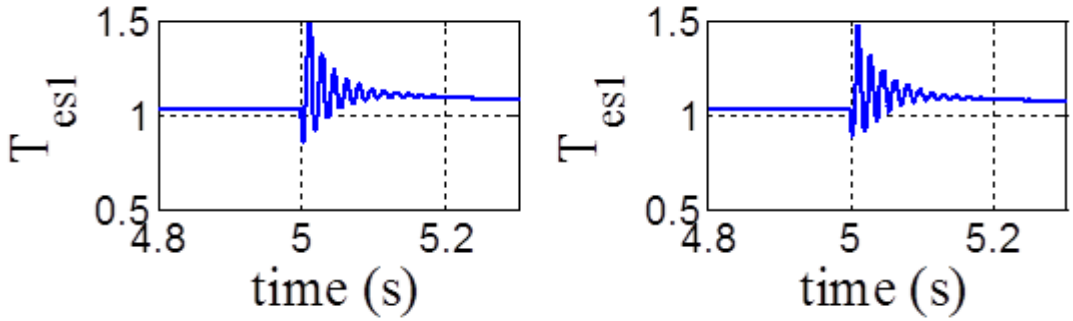

(b)

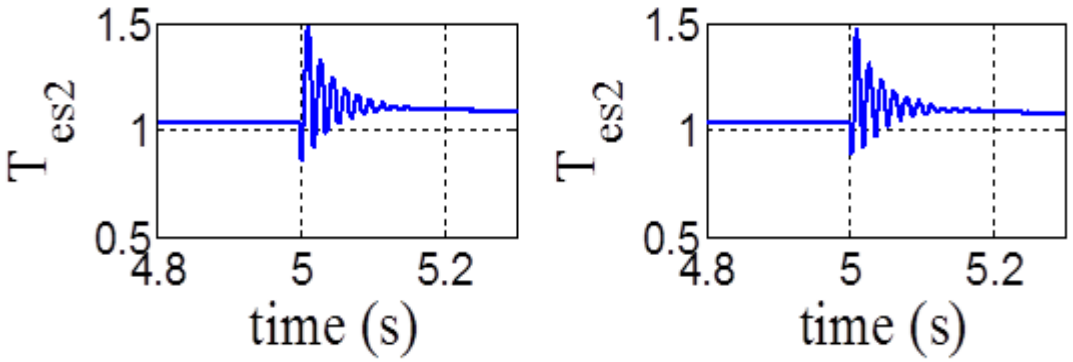

(c)

Figure 3.4: Responses of electrical torques of wind turbines (a) Response of wind turbine of Figure 2.1 (b) Response of Wind Turbine 1 of Figure 2.8 (c) Response of Wind Turbine 2 of Figure 2.8

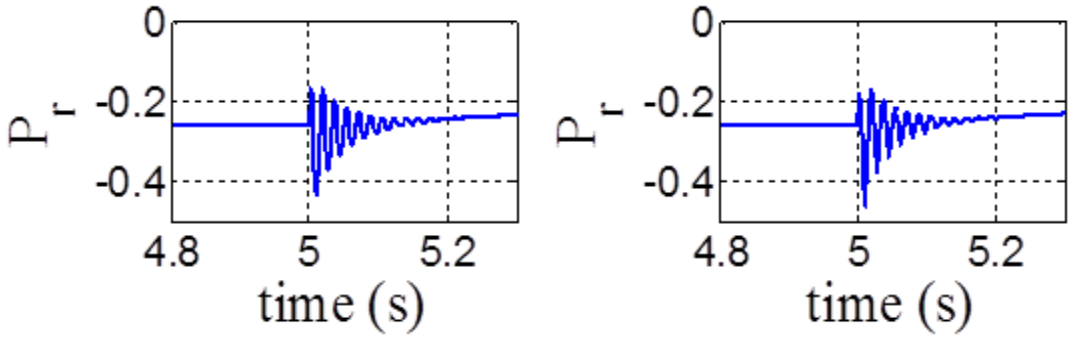

(a)

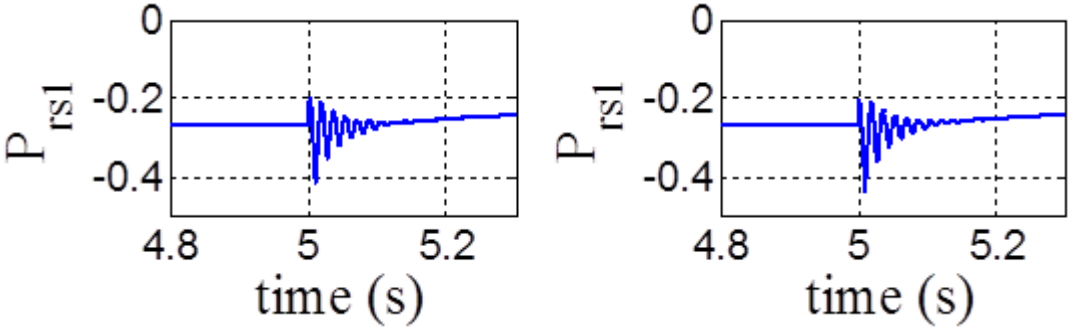

(b)

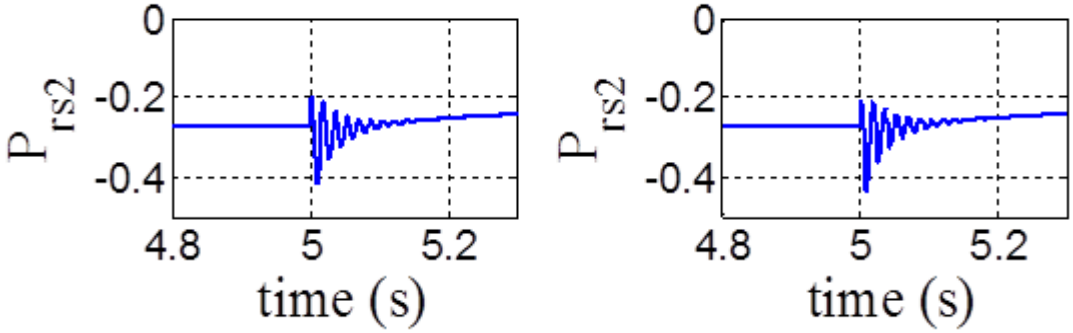

(c)

Figure 3.5: Responses of active power of rotor side converters (a) Response of Figure 2.1 (b) Response of Wind Turbine 1 of Figure 2.8 (c) Response of Wind Turbine 2 of Figure 2.8

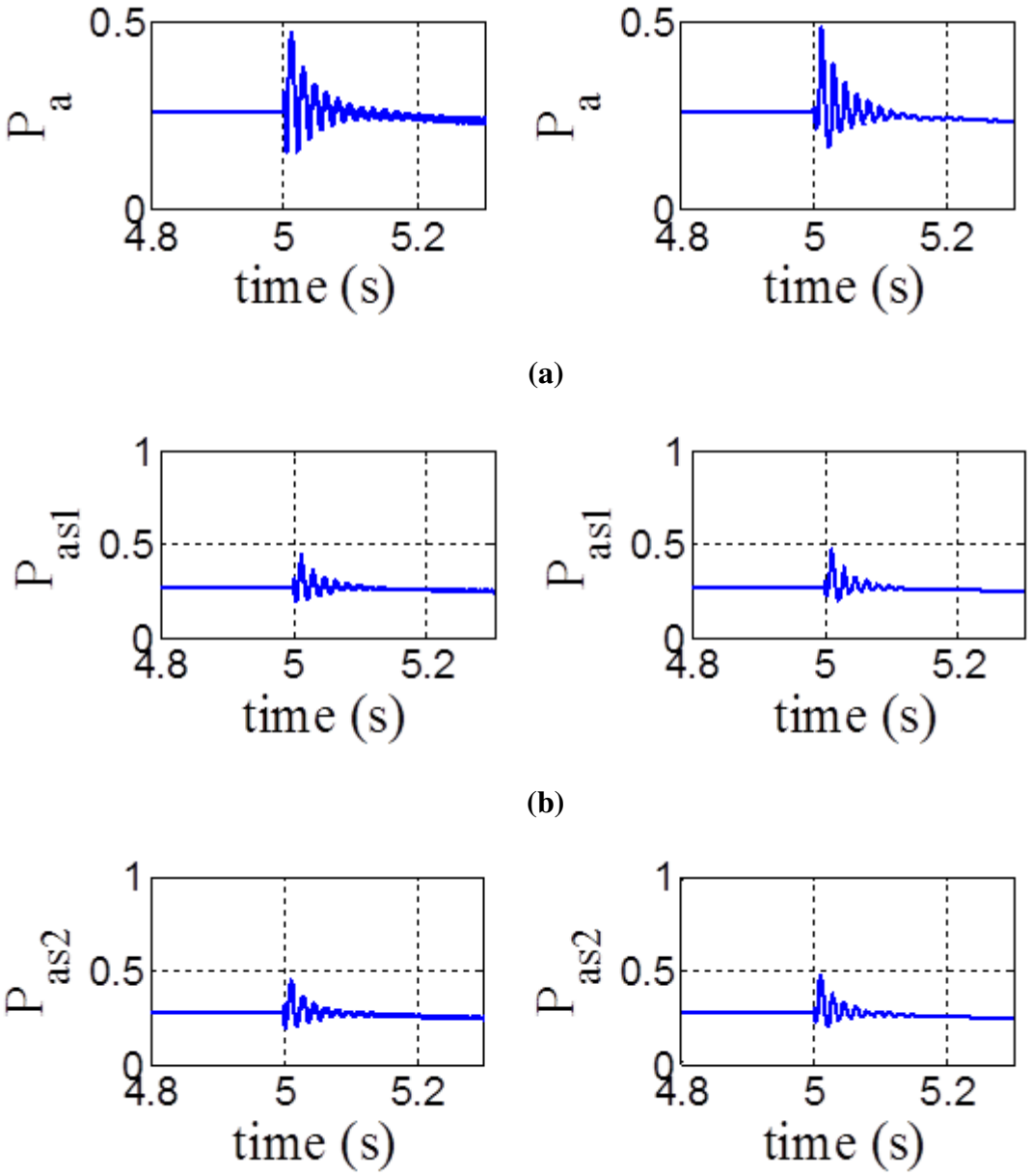

Figure 3.6: Responses of active power of grid side converters (a) Response of Figure 2.1 (b) Response of Wind Turbine 1 of Figure 2.8 (c) Response of Wind Turbine 2 of Figure 2.8

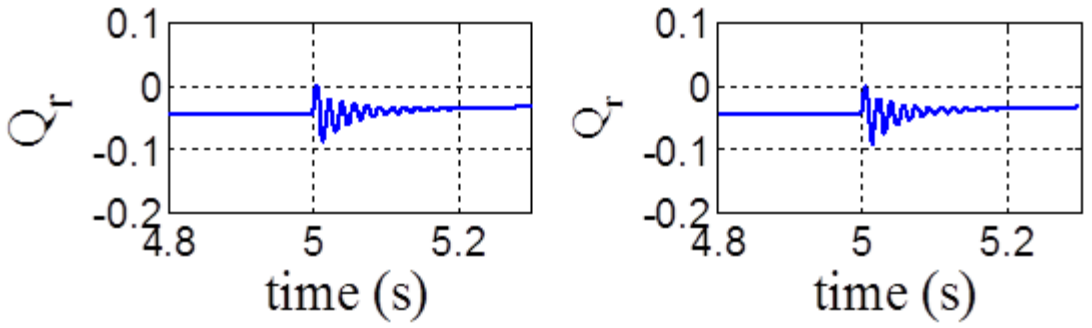

(a)

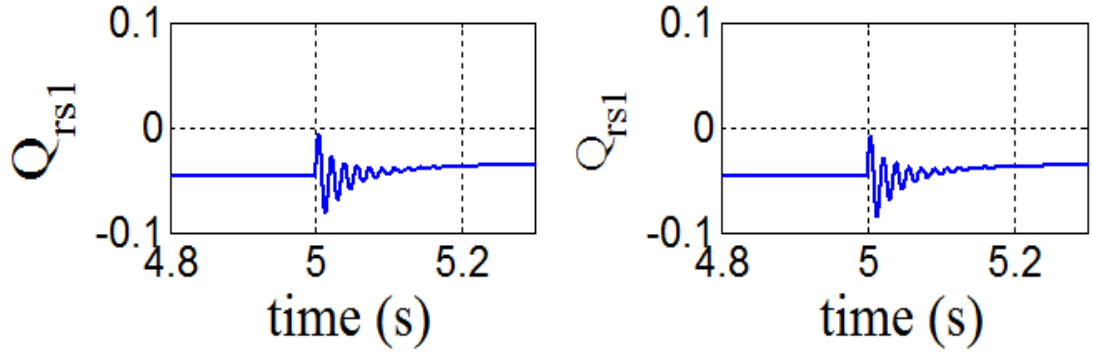

(b)

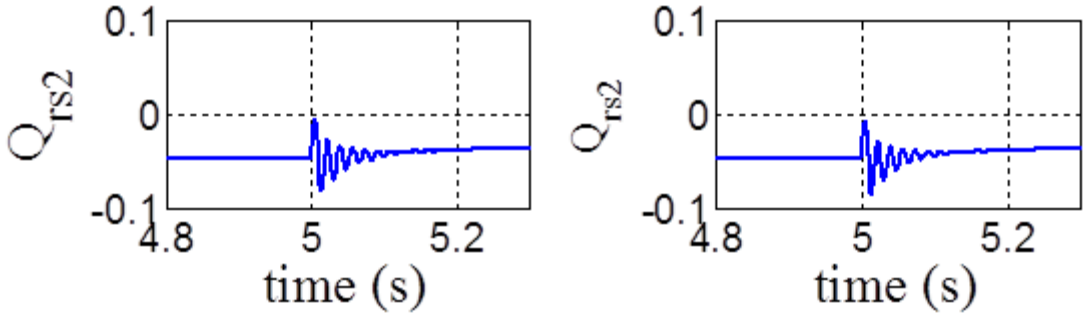

(c)

Figure 3.7: Responses of reactive power of rotor side converters (a) Response of Figure 2.1 (b) Response of Wind Turbine 1 of Figure 2.8 (c) Response of Wind Turbine 2 of Figure 2.8

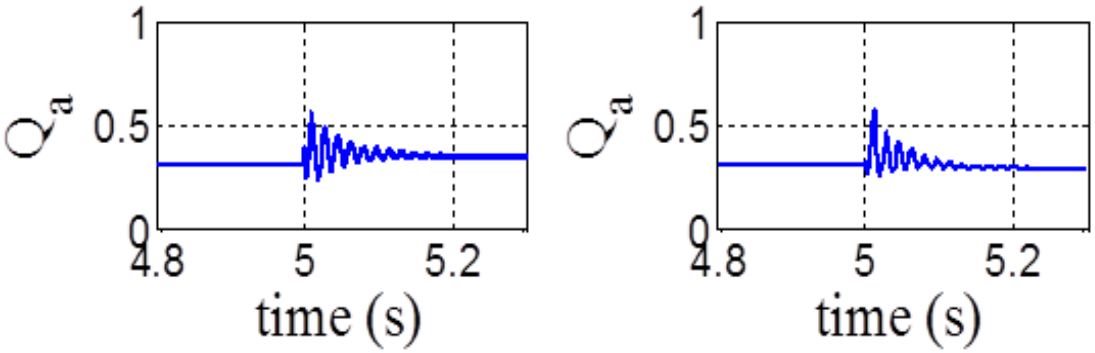

(a)

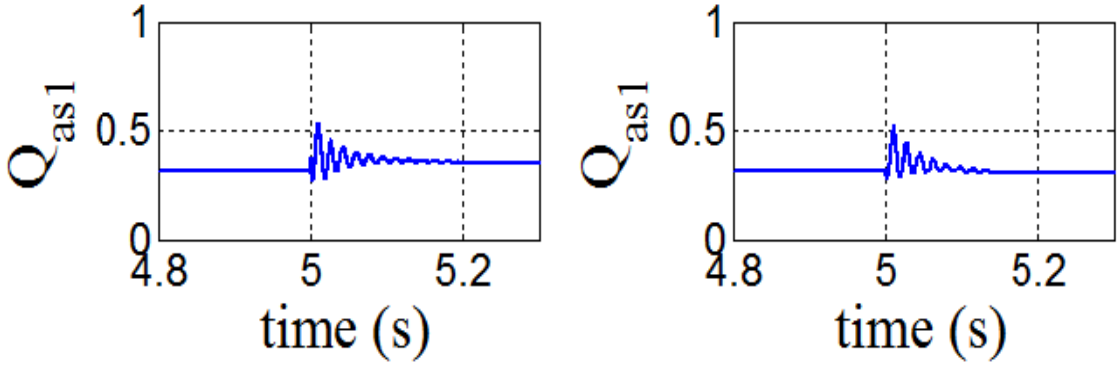

(b)

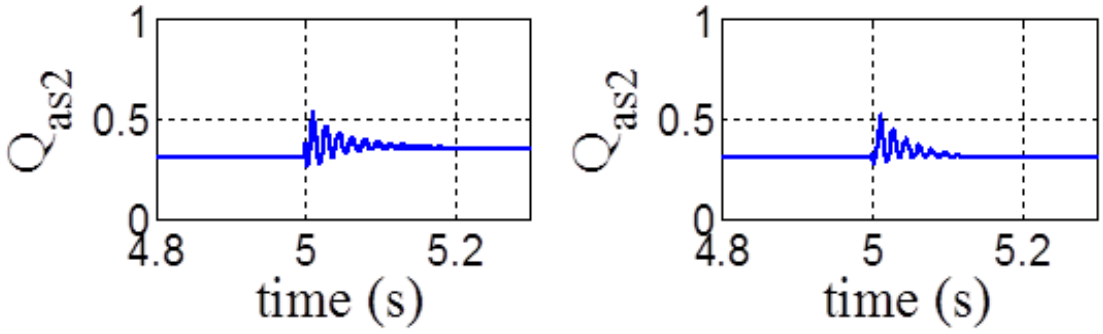

(c)

Figure 3.8: Responses of reactive power of grid side converters (a) Response of Figure 2.1 (b) Response of Wind Turbine 1 of Figure 2.8 (c) Response of Wind Turbine 2 of Figure 2.8

3.2 Case Study 2

At t=5.0 s., step change from 1200 V to 1350V is imposed on the reference signal of the DC-link voltage of the back-to-back converters at 13.5 m/s wind speed and 1 μH linking inductances to the models of both the systems developed in the PSCAD/EMTDC and MATLAB/SIMULINK environment for validation. The results, achieved from linear and non-linear models are then compared. The simulation results for case study 02 are presented from Figure 3.9 to Figure 3.16. Figure 3.9 presents results of rotor speed ω_r, ω_{rs1}, and ω_{rs2} of each turbine. Figure 3.10 describes dc link voltages V_{dc}, V_{dcs1},V_{dcs2} of ac-dc-ac back to back VSCs of both the systems. Figure 3.11 and Figure 3.12 presents simulation results of stator fluxes λ, $\lambda_{s1}, \lambda_{s2}$ and electrical torques T_e, T_{es1}, T_{es2}, respectively, of each of the turbines. Figure 3.13 and Figure 3.14 compares the simulation results of active power components of rotor side (P_r, P_{rs1}, P_{rs2}) and grid side converters (P_a, P_{as1}, P_{as2}), respectively. Figure 3.15 and Figure 3.16 present simulation results of reactive power components of rotor side (Q_r, Q_{rs1},Q_{rs2}) and grid side converters (Q_a, Q_{as1},Q_{as2}), respectively.

In these figures, left columns represent the simulation results achieved from linearized models whereas right columns represents the simulation results of non-linear models. It is noticed that the results of linearized models closely agree with the results from non-linear models.

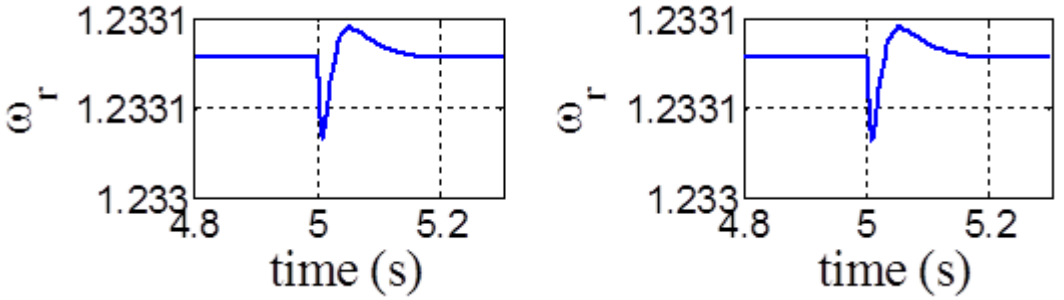

(a)

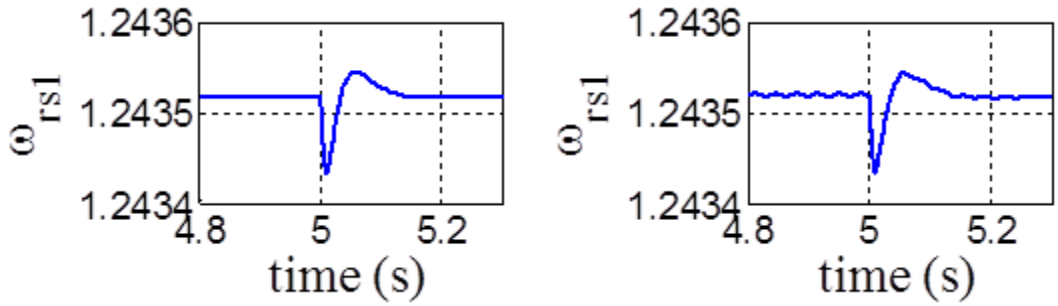

(b)

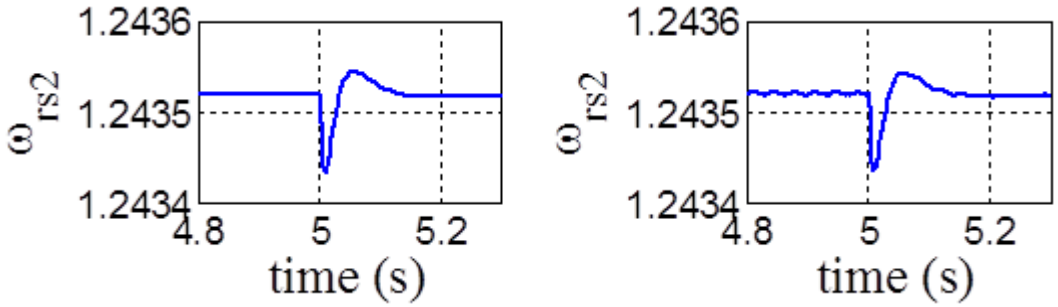

(c)

Figure 3.9: Responses of rotor speed of wind turbines (a) Response of wind turbine of Figure 2.1 (b) Response of Wind Turbine 1 of Figure 2.8 (c) Response of Wind Turbine 2 of Figure 2.8

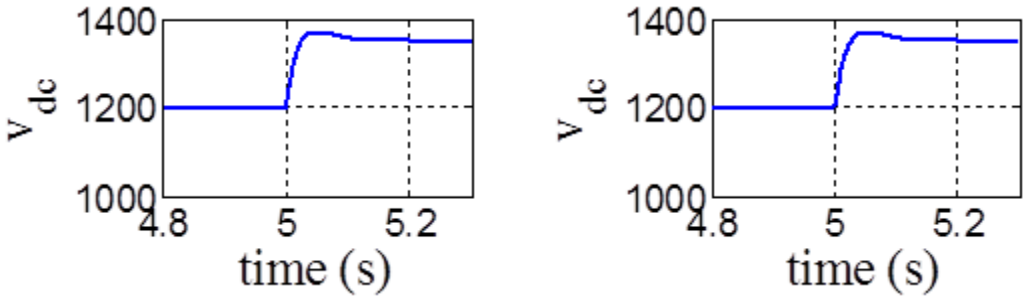

(a)

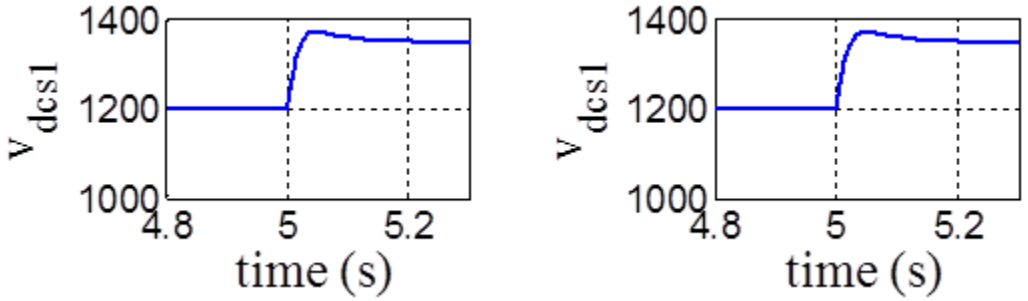

(b)

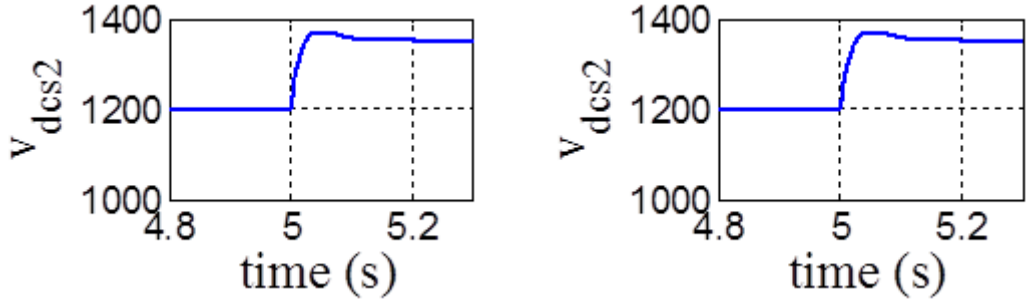

(c)

Figure 3.10: Responses of dc link voltages of ac-dc-ac back to back VSCs (a) Response of Figure 2.1 (b) Response of Wind Turbine 1 of Figure 2.8 (c) Response of Wind Turbine 2 of Figure 2.8

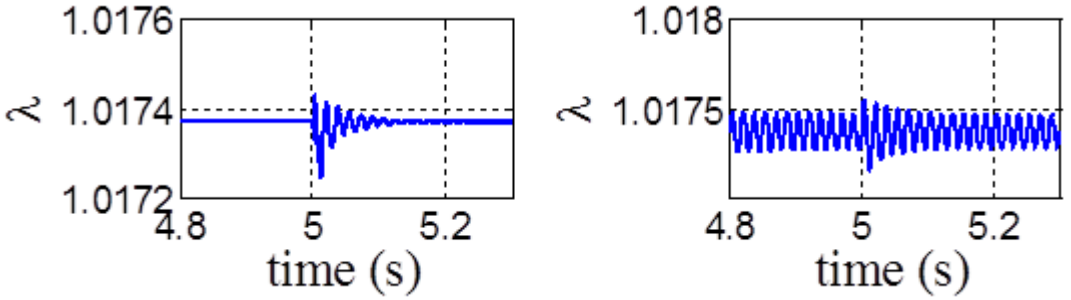

(a)

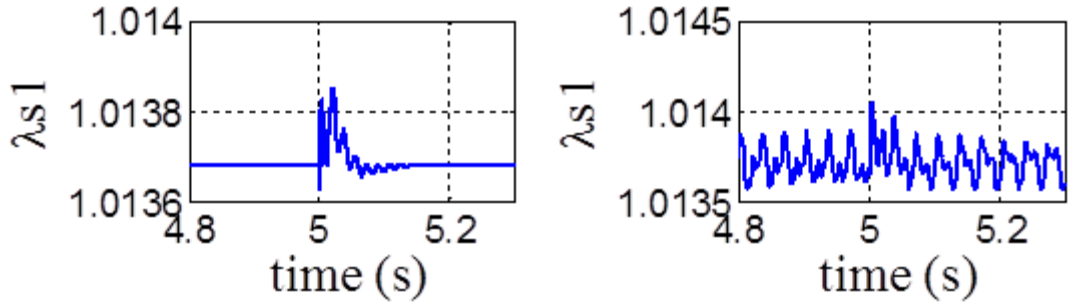

(b)

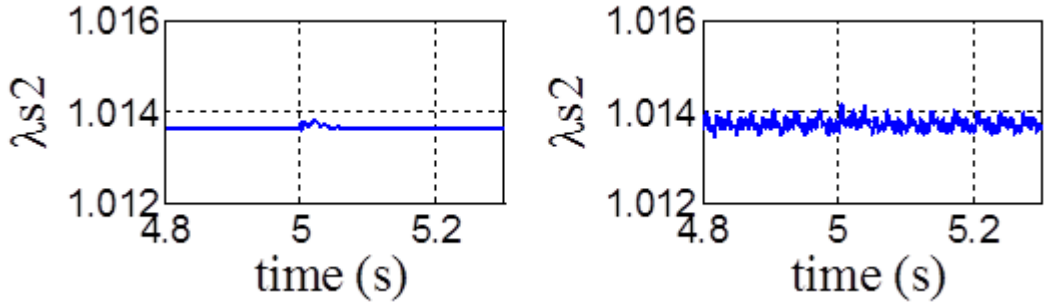

(c)

Figure 3.11: Responses of stator fluxes of wind turbines (a) Response of wind turbine of Figure 2.1 (b) Response of Wind Turbine 1 of Figure 2.8 (c) Response of Wind Turbine 2 of Figure 2.8

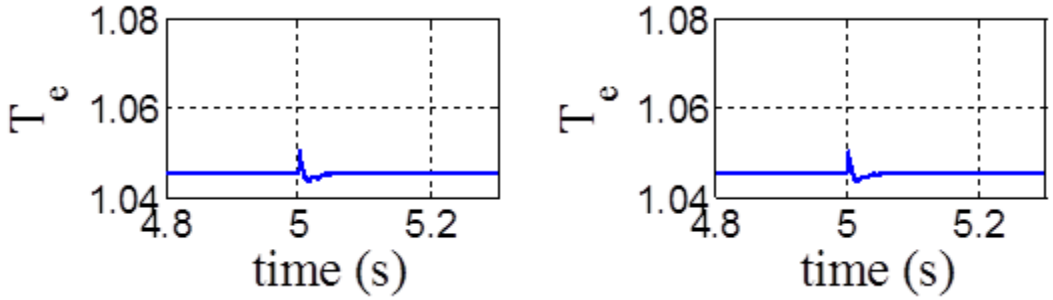

(a)

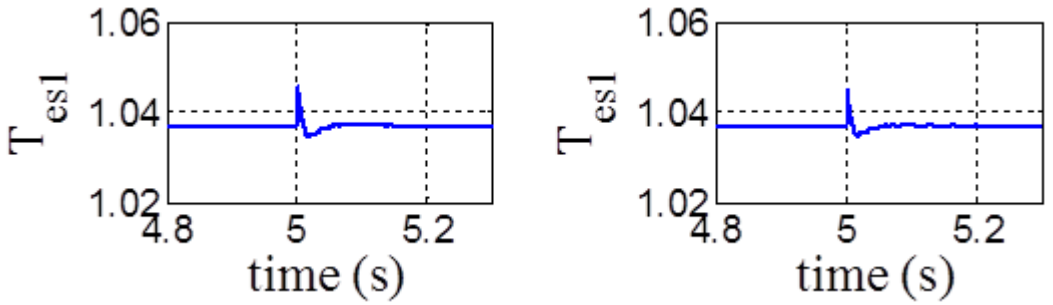

(b)

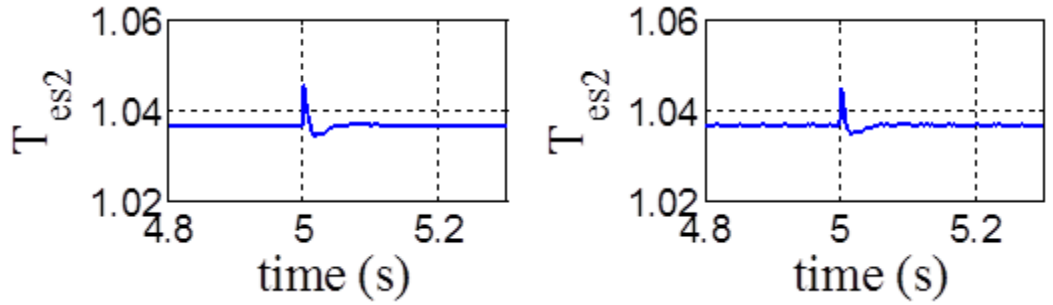

(c)

Figure 3.12: Responses of electrical torques of wind turbines (a) Response of wind turbine of Figure 2.1 (b) Response of Wind Turbine 1 of Figure 2.8 (c) Response of Wind Turbine 2 of Figure 2.8

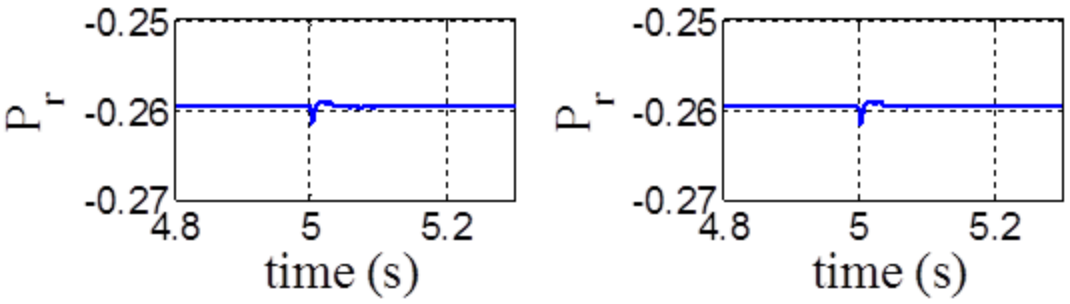

(a)

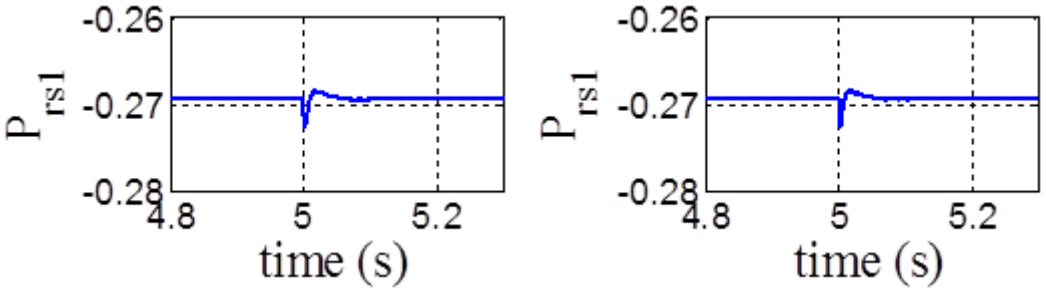

(b)

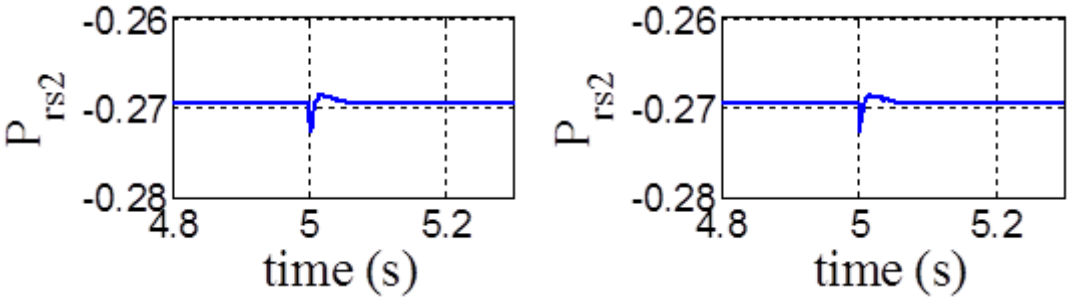

(c)

Figure 3.13: Responses of active power of rotor side converters (a) Response of Figure 2.1 (b) Response of Wind Turbine 1 of Figure 2.8 (c) Response of Wind Turbine 2 of Figure 2.8

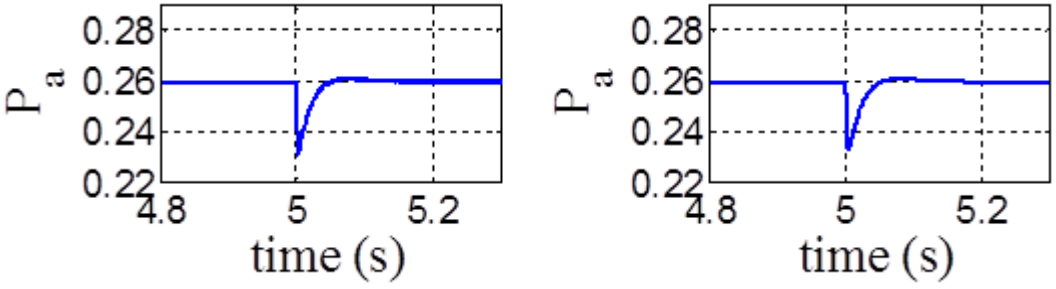

(a)

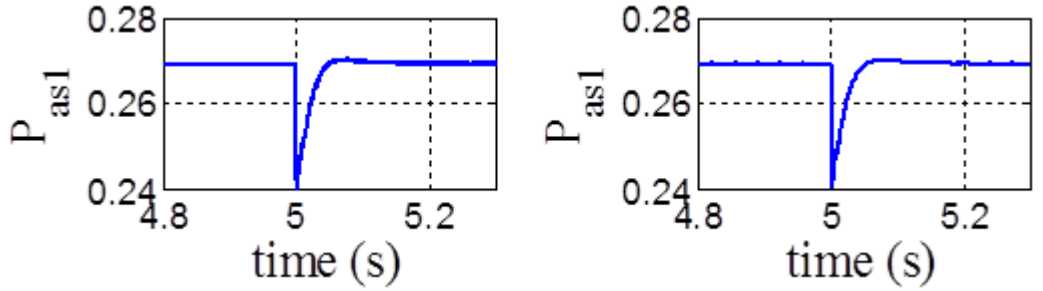

(b)

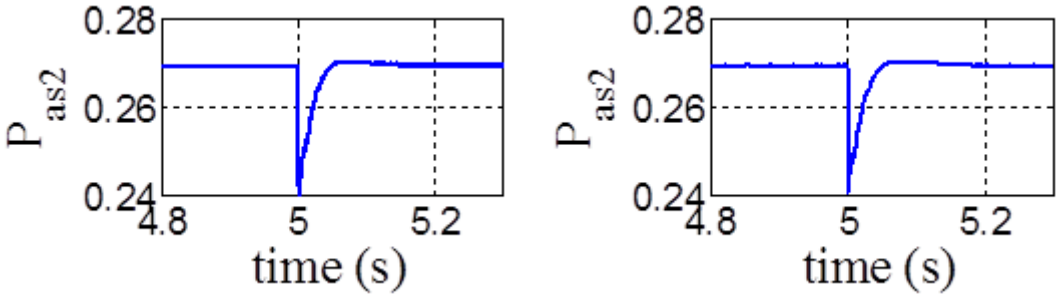

(c)

Figure 3.14: Responses of active power of grid side converters (a) Response of Figure 2.1 (b) Response of Wind Turbine 1 of Figure 2.8 (c) Response of Wind Turbine 2 of Figure 2.8

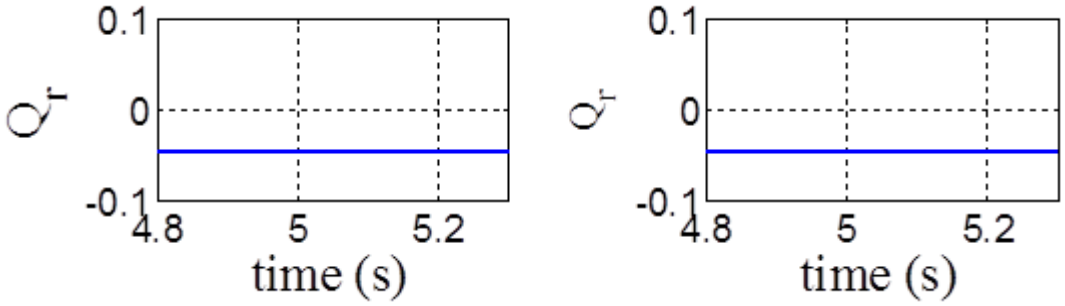

(a)

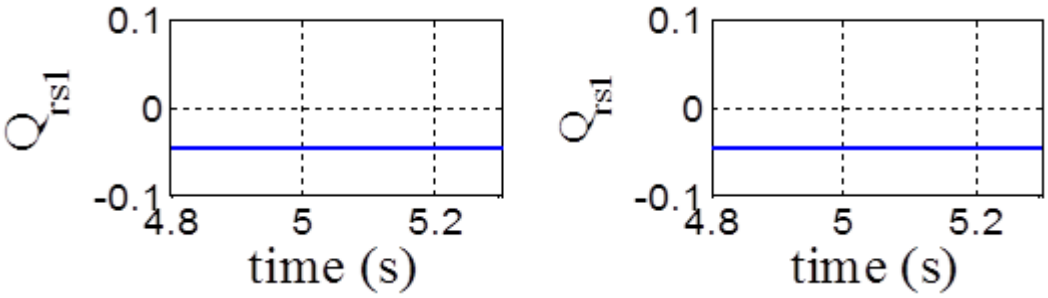

(b)

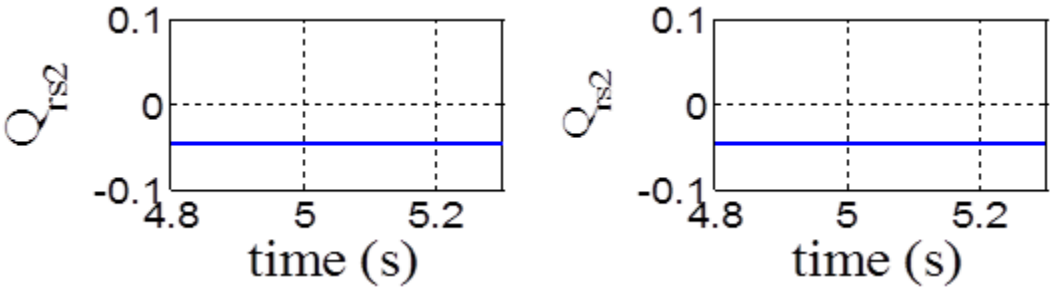

(c)

Figure 3.15: Responses of reactive power of rotor side converters (a) Response of Figure 2.1 (b) Response of Wind Turbine 1 of Figure 2.8 (c) Response of Wind Turbine 2 of Figure 2.8

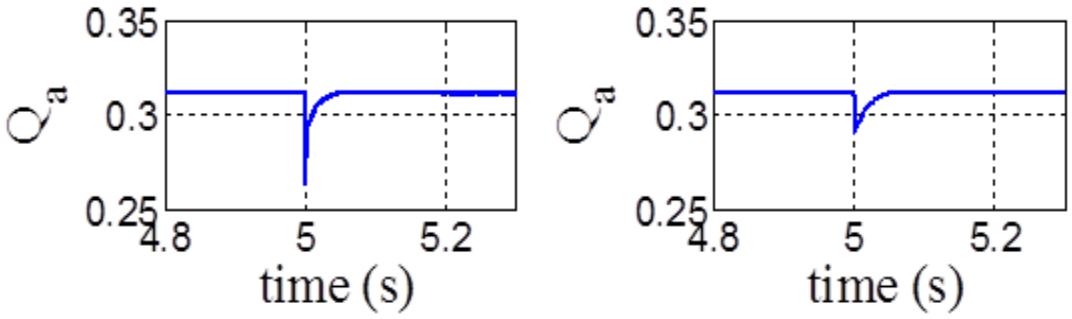

(a)

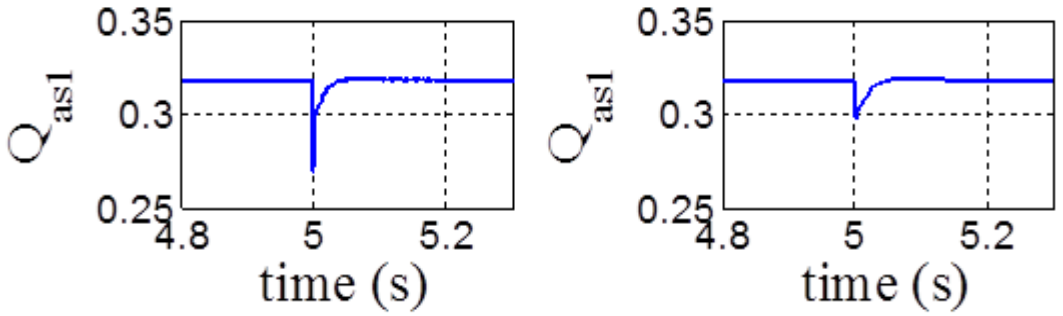

(b)

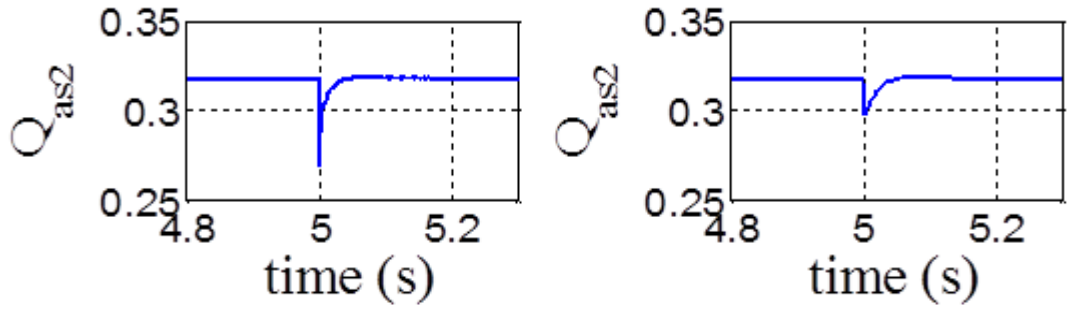

(c)

Figure 3.16: Responses of reactive power of grid side converters (a) Response of Figure 2.1 (b) Response of Wind Turbine 1 of Figure 2.8 (c) Response of Wind Turbine 2 of Figure 2.8

3.3 Summary and Conclusion

The linearized models developed in Chapter 2 have been verified with the simulation results of non-linear systems designed in the PSCAD/EMTDC environment. Model validation was carried out for two different conditions. Firstly, a 10% step change in grid voltage at t=5 s. was applied to both the linear and non-linear systems, and secondly, a step change from 1200V to 1350V of the dc link voltage of VSCs was applied. All the simulation results of both the linear and non-linear models of both the systems were compared and found to be identical.

Chapter 4

Modal Analysis- System Parametric Effects

The modal analysis of the two linearized systems, a single-turbine and a small wind farm both individually connected to a grid, developed in Chapter 2, are performed separately by changing different system parameters and operating conditions of the systems. For better understanding of intrinsic dynamic behavior and enhancement of system stability, this analysis is of utmost importance. Modal analysis also allows in figuring out the change in modal properties that occurs due to the change of system parameters and operating conditions. A brief detail of the terms participation factor, system stability, frequency of oscillations, and damping ratio are presented in this chapter, before modal analysis of the systems is performed. Eigenvalue sensitivity is then determined from the modal analysis by changing the linking inductances and wind speed.

4.1 Brief Description of Stability & Modal Analysis

Stability: The stability of the linearized models of grid-connected single wind power system and the grid-connected small wind farm is achieved by means of eigenvalue analysis.

Participation Factor: Effects of system parameters, on each eigenmode for linearized system, is determined by participation factor analysis. The element p_{ki} is denoted as participation factor and is given by:

$$p_{ki} = \frac{\partial \lambda_i}{\partial a_{kk}} \tag{4.1}$$

$$\text{where } \frac{\partial \lambda_i}{\partial a_{kk}} = \phi_{ki}\psi_{ik} \ , \tag{4.2}$$

where λ_i is the eigenvalue of the linearized system and a_{kk} is the diagonal element of state matrix A [26, 28, 29]; already discussed in Chapter 2. ϕ_{ki} is the k th entry of the right eigenvector ϕ_i of state matrix A; ψ_{ik} is the k th entry of the left eigenvector ψ_i of state matrix A [26,28].

Frequency of Oscillations and Damping Factor: Oscillatory mode of a system occurs for a complex eigenvalue. These eigenvalues always occur in conjugate pairs and is expressed as [26]:

$$\lambda_i = \sigma \pm j\beta \ , \tag{4.3}$$

where σ is the real part of the eigenvalue λ_i and β is the complex part. Frequency of oscillation (f_{osc}) in Hz is then expressed as:

$$f_{osc} = \frac{\beta}{2\pi} \tag{4.4}$$

The damping of the system depends on the real part of the eigenvalue. The damping factor (ζ) is written as:

$$\zeta = \frac{-\sigma}{\sqrt{\sigma^2+\beta^2}} \tag{4.5}$$

The rate of decay of amplitude of system oscillation is determined by ζ.

4.2 Sensitivity Analysis at very low Linking Inductances

In this section, relative participation factor analysis for dominant eigenvalue is studied. The dominant eigenmode are compared on the basis of participation of different states, for, linearized models; grid-connected DFIG-based single wind turbine and grid-connected DFIG-based small wind farm, developed in Chapter 2. Participation of states that are generated due to linking inductances, and wind speed, in eigenmodes are also observed. Then, eigenvalue loci are drawn to compare the intrinsic dynamic behavior of both the linearized systems. The behavior of frequency of oscillation and damping factor of linearized systems are analyzed. All these analysis are performed under low linking inductances.

4.2.1 Participation Factor Analysis

Participation factor, p_{ki}, analysis is carried out for both the linearized systems, developed in Chapter 2. However, the relative participation, $|p_{ki}|$, of a state variable in an eigenmode for both the systems is of prime interest, therefore, $|p_{ki}|$ is determined and presented in Table 4.1, Table 4.2 and Table 4.3. Additionally, relative participation factors which are less than 0.01 are considered zero in the tables.

Table 4.1 presents, the participation factor analysis for linearized DFIG-based single wind turbine system connected to a grid at a wind speed, V_w = 13.5m/s. and linking inductance, L_{link} = 1 μH. Table 4.2 analyzes the participation factors of linearized model of two DFIG-based wind turbine systems connected to a grid (small wind farm) by applying wind speed $V_{ws1} = V_{ws2}$=13.5 m/s. and linking inductances $L_{links1} = L_{links2}$= 1 μH.

Table-4.1: Participation factor analysis at wind speed $V_w = 13.5\, m/s$ and linking inductance $L_{link} = 1\ \mu H$

System State	$\boldsymbol{\lambda_{1,2}}$ $\boldsymbol{-2.05 \pm j2454040.18}$	$\boldsymbol{\lambda_{3,4}}$ $\boldsymbol{-2.06 \pm j244650.19}$	$\boldsymbol{\lambda_{29}}$ $\boldsymbol{-5.7646047357}$
V_{sd}	0.17	0.17	≈ 0
V_{sq}	0.17	0.17	≈ 0
V_d	0.08	0.08	≈ 0
V_q	0.08	0.08	≈ 0
i_{linkd}	0.25	0.25	≈ 0
i_{linkq}	0.25	0.25	≈ 0
ω_r	≈ 0	≈ 0	1.002
i_{rq}	≈ 0	≈ 0	0.01
x_{irq}	≈ 0	≈ 0	0.01
All other state	≈ 0	≈ 0	≈ 0

Participation of state variables in each dominant eigenmode is viewed in Table-4.1 and Table-4.2. V_{sds1} , V_{sqs1} , V_d , V_q , V_{sds2} , V_{sqs2}, $i_{linkds1}$, $i_{linkqs1}$, $i_{linkds2}$, $i_{linkqs2}$ of Table 4.2 and V_{sd} , V_{sq} , V_d , V_q, i_{linkd}, i_{linkq} of Table 4.1, are directly related to the system's linking inductances, present significant participation in eigenmode $\lambda_{1,2}$, $\lambda_{3,4}$, $\lambda_{5,6}$, $\lambda_{7,8}$ of linearized model of two-turbine system and in eigenmode $\lambda_{1,2}$, $\lambda_{3,4}$ of linearized model of single-turbine system, respectively. Participation of the state variables, ω_{rs1} and ω_{rs2} of Table 4.2 and the state variable ω_r of Table 4.1, are significant in eigenmode λ_{53}, λ_{54} and in eigenmode λ_{29}, respectively.

Table-4.2: Participation factor analysis at $V_{ws1} = 13.5\ m/s$ and $V_{ws2} = 13.5\ m/s$ and linking inductance $L_{links1} = 1\ \mu H$, $L_{links2} = 1\ \mu H$

System State	$\boldsymbol{\lambda_{1,2}}$ $\boldsymbol{-1.218 \pm j283289.2}$	$\boldsymbol{\lambda_{3,4}}$ $\boldsymbol{-1.223 \pm j282535.2}$	$\boldsymbol{\lambda_{5,6}}$ $\boldsymbol{-4.189 \pm j200467.4}$	$\boldsymbol{\lambda_{7,8}}$ $\boldsymbol{-4.211 \pm j199713.5}$	$\boldsymbol{\lambda_{53}}$ $\boldsymbol{-5.868}$	$\boldsymbol{\lambda_{54}}$ $\boldsymbol{-5.966}$
V_{sds1}	0.06	0.06	0.13	0.12	≈ 0	≈ 0
V_{sqs1}	0.06	0.06	0.13	0.13	≈ 0	≈ 0
V_{sds2}	0.06	0.06	0.13	0.12	≈ 0	≈ 0
V_{sqs2}	0.06	0.06	0.13	0.13	≈ 0	≈ 0
V_d	0.12	0.13	≈ 0	≈ 0	≈ 0	≈ 0
V_q	0.13	0.13	≈ 0	≈ 0	≈ 0	≈ 0
$i_{linkds1}$	0.12	0.12	0.12	0.12	≈ 0	≈ 0
$i_{linkqs1}$	0.12	0.12	0.12	0.12	≈ 0	≈ 0
$i_{linkds2}$	0.12	0.12	0.12	0.12	≈ 0	≈ 0
$i_{linkqs2}$	0.12	0.12	0.12	0.12	≈ 0	≈ 0
ω_{rs1}	≈ 0	≈ 0	≈ 0	≈ 0	0.5	0.51
ω_{rs2}	≈ 0	≈ 0	≈ 0	≈ 0	0.5	0.51
i_{rqs1}	≈ 0	≈ 0	≈ 0	≈ 0	≈ 0	≈ 0
i_{rqs2}	≈ 0	≈ 0	≈ 0	≈ 0	≈ 0	≈ 0
x_{irqs1}	≈ 0	≈ 0	≈ 0	≈ 0	≈ 0	0.01
x_{irqs2}	≈ 0	≈ 0	≈ 0	≈ 0	≈ 0	0.01
All other state	≈ 0	≈ 0	≈ 0	≈ 0	≈ 0	≈ 0

Same wind speed and linking inductances are imposed on both the turbines of the linearized model of grid-connected two DFIG-based wind power system. So, in Table 4.2 the participation of the states, of Wind Turbine 1 and Wind Turbine 2 are nearly equal in each eigenmode. It can be stated from Table 4.2, that on application of same parametric conditions on both the turbines, the system states have equal participation in each eigenmode. But, the significant participation of states, of Wind Turbine 1 and of Wind Turbine 2 in each eigenmode are not decoupled, thus, cannot be specified which state corresponds to which eigenmode.

To minimize this problem, different wind speed and linking inductances are applied to each turbine system of linearized model of grid-connected two DFIG-based wind power systems and participation factor analysis is conducted in Table-4.3. In this table, analysis is performed by applying different wind speed V_{ws1}=13.5 m/s., V_{ws2}=7 m/s. and linking inductances L_{links1}=1 μH, and L_{links2}= 0.5 μH.

From Table 4.3, it is noticed that the participation of states, of Wind Turbine 1 and Wind Turbine 2, on each mode, are decoupled. Participation of states, V_{sds1} , V_{sqs1} , $i_{linkds1}$, $i_{linkqs1}$ of Wind Turbine 1 in eigenmode $\lambda_{1,2}$ and $\lambda_{3,4}$ are major; and the participation of states like V_{sds2} , V_{sqs2} , $i_{linkds2}$, and $i_{linkqs2}$ of Wind Turbine 2 in eigenmode $\lambda_{5,6}$ and $\lambda_{7,8}$ are noteworthy. Similarly, on eigenvalue λ_{53} and λ_{54}, participation of two turbine states, are decoupled; and wind speed change of Wind Turbine 1 and Wind Turbine 2, will affect the sensitivity of eigenmode λ_{54} and λ_{53}, respectively.

Only those eigenvalues of linearized models are considered in Table 4.1, 4.2 and 4.3, on which, system states related to linking inductances and applied wind speed, are involved; as stability analysis is carried out in this thesis for different linking inductances and for

Table-4.3: Participation factor analysis at $V_{ws1} = 13.5\ m/s$ and $V_{ws2} = 7\ m/s$ and linking inductance $L_{links1} = 1\ \mu H$, $L_{links2} = 0.5\ \mu H$

System State	$\boldsymbol{\lambda_{1,2}}$ $\boldsymbol{-1.907 \pm j248673.2}$	$\boldsymbol{\lambda_{3,4}}$ $\boldsymbol{-1.916 \pm j247919}$	$\boldsymbol{\lambda_{53}}$ $\boldsymbol{-2.9187}$	$\boldsymbol{\lambda_{54}}$ $\boldsymbol{-5.9246}$	$\boldsymbol{\lambda_{5,6}}$ $\boldsymbol{-7.98 \pm j102472.4}$	$\boldsymbol{\lambda_{7,8}}$ $\boldsymbol{-8.026 \pm j1.017}$
V_{sds1}	0.16	0.16	≈ 0	≈ 0	0.03	0.03
V_{sqs1}	0.16	0.16	≈ 0	≈ 0	0.03	0.03
V_{sds2}	≈ 0	≈ 0	≈ 0	≈ 0	0.19	0.19
V_{sqs2}	≈ 0	≈ 0	≈ 0	≈ 0	0.19	1.19
V_d	0.09	0.09	≈ 0	≈ 0	0.03	0.03
V_q	0.09	0.09	≈ 0	≈ 0	0.03	0.03
$i_{linkds1}$	0.24	0.24	≈ 0	≈ 0	0.01	0.01
$i_{linkqs1}$	0.24	0.24	≈ 0	≈ 0	0.01	0.01
$i_{linkds2}$	≈ 0	≈ 0	≈ 0	≈ 0	0.24	0.24
$i_{linkqs2}$	≈ 0	≈ 0	≈ 0	≈ 0	0.24	0.24
ω_{rs1}	≈ 0	≈ 0	≈ 0	1	≈ 0	≈ 0
ω_{rs2}	≈ 0	≈ 0	1.005	≈ 0	≈ 0	≈ 0
i_{rqs1}	≈ 0	≈ 0	≈ 0	0.01	≈ 0	≈ 0
i_{rqs2}	≈ 0	≈ 0	≈ 0	≈ 0	≈ 0	≈ 0
x_{irqs1}	≈ 0	≈ 0	≈ 0	0.01	≈ 0	≈ 0
x_{irqs2}	≈ 0	≈ 0	0.01	≈ 0	≈ 0	≈ 0
All other state	≈ 0	≈ 0	≈ 0	≈ 0	≈ 0	≈ 0

different wind speed. On the basis of this discussion, eigenvalue loci are drawn for the change in system's linking inductances and wind speed.

4.2.2 Eigenvalue, Frequency of Oscillation and Damping Factor

Figure 4.1 (a)-(c) shows the eigenvalue loci for change in linking inductances from 0.5 μH to 5 μH at constant wind speed of 13.5 m/s. For two-turbine system connected to a grid, same valued linking inductances and wind speed are applied to each of the turbines. In Figure 4.1, the eigenvalues are denoted as λ01 and λ02, determined from the linearized models of DFIG-based single-turbine system and wind farm, respectively. It is observed from Figure 4.1, that with the increase of linking inductances, eigenvalues move far from the imaginary axis. Also the magnitude of the imaginary part is decreasing while the magnitude of real part is increasing. So at larger linking inductances, both the systems are better damped and frequency of oscillations decays. Also, it is noticed from Figure 4.1, that the change in pattern of eigenvalue loci for both the systems, are identical.

Figure 4.2 presents frequency of oscillations (f_{osc}) and damping ratio (ζ), that are calculated from the eigenvalues plotted in Figure 4.1. In Figure 4.2, the eigenvalues are denoted as λ01 and λ02, determined from linearized models of DFIG-based single-turbine system and wind farm, respectively. It is also noticed that oscillatory frequency will be lower and damping ratio will increase with increase in linking inductance for both the systems. The nature of oscillation frequency and damping ratio, of single-turbine system and two-turbine system are nearly same, depends on how dominant the eigenvalues are.

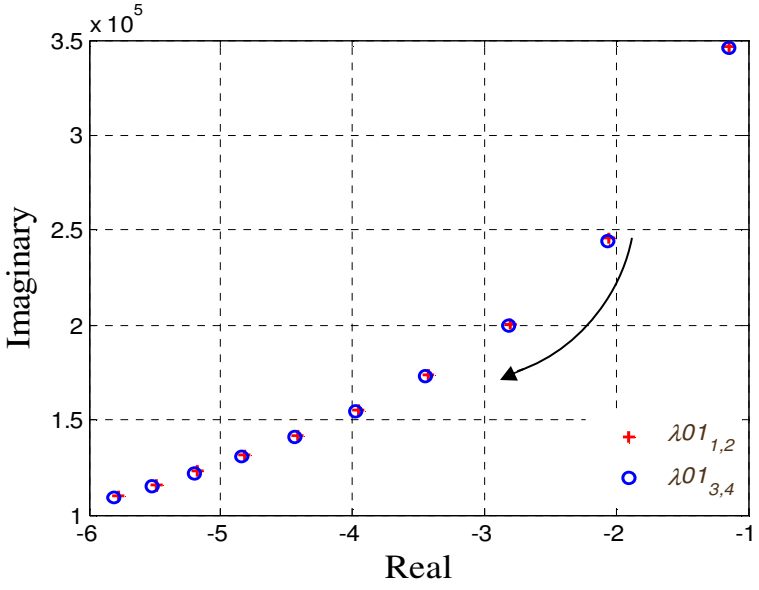

(a)

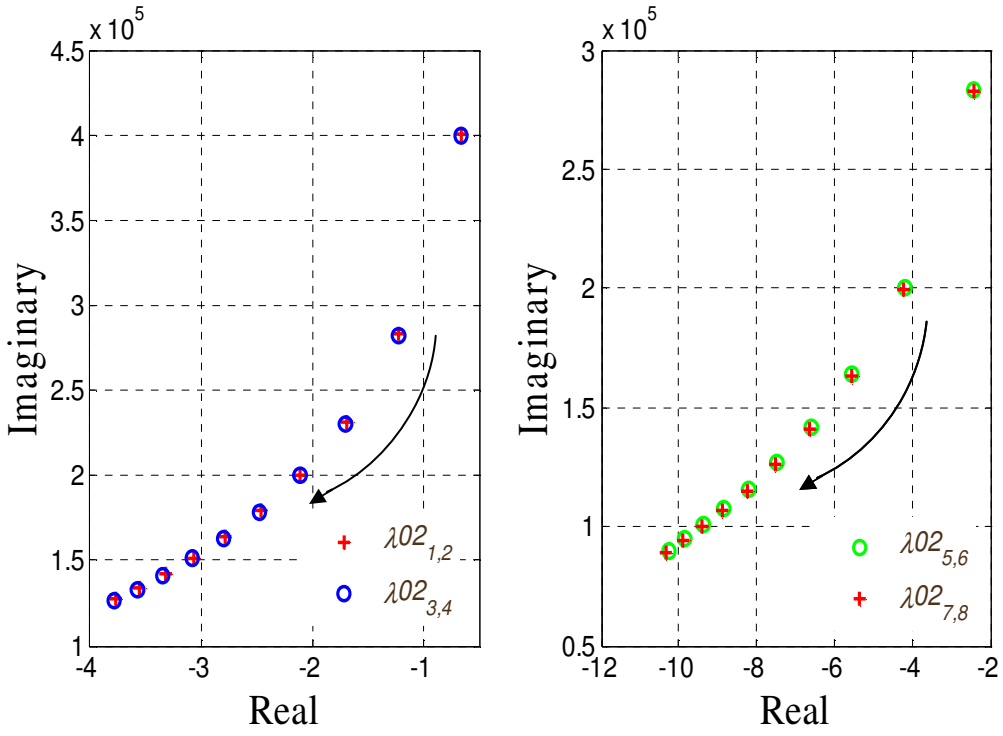

(b) **(c)**

Figure 4.1: Eigenvalue loci for change in linking inductances (a) $\lambda_{1,2}$ and $\lambda_{3,4}$ for single-turbine connected to a grid (b) $\lambda_{1,2}$ and $\lambda_{3,4}$ for two-turbine system connected to a grid (c) $\lambda_{5,6}$ and $\lambda_{7,8}$ for two-turbine system connected to a grid

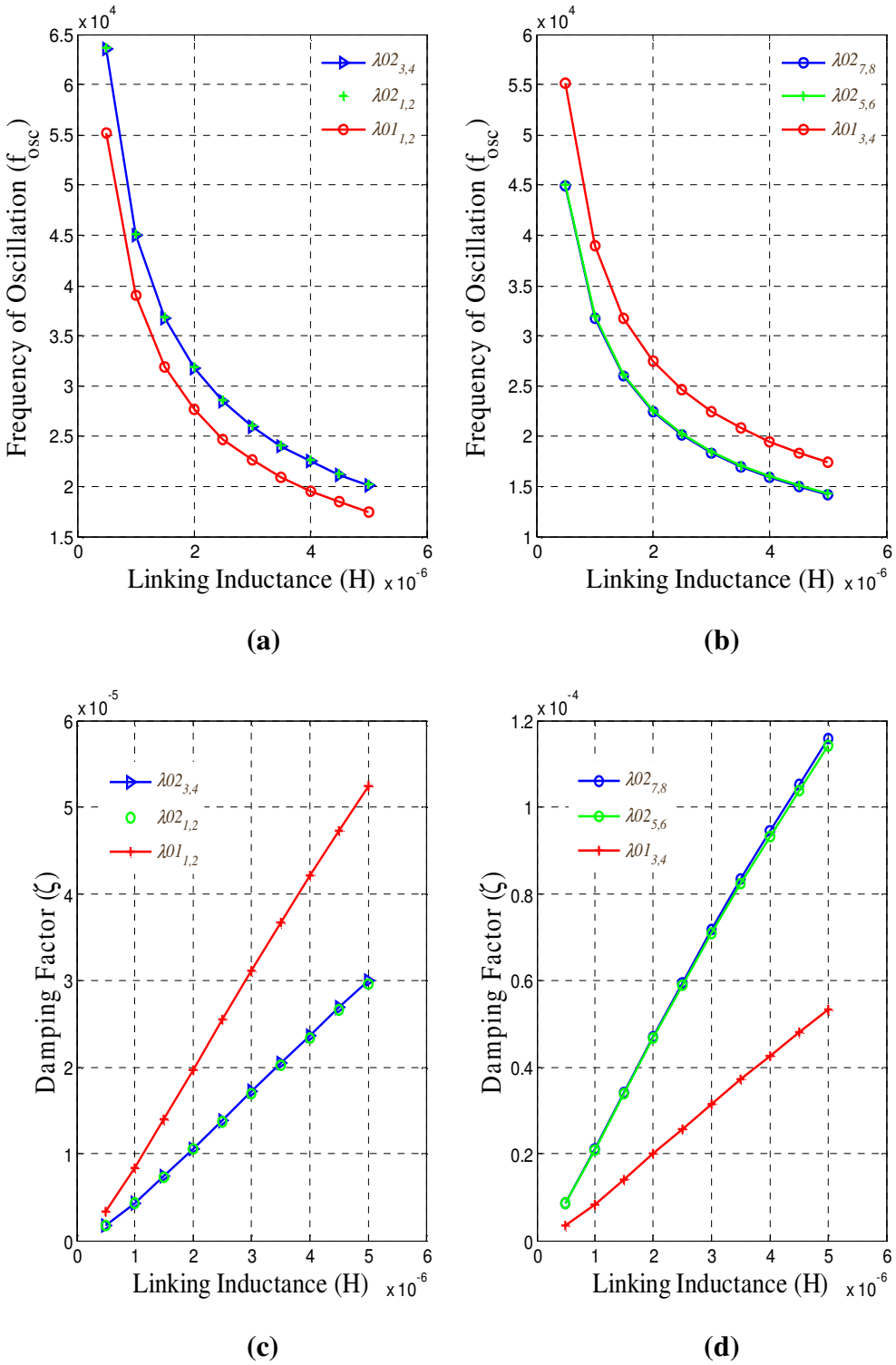

Figure 4.2: Frequency of oscillation (f_{osc}) and damping Factor (ζ) of eigenvalues of Figure 4.1 (a) Frequency of oscillation (f_{osc}) (b) Frequency of oscillation (f_{osc}) (c) damping Factor (ζ) (d) damping Factor (ζ)

Figure 4.3 describes and compares the change in real part of dominant eigenvalues (σ) of two different linearized models, with change in linking inductances varying from 0.5 μH to 5 μH at a constant wind speed of 13.5 m/s. It is also observed that with rise in linking inductances, the magnitudes of real part of dominant eigenvalues increase for both the systems.

From Figure 4.1 to Figure 4.3, it is observed that with change in linking inductances, eigenvalues, $\lambda_{1,2}$ and $\lambda_{3,4}$ for single wind power system connected to a grid and eigenvalues, $\lambda_{1,2}$, $\lambda_{3,4,}$ $\lambda_{5,6}$ and $\lambda_{7,8}$ for two wind power system connected to a grid, vary

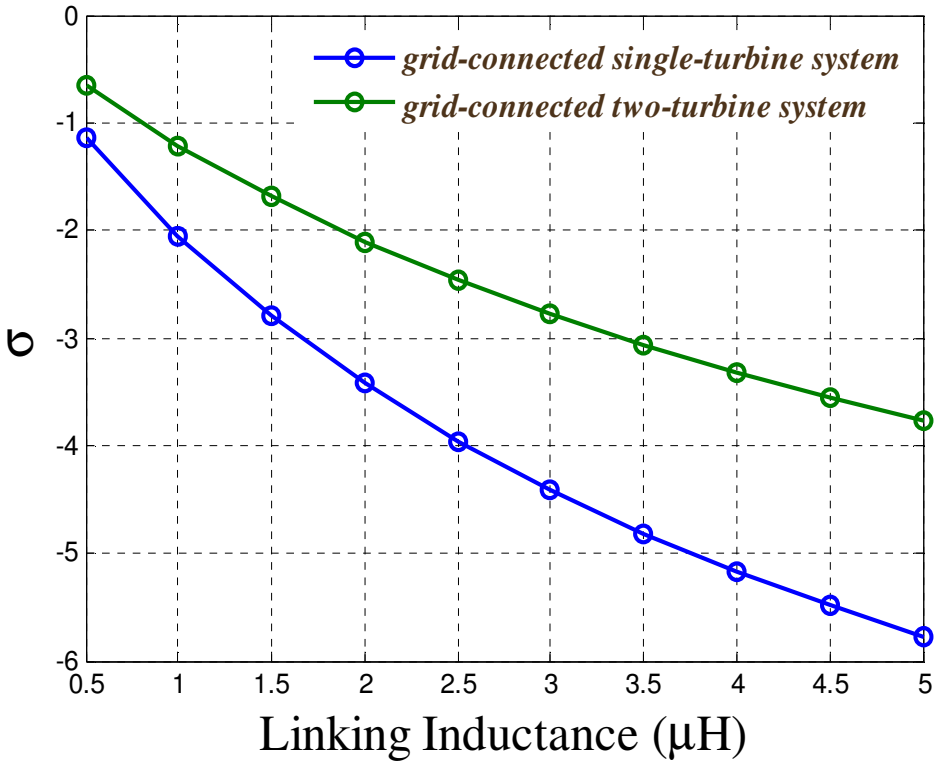

Figure 4.3: Graph for change in linking inductances with real part of dominant eigenvalue (σ) of linearized model grid-connected single-turbine system and grid-connected two-turbine systems, with change in linking inductances

at a wide range. This happens, because the participation of the states generated from linking inductances of the systems in that particular eigenmodes, are major that are already detailed in Table 4.1 and in Table 4.2. Table 4.4 illustrates, that at same condition (for change in linking inductances at constant wind speed) the eigenvalue λ_{29} of linearized model of single wind power system and λ_{53} and λ_{54} of linearized model of two wind power systems connected to a grid, are nearly constant. The states related to linking inductances have no major participation on these eigenmodes.

Table-4.4: Change in eigenvalues λ_{29} of linearized model of Figure 2.1 and λ_{53} and λ_{54} of linearized model of Figure 2.8 with inductances changes from 0.5 µH to 5 µH

Linking Inductance (µH)	**Grid-Connected Single -Turbine**	**Grid-Connected Two-Turbine**	
	λ_{29}	**λ_{53}**	**λ_{54}**
0.5	-5.754	-5.876	-5.974
1	-5.765	-5.868	-5.966
1.5	-5.765	-5.824	-5.915
2	-5.765	-5.876	-5.974
2.5	-5.768	-5.845	-5.939
3	-5.769	-5.876	-5.975
3.5	-5.786	-5.866	-5.965
4	-5.802	-5.869	-5.967
4.5	-5.802	-5.876	-5.975
5	-5.757	-5.859	-5.956

Figure 4.4 (a)-(c) shows the eigenvalue loci for change in wind speed from 6 m/s to 14 m/s at constant linking inductances of 1 μH. For two-turbine system connected to a grid, the linking inductances and wind speed applied to each of the turbines are same. It is observed in Figure 4.4 that with the rise in wind speed, eigenvalues λ_{29} of linearized model of grid-connected single DFIG-based wind power system and λ_{53} and λ_{54} of linearized model of grid-connected small wind farm, move far from imaginary axis. Figure 4.4 illustrates that, these eigenmodes are non-oscillatory by nature.

Figure 4.5 shows that with change in wind speed, there is not much change on dominant eigenvalues of both the systems. As was discussed previously, that the participation of system states related to linking inductances are significant on dominant eigenvalues, whereas the participation of the states related to wind speed on dominant eigenvalue are insignificant.

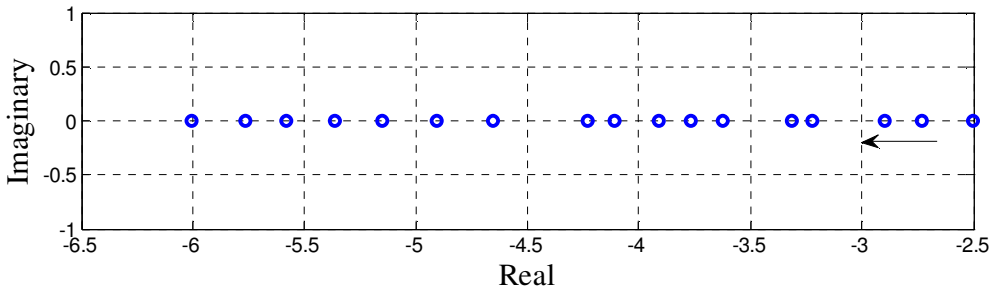

(a)

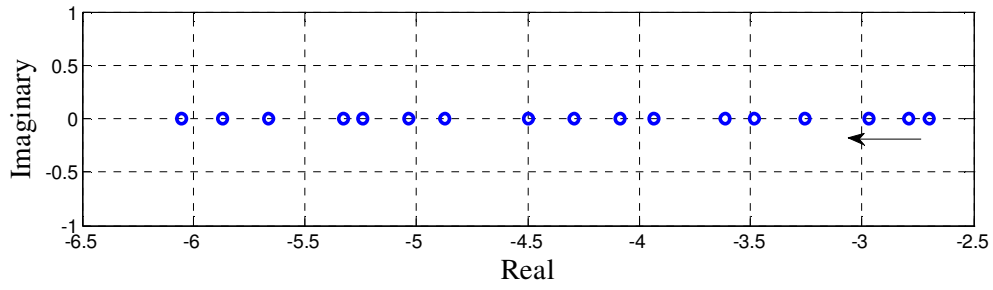

(b)

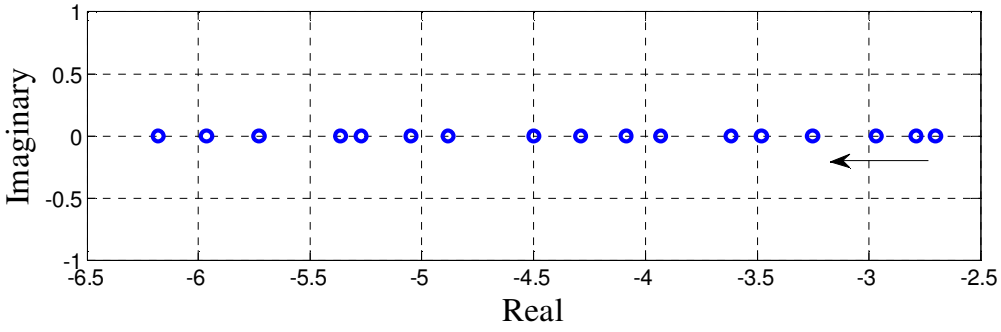

(c)

Figure 4.4: Eigenvalue loci for change in wind speed **(a)** λ_{29} for single-turbine connected to a grid. **(b)** λ_{53} for two-turbine system connected to a grid **(c)** λ_{54} for two-turbine system connected to a grid

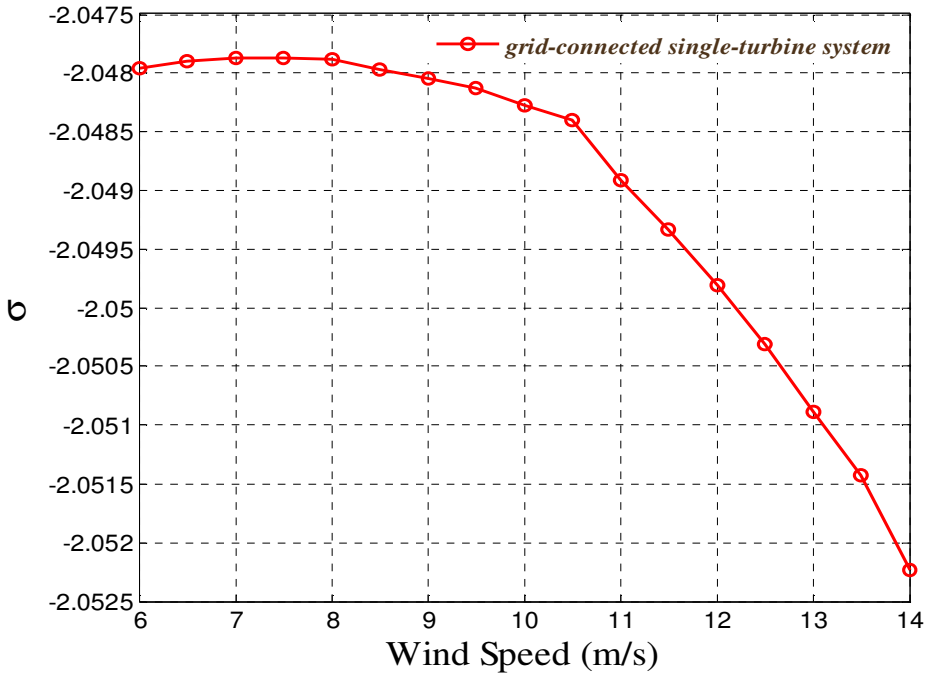

(a)

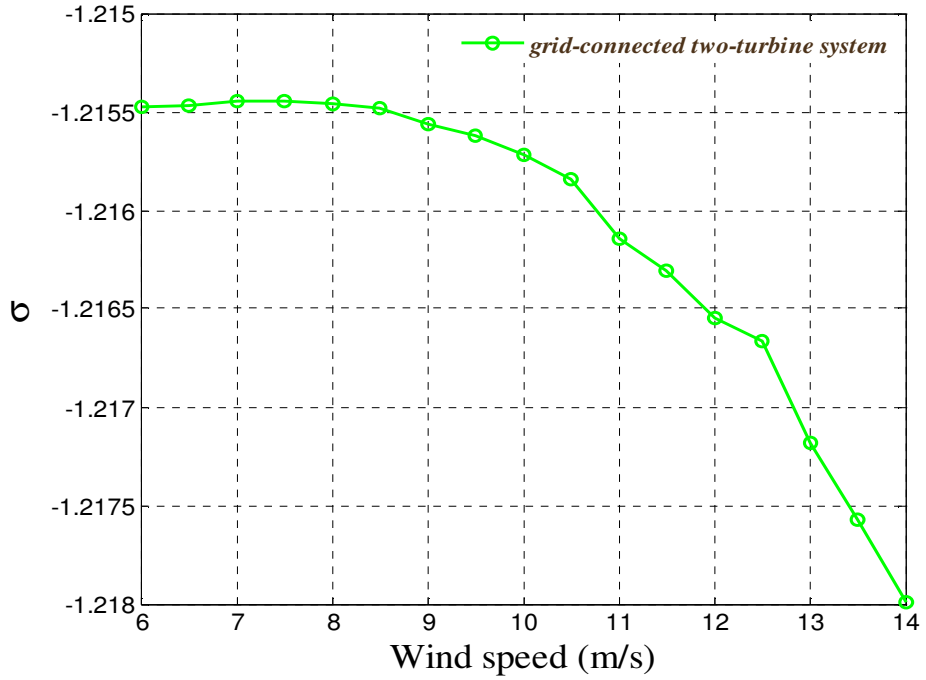

(b)

Figure 4.5: Graph for change in wind speed with real part of dominant eigenvalue for **(a)** Linearized model of Figure 2.1 and **(b)** Linearized model of Figure 2.8

4.3 Sensitivity analysis at High Linking Inductances

A case study is performed, in which the wind power systems are considered to be far away from the grid and that is connected to a transmission line with 0.32 mH/km [30]. In this scenario, eigenvalue sensitivity for both the linearized models of grid-connected DFIG-based single wind turbine system and grid-connected small wind farm, are analyzed. Figure 4.6 shows, the shifting of real part of dominant eigenvalue with the change in linking inductances and change in wind speed. From Figure 4.6 (a), it is observed that, with increase in linking inductance from 0.32 mH to 2 mH at constant wind speed of 13.5 m/s., the real part of dominant eigenvalues swing toward the instability zone for both the linearized models. In Figure 4.6 (b), the magnitude of real part of dominant eigenvalue is also increasing and going far from imaginary axis with the increase in wind speed from 6 m/s to 14 m/s at constant linking inductances of 0.32 mH for both the linearized models.

Figure 4.7 presents that at high linking inductance, both the models have non-oscillatory dominant eigenmodes. Both, in the figures 4.6 and 4.7, same wind speed and linking inductances are applied at same time to draw intrinsic dynamic nature of two-turbine system connected to a grid. Thus, in conclusion, at a high linking inductance, the nature of dominant eigenvalues is identical for both the systems.

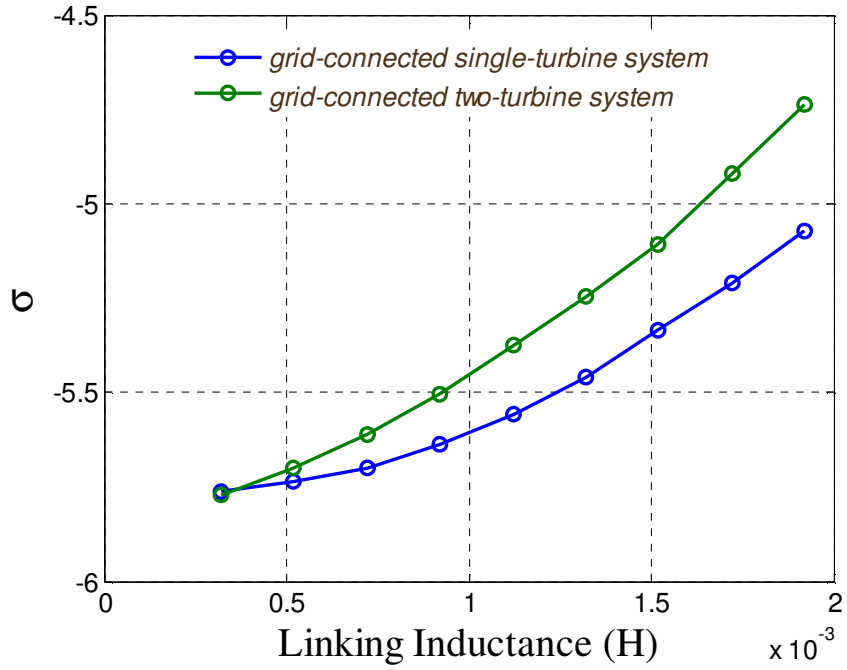

(a)

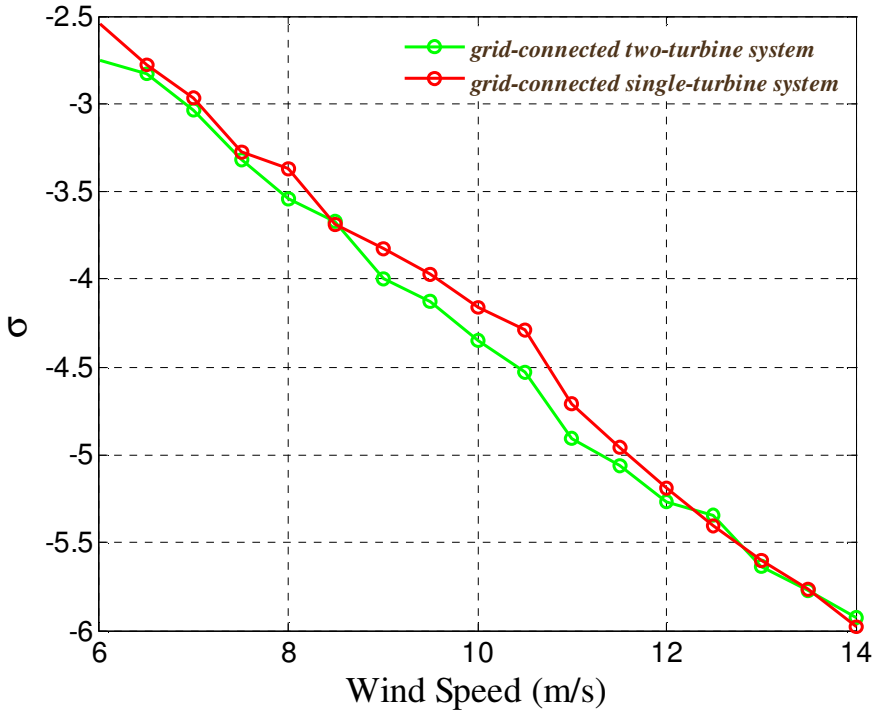

(b)

Figure 4.6: Graph for change in system parameters with real part of dominant eigenvalue **(a)** Change in linking inductances **(b)** Change in wind speed

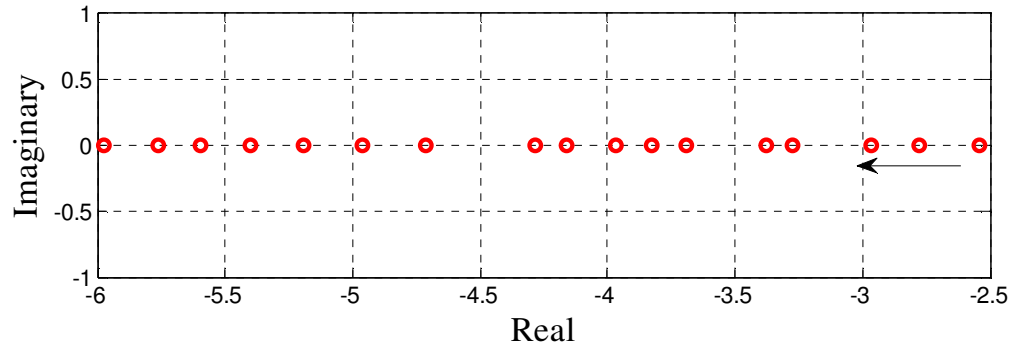

(a)

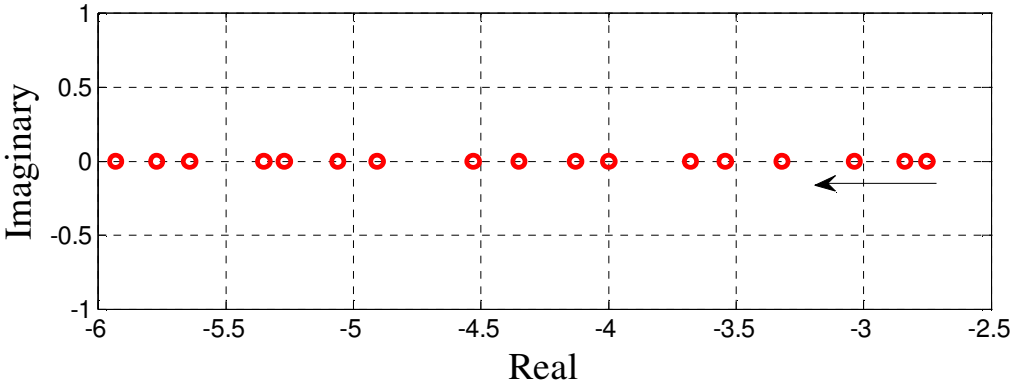

(b)

Figure 4.7: Dominant eigenvalue loci draw for change in wind speed from 6 m/s to 14 m/s at linking inductance 0.00032 H (a) Linearized model of grid-connected single-turbine and (b) Linearized model of grid-connected small wind farm

4.4 Summary and Conclusion

This chapter has studied the small-signal stability, the system's parametric effects on stability and modal analysis of the two linearized models developed in Chapter 2. The system's parametric effects were analyzed using a participation factor. Modal analysis was carried out by determining participation factor, damping factor and frequency of oscillation of dominant eigenvalues of the systems. This study was conducted in the MATLAB/SIMULINK environment. In conclusion, under the same operating conditions and system parameters, the dynamic behavior of a multi-unit wind power system (farm)

is very similar to that of a single-unit wind power system connected to a grid; also, the system parameters exhibit nearly the same effects on the stability of both aforementioned systems.

Chapter 5

Summary, Conclusions and Future Works

5.1 Summary and Conclusions

Summary and conclusions of the thesis are stated below:

- Detailed non-linear mathematical models as well as linearization of a grid-connected single DFIG-based turbine and a two DFIG-based wind turbine system connected to a grid have been presented;
- Two ac-dc-ac back-to-back VSCs, PLL, rotor current controller block, dc bus voltage current controller block, reference signal generator, stator flux observer, current control loop for a grid side VSC system, DC voltage controller with feed-forward block are introduced with each wind turbine system. Also, the role of each controller block is explained in detail, and non-linear equations as well as linearization are generated for each individual block;
- The system's mathematical model is introduced in a dq-frame to avoid the complexity of three phase circuits;
- Participation factor analysis is carried out to determine the system parametric effects on each eigenmode for systems;
- The intrinsic dynamic behaviors of grid-connected single-turbine system and a grid-connected two-turbine system are analyzed individually by observing the

pattern of eigenvalue loci, frequency of oscillation, and damping ratio. This study is performed by changing system's parameters and operating conditions such as by linking inductance and wind speed;

- A comparative study of eigenvalue sensitivity, system parametric effects and system stability is presented for a grid-connected single wind-power system to that of a grid-connected two wind power system;
- Finally, to assess the stability, dynamic behavior, and effects of different system parameters in a wind farm constituted entirely with identical wind power systems, it is sufficient to only study one of the constituting wind power systems, as a good approximation.

5.2 Future Work

The scope of future work is discussed as follows:

- It is necessary to lump the two turbines into one single-turbine and compare the output result of the lumped system with that of two-turbine system.
- Extended research can be performed on disturbances generated by mechanical parts of the wind turbine and affecting the electrical system.
- Interaction between a wind farm with an HVDC system and FACTS controllers can be studied.

References

[1] T. Ackermann, *Wind Power in Power Systems*. Chichester, UK: Wiley, 2005.

[2] G. L. Johnson, *Wind Energy Systems*. USA: Pentrice Hall, 1985.

[3] T. Burton, N. Jenkins, D. Sharpe, E. Bossanyi, *Wind Energy Handbook*, 2nd Ed., Chichester, UK: Wiley, 2011.

[4] S. Heier, *Grid Integration of Wind Energy Conversion Systems*, 2nd Ed., Chichester, UK: Wiley, 2006.

[5] Global Wind Energy Council (GWEC), "http://www.gwec.net/wp-content/uploads/2013/02/GWEC-PRstats-2012_english.pdf", Belgium, Feb. 2013.

[6] Global Wind Energy Outlook (GWEO), "http://www.gwec.net/wp-content/uploads/2012/11/GWEO_2012_lowRes.pdf", Belgium, Nov. 2012.

[7] Energy Efficiency & Renewable Energy (EERE), "http://www2.eere.energy.gov/wind/inside_a_wind_turbine.html", USA, Jan. 2013.

[8] Union of Concerned Scientists (UCS), "http://www.ucsusa.org/clean_energy/our-energy-choices/renewable-energy/how-wind-energy-works.html", USA, Dec. 2009.

[9] J.F. Manwell, J. G. Magowan, A.L. Rogers, *Wind Energy Explained: Theory, Design and Application*. Chichester, UK: Wiley, 2009.

[10] American Wind Energy Association (AWEA), "http://www.awea.org/issues/supply_chain/Anatomy-of-a-Wind-Turbine.cfm", USA, 2013.

[11] Green Rhino Energy, "http://www.greenrhinoenergy.com/renewable/wind/", 2013.

[12] M. R. Patel, *Wind and Solar Power Systems*. Florida, USA: CRC Press, 1999.

[13] O. A. Lara, N. Jenkins, J. Ekanayake, P. Cartwright, M. Hughes, *Wind Energy Generation: Modelling and Control*. Chichester, UK: Wiley, 2009.

[14] A. W. Manyonge, R. M. Ochieng, F. N. Onyango , J. M. Shichikha, "Mathematical Modelling of Wind Turbine in a Wind Energy Conversion System: Power Coefficient Analysis", *Applied Mathematical Sciences*, Vol. 6, no. 91, pp. 4527 – 4536, Apr. 2012.

[15] F. D. Bianchi, H. D. Battista, R. J. Mantz, *Wind Turbine Control Systems: Principles, Modeling and Gain Scheduling Design*. London, UK: Springer, 2007.

[16] A. Yazdani, R. Iravani, *Voltage-Sourced Converters in Power Systems: Modeling, Control, and Applications*. Hoboken, New Jersey: IEEE/Wile, 2010.

[17] A. R. Jha, *Wind Turbine Technology*. Florida: USA, C.R.C Press, 2011.

[18] F. Mei, B. C. Pal, "Modelling and Small-Signal Analysis of a Grid Connected Doubly- Fed Induction Generator", *IEEE Power Engineering Society General Meeting*, Vol. 3, pp. 2101-2108, Jun. 2005.

[19] L. Rouco, and J. L. Zamora, "Dynamic Patterns and Model Order Reduction in Small-signal Models of Doubly Fed Induction Generators for Wind Power Applications", *IEEE Power Eng. Soc. Gen. Meeting*, pp.1-8, 2006.

[20] F. Mei, and B. Pal, "Modal Analysis of Grid-Connected Doubly Fed Induction Generators", *IEEE Trans. Of Energy Conv.*, Vol. 22, no. 3, pp. 728-736, Sep. 2007.

[21] L. Sigrist, and L. Rouco, "Design of Damping Controllers for Doubly Fed Induction Generators Using Eigenvalue Sensitivities", *IEEE Power Sys. Conf. & Expo. PSCE'09*, Seattle, WA, USA, pp.1-7, Mar. 2009.

[22] L. Yang, Z. Xu, J. Østergaard, Z. Y. Don, K. P. Wong, and X. Ma, "Oscillatory Stability and Eigenvalue Sensitivity Analysis of A DFIG Wind Turbine System", *IEEE Trans. of Energy Conv.*, Vol. 26, no. 1, pp. 328-329, Mar. 2011

[23] A. Ostadi, A. Yazdani, and R. K. Varma, "Modeling and Stability Analysis of a DFIG-Based Wind-Power Generator Interfaced With a Series-Compensated Line", *IEEE Trans. on Power Delivery*, Vol. 24, no. 3, pp. 1504-1514, July 2009.

[24] W. Leonhard, *Control of Electrical Drives*. New York, USA: Springer, 3rd ed., 2001.

[25] Md. Hilal, Md. Maaroufi, and Md. Ouassaid, "Doubly Fed Induction Generator Wind Turbine Control for a maximum Power Extraction", *Int. Conf. on Multimedia Comp. and Sys. (ICMCS), IEEE*, Apr. 2011, pp.1-7.

[26] P. Kundar, *Power system stability and control*, New York, USA: McGraw-Hill, 1994.

[27] PSCAD/EMTDC, *Manitoba HVDC Research Centre*, V. 4.2 Winnipeg, MB, Canada.

[28] P. W. Sauer, M. A. Pai, "Power system dynamics and stability", *Prentice Hall*, Upper Saddle River, New Jersey, USA, 1998.

[29] B. Porter & R. Crossley, *Modal Control: Theory and Applications*. London, UK: Taylor & Francis, 1972.

[30] W. Kling, P. Bresesti, I. Valadè, D. Canever, R. Hendriks, "Transmission systems for offshore wind farms in the Netherlands", In s.n. (Ed.), *Copenhagen Offshore Wind Conference Proceedings* , Copenhagen , Oct. 2005, pp. 1-7.

Appendices

Appendix A

Table

System parameters used in Figure 2.1 and Figure 2.8

Turbine Parameters		
Quantity	***Value***	***Comments***
r	*35.25 m*	*Rotor radius*
A	*3904 m^2*	*Rotor swept area*
C_{pmax}	*0.421*	*Performance coefficient*
λ_{opt}	*6.85*	*Optimal tip speed ratio*
N	*180*	*Gear box ratio including machine number of poles*
ρ	*1.225 kg/m^3*	*Air density*
H	*0.5s*	*Inertia constant*
Generator Parameters		
P_b	*1.678 MW*	*Base power*
V_b	*1878 V*	*Base voltage*
i_b	*596 A*	*Base current*
ω_b	*377 rad/s*	*Base frequency*
T_b	*4.451 kN m*	*Base torque*
R_s	*29 mΩ*	*Stator resistance*
R_r	*26 mΩ*	*Rotor resistance*
L_m	*34.52 mH*	*Magnetizing inductance*
L_s	*35.12 mH*	*Stator inductance*
L_r	*35.12 mH*	*Rotor inductance*
τ_s	*1.21 s*	*Stator time constant*
τ_r	*1.35 s*	*Rotor time constant*
N_t	*1*	*Rotor/stator turn ratio*
VSC Parameters		

$T_{rs-power}$	*400 kVA*	T_{rs} *Transformer nominal power*
$T_{rs-voltage\ ratio}$	*2.3/ 0.6 kV*	*At rotor side winding, 0.6 kV and at grid side 2.3 kV-* N_{tc}
$T_{rs-reactance}$	*239 μH*	*At 0.6 kV side*
$T_{rs-resistance}$	*9.0 mΩ*	*Ohomic resistance loss at 0.6 kV side*
L_a	*764 μH*	*Grid side converter ac-side terminal inductance*
R_a	*35 mΩ*	*Grid side converter ac-side terminal resistance*
C_f	*50 μf*	*Shunt capacitor at PCC*
C_{dc}	4000 *μf*	*DC side capacitor of two VSC*
L_{link}	*0.32 mH/km*	*Based on distance between wind power system and transmission network*
C_{link}	*25 μf*	*Shunt capacitor at machine and linking inductance meet point*
Transmission line Parameters		
V_g	*13.8 kV*	*rms value of grid voltage l-l*
L_g	*17.13 mH*	Inductance at Transmission line
R_g	*682.9 mΩ*	Resistance at Transmission line
$T_{rg-power}$	*2.0 MVA*	T_{rg} *Transformer nominal power*
$T_{rg-Voltage\ ratio}$	*13.8/2.3 kV*	*At grid side winding, 13.8 kV and the turn ratio is* N_{tg}
$T_{rg-inductance}$	*0.1 pu*	*Transmission line Transformer leakage inductance*
$T_{rg-resistance}$	*0.02 pu*	*Transmission line Transformer ohomic resistance*

Controller Parameters

$$K_r(s) = 17.97 + \frac{333.33}{s};$$

$$K_a(s) = 0.764 + \frac{4.7}{s};$$

$$G(s) = \frac{0.16}{1+0.00048s};$$

$$K_{pr}(s) = \frac{1}{0.001s+1};$$

$$K_v(s) = 0.899 + \frac{17.241}{s};$$

$$G_f(s) = \frac{1}{1+0.000008s};$$

$$H_s(s) = \frac{142680(s^2+568516)(s^2+166s+6889)}{s(s^2+1508s+568516)(s^2+964s+232324)};$$

Appendix B

Linearized Mathematical Model of Wind turbine 1 & Wind turbine 2 of Small Wind Farm

$$\frac{d\Delta\lambda_{s1}}{dt} = -\frac{\Delta\lambda_{s1}}{\tau_{ss1}} + \Delta V_{sds1} + \frac{L_{ms1}\Delta i_{rds1}}{\tau_{ss1}} \quad (1)$$

$$\frac{d\Delta\alpha_{s1}}{dt} = \left[\frac{V_{sq0s1}}{\lambda_{0s1}^2} + \frac{L_{ms1}i_{rq0s1}}{\lambda_{0s1}^2\tau_{ss1}}\right]\Delta\lambda_{s1} - \frac{1}{\lambda_{0s1}}\Delta V_{sqs1} - \frac{L_{ms1}}{\tau_{ss1}\lambda_{0s1}}\Delta i_{rqs1} \quad (2)$$

$$\frac{d\Delta V_{sds1}}{dt} = \frac{1}{C_{links1}}\Delta I_{linkds1} - \frac{1}{C_{links1}}\Delta I_{sds1} - \frac{1}{C_{links1}}\Delta I_{mds1} + \omega_{0s1}\Delta V_{sqs1} + V_{sq0s1}\Delta\omega_{s1} \quad (3)$$

$$\frac{d\Delta V_{sqs1}}{dt} = \frac{1}{C_{links1}}\Delta I_{linkqs1} - \frac{1}{C_{links1}}\Delta I_{sqs1} - \frac{1}{C_{links1}}\Delta I_{mqs1} - \omega_{0s1}\Delta V_{sds1} - V_{sd0s1}\Delta\omega_{s1} \quad (4)$$

$$\frac{dV_{dcs1}}{dt} = -\frac{3}{2C_{dcs1}V_{dc0s1}}\left[V_{rd0s1}\Delta i_{rds1} + i_{rd0s1}\Delta V_{rds1} + V_{rq0s1}\Delta i_{rqs1} + i_{rq0s1}\Delta V_{rqs1} + V_{ad0s1}\Delta i_{ads1} + i_{ad0s1}\Delta V_{ads1} + V_{aq0s1}\Delta i_{aqs1} + i_{aq0s1}\Delta V_{aqs1}\right] \quad (5)$$

$$\frac{d\Delta\omega_{rs1}}{dt} = \frac{1}{J_{s1}\omega_{r0s1}}\Delta P_{turs1} - \frac{1}{J_{s1}\omega_{r0s1}}\Delta P_{es1} \quad (6)$$

$$\frac{d\Delta\beta_{ls1}}{dt} = -H(s)_{s1}\Delta Vsql_{s1} \quad (7)$$

$$\frac{d\Delta i_{rds1}}{dt} = \left(-\frac{R_{rs1}}{\eta_{s1}} - \frac{L_{ms1}^2}{L_{ss1}\tau_{ss1}\eta_{s1}} - \frac{K_{rps1}R_{rs1}}{\eta_{s1}}\right)\Delta i_{rds1} + i_{rq0s1}\Delta\omega_{s1} + \frac{L_{ms1}}{L_{ss1}\eta_{s1}\tau_{ss1}}\Delta\lambda_{s1} + \frac{K_{rps1}R_{rs1}}{\eta_{s1}}\Delta i_{rdrefs1} + \frac{K_{ris1}R_{rs1}}{\eta_{s1}}\Delta x_{irds1} \quad (8)$$

$$\frac{d\Delta i_{rqs1}}{dt} = \left(-\frac{R_{rs1}}{\eta_{s1}} - \frac{K_{rps1}R_{rs1}}{\eta_{s1}}\right)\Delta i_{rqs1} + \left[-i_{rd0s1} - \frac{L_{ms1}\lambda_{0s1}}{L_{ss1}\eta_{s1}}\right]\Delta\omega_{s1} + \frac{K_{rps1}R_{rs1}}{\eta_{s1}}\Delta i_{rqrefs1} + \frac{K_{ris1}R_{rs1}}{\eta_{s1}}\Delta x_{irqs1} \quad (9)$$

$$\frac{d\Delta i_{ads1}}{dt} = \frac{K_{aps1}}{L_{as1}}\Delta i_{adrefs1} - \left(\frac{K_{aps1}}{L_{as1}} + \frac{R_{as1}}{L_{as1}}\right)\Delta i_{ads1} - \frac{1}{N_{tcs1}L_{as1}}\Delta V_{sdls1} + G_{fs1}\frac{\Delta V_{sdls1}}{N_{tcs1}L_{as1}} \quad (10)$$

$$\frac{d\Delta i_{linkds1}}{dt} = \frac{\Delta V_d}{L_{links1}} - \frac{\Delta V_{sds1}}{L_{links1}} + \omega_{0s1}\Delta i_{linkqs1} + i_{linkq0s1}\Delta\omega_{s1} \quad (12)$$

$$\frac{d\Delta i_{linkqs1}}{dt} = \frac{\Delta V_q}{L_{links1}} - \frac{\Delta V_{sqs1}}{L_{links1}} - \omega_{0s1}\Delta i_{linkds1} - i_{linkd0s1}\Delta\omega_{s1} \quad (13)$$

$$\frac{d\Delta x_{irds1}}{dt} = \Delta i_{rdrefs1} - \Delta i_{rds1} \quad (14)$$

$$\frac{d\Delta x_{irqs1}}{dt} = \Delta i_{rqrefs1} - \Delta i_{rqs1} \quad (15)$$

$$\frac{d\Delta x_{iads1}}{dt} = \Delta i_{adrefs1} - \Delta i_{ads1} \quad (16)$$

$$\frac{d\Delta x_{iaqs1}}{dt} = \Delta i_{aqrefs1} - \Delta i_{aqs1} \quad (17)$$

$$\frac{d\Delta x_{v1s1}}{dt} = \Delta x_{v2s1} \quad (18)$$

$$\frac{d\Delta x_{v2s1}}{dt} = \frac{V_{dcref0s1}\Delta V_{dcrefs1}}{T_{s1}} - \frac{V_{dc0s1}\Delta V_{dcs1}}{T_{s1}} - \frac{\Delta x_{v2s1}}{T_{s1}} \quad (19)$$

$$\frac{d\Delta X_{prs1}}{dt} = \frac{3}{2}\frac{\left[V_{rd0s1}\Delta i_{rds1} + i_{rd0s1}\Delta V_{rds1} + V_{rq0s1}\Delta i_{rqs1} + i_{rq0s1}\Delta V_{rqs1}\right]}{T_{5s1}} + \frac{3}{2}\frac{\left[V_{ad0s1}\Delta i_{ads1} + i_{ad0s1}\Delta V_{ads1} + V_{aq0s1}\Delta i_{aqs1} + i_{aq0s1}\Delta V_{aqs1}\right]}{T_{5s1}} - \frac{\Delta X_{prs1}}{T_{5s1}} \quad (20)$$

$$\frac{d\Delta X_{fds1}}{dt} = \frac{\Delta V_{sdls1}}{N_{tcs1}T_{4s1}} - \frac{\Delta X_{fds1}}{T_{4s1}} \quad (21)$$

$$\frac{d\Delta X_{fqs1}}{dt} = \frac{\Delta V_{sqls1}}{N_{tcs1}T_{4s1}} - \frac{\Delta X_{fqs1}}{T_{4s1}} \quad (22)$$

$$\frac{d\Delta h_{1s1}}{dt} = \Delta h_{2s1} \quad (23)$$

$$\frac{d\Delta h_{2s1}}{dt} = \Delta h_{3s1} \quad (24)$$

$$\frac{d\Delta h_{3s1}}{dt} = \Delta h_{4s1} \quad (25)$$

$$\frac{d\Delta h_{4s1}}{dt} = \Delta h_{5s1} \tag{26}$$

$$\frac{d\Delta h_{5s1}}{dt} = \Delta V_{sqls1} - (\beta_{13} + \beta_{11})\Delta h_{5s1} - (\beta_{14} + \beta_{11}\beta_{13} + \beta_{12})\Delta h_{4s1} - (\beta_{12}\beta_{13} + \beta_{11}\beta_{14})\Delta h_{3s1} - \beta_{12}\beta_{14}\Delta h_{2s1} \tag{27}$$

List of Constant used in above equations

β_{11}=1508; β_{12}=568516; β_{13}=964; β_{14}=232324; generated due to $H_s(s)_{s1}$

$T_{s1} = 0.00048$; generated due to $G(s)_{s1}$

$T_{4s1} = 8 \times 10\text{^} - 6$; generated due to $G_f(s)_{s1}$

$T_{5s1} = 0.001$; generated due to $K_{pr_{s1}}$

$K_{rp_{s1}}$ and $K_{ri_{s1}}$ are proportional and integral constant generated due to PI controller $K_{r_{s1}}$

$K_{ap_{s1}}$ and $K_{ai_{s1}}$ are proportional and integral constant generated due to PI controller $K_{a_{s1}}$

The linearized mathematical model generated due to wind turbine 2 of the wind farm is exactly same with the wind turbine 1. Another 27 identical equations will be generated with subscript s2 for wind turbine 2.

Linearized Mathematical Model of the Distribution Network of Small Wind Farm

$$\frac{d\Delta i_{gd}}{dt} = -\frac{1}{L_g}\hat{V}_g \sin\alpha_{0s1}\Delta\alpha_{s1} - \frac{R_g}{L_g}\Delta i_{gd} + \omega_{0s1}\Delta i_{gq} + i_{gq0}\Delta\omega_{s1} - \frac{N_{tg}}{L_g}\Delta V_d \tag{28}$$

$$\frac{d\Delta i_{gq}}{dt} = \frac{1}{L_g}\hat{V}_g \cos\alpha_{0s1}\Delta\alpha_{s1} - \frac{R_g}{L_g}\Delta i_{gq} - \omega_{0s1}\Delta i_{gd} - i_{gd0}\Delta\omega_{s1} - \frac{N_{tg}}{L_g}\Delta V_q \tag{29}$$

$$\frac{d\Delta V_d}{dt} = \frac{N_{tg}}{C_f}\Delta i_{gd} - \frac{1}{C_f}\Delta(i_{linkds1} + i_{linkds2}) + \omega_{0s1}\Delta V_q + V_{q0}\Delta\omega_{s1} \tag{30}$$

$$\frac{d\Delta V_q}{dt} = \frac{N_{tg}}{C_f}\Delta i_{gq} - \frac{1}{C_f}\Delta(i_{linkqs1} + i_{linkqs2}) - \omega_{0s1}\Delta V_d - V_{d0}\Delta\omega_{s1} \tag{31}$$

Vita

NAME:	Baishakhi Dhar
POST-SECONDARY EDUCATION:	Western University London, Ontario 2011-2013 M.E.Sc.
	Jadavpur University Kolkata, India 2006-2008 M.E
AWARDS:	Western Engineering Scholarship (WES) since May 2011
RELATED WORK	Research Assistant Western University 2011-2013
	Teaching Assistant Western University 2011-2013